

Photocatalytic, electrocatalytic and photoelectrocatalytic degradation of pharmaceuticals in aqueous media: Analytical methods, mechanisms, simulations, catalysts and reactors

Belisa A. Marinho^{a,*}, Luka Suhadolnik^a, Blaž Likozar^b, Matej Huš^{b,c}, Živa Marinko^{a,d}, Miran Čeh^a

^a Department for Nanostructured Materials, Jožef Stefan Institute, Jamova 39, 1000, Ljubljana, Slovenia

^b Department of Catalysis and Chemical Reaction Engineering, National Institute of Chemistry, Hajdrihova 19, SI-1000, Ljubljana, Slovenia

^c Association for Technical Culture of Slovenia (ZOTKS), Zaloška 65, 1000, Ljubljana, Slovenia

^d Jožef Stefan International Postgraduate School, Jamova 39, 1000, Ljubljana, Slovenia

ARTICLE INFO

Handling Editor: Zhen Leng

Keywords:

Advanced oxidation process
Persistent organic compounds
Pharmaceutical by-products
Degradation mechanism
Reactor design
Analytical methods

ABSTRACT

Pharmaceuticals are used every day in most parts of the world and great proportions of these substances are excreted unaltered or as active sub-products, posing a threat of pollution. To protect the aquatic ecosystems, innovative solutions such as photocatalysis, electrocatalysis and photoelectrocatalysis are required. In this article we provide a comprehensive review of photo- and electrocatalytic techniques for the removal of pharmaceuticals from water and wastewaters. The analytical and toxicity methods commonly used to study the degradation of pharmaceuticals are presented, and it is pointed high performance liquid chromatography analysis as the most common analytical method to evaluate the efficiency in the pharmaceutical's degradation. However, it is also highlighted that the evaluation of the toxicity is fundamental to ensure adequate treatment. The determination of the reactive species and the mechanistic evaluation of pharmaceuticals degradation are essential to understanding and enhancing the degradation process. A deep discussion of photocatalysis, electrocatalysis and photoelectrocatalysis principles and practical examples of their application in pharmaceuticals treatment is presented. The catalytic materials and the reactors used in these processes for the removal of pollutants are reviewed focusing on some representative examples. The reusability of catalysts is still restricted to a few reuse cycles. It was observed very limited results in the treatment of larger amounts of effluent and a lack of information about process costs, which were correlated to the difficulty of application of these techniques on real scale. Finally, the main advantages of photocatalysis, electrocatalysis and photoelectrocatalysis as high efficiency on pharmaceuticals degradation, and the main drawbacks, as the low quantum efficiency and/or high energetic consume are pointed out along with alternatives to overcome these limitations.

1. Introduction

Pharmaceuticals are an important class of substances used for healing and preventing diseases as well as improving the quality of life. Nevertheless, they are also emerging as environmental pollutants that can adversely affect the aquatic environment and so have long-term consequences for human health (Zhou et al., 2020). They reach the natural environment in its development stage as raw materials, during the production, transportation and storage, as well as through domestic sewage, hospitals and industrial wastewater, livestock farming, and

solid-waste leachate, among other daily human activities (Rodriguez-Mozaz et al., 2020). The situation is worsened by their indiscriminate use (without medical planning) coupled with improper disposal (de Oliveira et al., 2020). Several classes of pharmaceuticals used in human medicine are only partially metabolized by the organism, and are excreted unaltered or in active forms. For example, more than 75% of the antibiotics from the tetracyclines family are excreted as active metabolites (Xu et al., 2021).

Numerous pharmaceuticals were already found in surface, ground and drinking water in concentrations from parts-per-trillion (ng/L) to

* Corresponding author.

E-mail address: belisa.alcantara.marinho@ijs.si (B.A. Marinho).

<https://doi.org/10.1016/j.jclepro.2022.131061>

Received 7 September 2021; Received in revised form 16 February 2022; Accepted 19 February 2022

Available online 23 February 2022

0959-6526/© 2022 The Authors.

Published by Elsevier Ltd.

This is an open access article under the CC BY-NC-ND license

(<http://creativecommons.org/licenses/by-nc-nd/4.0/>).

parts-per-billion ($\mu\text{g/L}$) (Yang et al., 2017). In Europe, the most frequently detected and quantified pharmaceuticals in environmental samples include three antibiotics (sulfamethoxazole, trimethoprim and clarithromycin), four analgesic anti-inflammatory drugs (diclofenac, ibuprofen, naproxen, paracetamol (acetaminophen) and ketoprofen) and two psychotropic drugs (carbamazepine and venlafaxine) (Fekadu et al., 2019).

Once pharmaceuticals or their by-products reach the environment, they can cause multiple adverse effects, such as aquatic toxicity, the growth of resistant and multi-resistance pathogenic bacteria, the transference of an antibiotic-resistant gene to a new generation of microorganisms (making them more resistant than before), genotoxicity, endocrine disorders and other harmful ecotoxicological effects (Jose et al., 2020).

There are still no specific laws or discharge limits for effluents containing pharmaceuticals. However, the Decision (EU) 2018/840 introduces a watch list of substances for EU-wide monitoring, which includes four pharmaceutical compounds/classes (17- α -ethinylestradiol, macrolide antibiotics, amoxicillin, ciprofloxacin) (European Commission, 2018). The Swiss Water Protection Act proposes evaluating the effectiveness of wastewater treatment in plants that have implemented advanced treatments with either ozone or activated carbon. This act lists 12 indicator substances that must be abated, on average, by 80% over the whole treatment plant. Among the 12 indicator substances, 10 of them are pharmaceuticals (amisulpride, carbamazepine, citalopram, clarithromycin, diclofenac, hydrochlorothiazide, metoprolol, venlafaxine, candesartan, irbesartan) (Joint Norman Water Europe Position Paper, 2019). Despite not specifying the monitoring of pharmaceuticals, the US Unregulated Contaminant Monitoring Rule (UCMR) and the Australian Drinking Water Guidelines (ADWG) list 30 chemical contaminants to be monitored and strategies for managing drinking-water systems, respectively (NHMRC, 2018; U.S.EPA, 2016).

Conventional water- and wastewater-treatment plants (WWTPs) were originally designed for the removal of suspended solids and biodegradable organic matter; as such they exhibit variable removal efficiencies (from 0 to 100%) for pharmaceuticals (Desbordes et al., 2018). For antibiotics, values of 4% for ofloxacin and 74% for amoxicillin removal were already reported (Yang et al., 2017). It is clear that conventional wastewater treatments fall short of the required efficiency. Several alternative technologies have been studied and applied to reduce the potential risk of pharmaceuticals to the environment and human health, including membrane filtration (Bhattacharya et al., 2020; Heo et al., 2019; Reddy et al., 2017), adsorption (Escudero-Curiel et al., 2021; Jaria et al., 2021; Jia et al., 2021; Liu et al., 2021), Fenton processes (Hong et al., 2020; Mitsika et al., 2021; Scaria et al., 2021; Talwar et al., 2021), ozonation (Kharel et al., 2020; Kim et al., 2020; Mathon et al., 2021; C. Wang et al., 2020), sulfate radical-based oxidation (Smaali et al., 2021; Telegang Chekem et al., 2020; Wang et al., 2020; Zhang et al., 2021), and ionizing radiation (Reinholds et al., 2017; Sági et al., 2018; Shen et al., 2019a, 2019b). However, an effective, safe, low-cost, high-technology-readiness-level (TRL) alternative, which could be a concrete option to be used together with a conventional treatment, still needs to be developed. The combination of an appropriate catalyst with an optimized reactor design allows the effective use of the catalyst active sites and should enhance the system efficiency along with economic advantages (Darvishi et al., 2016).

In this context, photocatalysis, electrocatalysis and photoelectrocatalysis with immobilized catalysts are promising technologies because of their environmental friendliness, easy operation, lack of sludge generation, high removal rate of emerging pollutants (>80%), effectiveness in disinfection and the possibility of solar-energy utilization (Espindola and Vilar, 2020). In fact, concerning the research on pharmaceuticals' degradation, these three technologies combined exhibit exponential growth and correspond to almost 20% of the published studies in the past 20 years (between 2000 and 2020), as shown in Fig. 1.

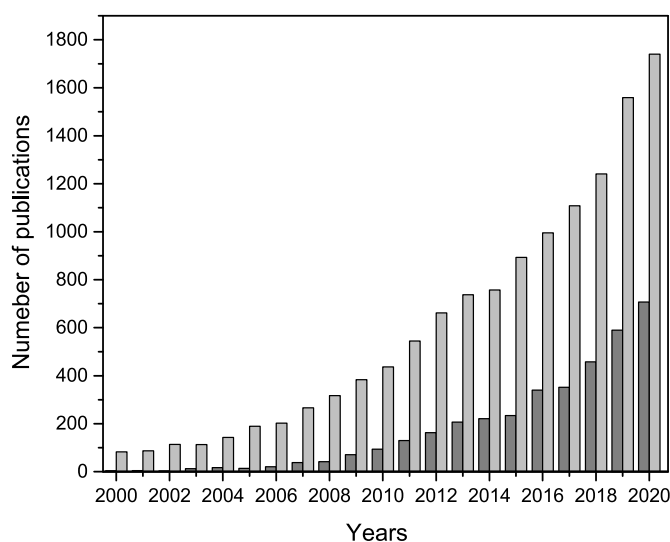


Fig. 1. Number of publications per year (2000–2020). Search terms: ■ “pharmaceutica* and (photocataly* or electrocataly* or photoelectrocataly*)”. Results: total of 3724 documents; ■ “pharmaceutica* and degradation”. Results: total of 12,572 documents. Source: Web of Science on August 2021.

Review articles focused on the treatment of water and wastewater contaminated with pharmaceuticals are generally: i) very specific, limited to a single treatment technique or contaminant (Abdurahman and Abdullah, 2020; Awofiranye et al., 2020; Mohapatra et al., 2014b; Prasannamedha and Kumar, 2020; Sodhi et al., 2021), or ii) very embracing, exploring several classes of treatment or compounds (Alharbi and Price, 2017; Bourgin et al., 2018; de Oliveira et al., 2020; Dhargar and Kumar, 2020; Espindola and Vilar, 2020; Kanakaraju et al., 2018). There is a lack of reviews that cover pharmaceuticals' degradation by photocatalytic, electrocatalytic, and photoelectrocatalytic processes. This review will critically review and compare the fundamentals, efficiencies and applicability potential of photocatalysis (PC), electrocatalysis (EC) and photoelectrocatalysis (PEC) in terms of the degradation of the pharmaceutical. Since Fenton and other Iron-based processes are already very well discussed and reviewed in other works (Brillas, 2020; Ismail et al., 2021; Moreira et al., 2017), in this review we will focus on the use of other catalysts, including TiO_2 , BDD and heterostructured materials. We present an overview of the analytical techniques necessary to follow the concentration of pharmaceuticals and by-products formed, along with the toxicity tests more appropriate to evaluate the final quality of the treated water. The catalysts commonly used and their characteristics, as well as the design of the reactors combined with different sources of radiation for batch and continuous treatment, are also discussed. The high efficiency on pharmaceuticals degradation is one of the main advantages of PC, EC and PEC processes. However, some drawbacks, including the low quantum efficiency of commercial catalysts and/or high energetic consumption, still difficult the application of these processes on larger scale. Some challenges and alternatives to overcome these limitations are emphasized in the prospects section.

2. Detection, quantification and toxicity evaluation of pharmaceuticals

During the degradation of pharmaceuticals, it is essential to monitor the specific compound's decay, its mineralization, the formation of by-products, and the toxicity of the final effluent. To understand the steps involved in the degradation process, it is desirable to evaluate the oxidative (OH^\bullet , $\text{O}_2^{\bullet-}$, HO_2^\bullet , $\text{SO}_5^{\bullet-}$) and reducing (e_{aq}^-) species formed during the catalytic reaction. Only an evaluation of all these parameters provides a complete view of the degradation process. Table 1 shows the

Table 1

Techniques most used to check the viability of a particular degradation process.

PERFORMANCE	BY-PRODUCTS IDENTIFICATION	REACTIVE SPECIES IDENTIFICATION	TOXICITY
<u>MINERALIZATION</u>	• HPLC	• FLUORESCENCE	• <i>Pseudokirchneriella subcapitata</i>
• TOC	• GC-MS	• QUENCHING	• <i>Vibrio fischeri</i>
<u>GENERAL ANALYSIS</u>	• LC-MS	• HPLC	• <i>Daphnia magna</i>
• UV-VIS	• IC	• EPR	
• COD			
<u>COMPOUNDS DECAY</u>			
• HPLC/GC			
• UV-VIS			
• ELECTROCHEMISTRY			

techniques most used to check the viability of a particular degradation process.

The decay kinetics of the initial pollutant is usually evaluated by high-performance liquid chromatography (HPLC) or gas chromatography (GC), noting that sample preparation for HPLC is usually easier than that for GC (Feier et al., 2018). Furthermore, the low volatility and/or poor thermal stability of some pharmaceuticals can limit the applicability of GC analysis (Brillas and Sirés, 2015). In fact, as shown in Table 2, liquid chromatography with separation through a reverse-phase C18 column is the primary method used to follow the decay of pharmaceuticals. Nevertheless, for specific compounds, including ampicillin, paracetamol and ciprofloxacin, alternative, simpler methods, such as electrochemical sensors (Raymundo-Pereira et al., 2017; Yang et al., 2017), Raman (He et al., 2010) and ultraviolet-visible spectroscopies (Gupta et al., 2021), can also be used. It is important to mention that for all techniques, depending on the pharmaceutical's initial concentration and the method's sensibility, pre-concentration of the samples might be required. Solid-phase extraction (SPE), liquid-liquid extraction (LLE), liquid-liquid micro-extraction (LLME) and solid-phase microextraction (SPME) are the most common sample-preparation techniques used for pharmaceutical monitoring (Feier et al., 2018).

Evaluating the decay of the total organic carbon (TOC), chemical oxygen demand (COD) and UV-vis spectra (200–300 nm) can also provide useful information about the mineralization, organics oxidation, and aromatic or unsaturated molecules' abatement, respectively (Brillas and Sirés, 2015).

A crucial task that concerns pharmaceuticals' degradation is the elucidation of the reaction mechanism, which can be achieved through the detection of intermediates and by-products, and the detection/determination of the reactive species that are formed (Brillas and Sirés, 2015; Zhang et al., 2021).

Cyclic and aromatic intermediates and low-molecular-weight carboxylic acids are usually detected by liquid chromatography with a variety of mass-spectrometry detectors (LC-MS, LC-MS-MS, LC-QTOF-MS, LC-QTOF-MS-MS, UPLC-MS, UPLC-MS-MS, etc.). Gaseous chromatography is an alternative for detecting small molecules containing -OH groups, because they can be derivatized. In this case, both polar and non-polar columns can be used for the separation of intermediates (Brillas and Sirés, 2015). Another strategy is determining low-molecular-weight carboxylic acids, formed through the successive oxidative cleavage of aromatic products, by ion-exclusion chromatography. In this case, a regular HPLC can be equipped with an appropriated column (Bio-rad Aminex HPX 87H column 300 mm × 7.8 mm (i.d.) or Phenomenex Rezex™ ROA-Organic Acid H+ (8%) 300 mm × 7.8 mm) and a simple 4 mM H₂SO₄ solution can be used as the mobile phase (Espíndola et al., 2019; Guinea et al., 2010). Finally, inorganic ions that can form (e.g., Cl⁻, SO₄²⁻, F⁻, NH₄⁺, NO₃⁻, etc.) can be accurately quantified by ionic chromatography, using appropriate anion/cation columns and a conductivity detector (Brillas and Sirés, 2015).

Concerning the identification, quantification and determination of the reactive species' contribution during the pharmaceuticals' removal by advanced oxidation processes (AOPs), the most common methods are electron paramagnetic resonance (EPR), HPLC and quenching

experiments, respectively (M. He et al., 2021). EPR is a technique capable of identifying molecules with one or more unpaired electrons, as radicals, providing an effective way to detect the reactive species formed during the catalytic processes. However, as the reactive species are very reactive and have a short lifetime (~μs), their direct detection is difficult. Thus, the EPR spin-trap method is based on the use of trap agents to derivatize the reactive species into longer-lifetime species, allowing their identification. The commonly employed trap agents are 5,5-Dimethyl-1-pyrroline N-oxide (DMPO) for OH[•], SO₄^{•-} and O₂^{•-}, and 2,2,6,6-Tetramethylpiperidine (TEMP) for singlet oxygen (¹O₂) (Wang et al., 2020). After the spin-adduct DMPO-OH[•] forms, the molecule's lifetime is increased to 55 min (He et al., 2021).

The principle of using HPLC to quantify the reactive species is also based on the strategy of generating stabilized intermediates through the reaction with trap agents. In this case, the preferable trap agents include benzoic acid, hydroxybenzoic acid, terephthalic acid and dimethyl sulfoxide (Wang and Wang, 2020). By correlating the concentration of the intermediates with the reactive species, it is possible to determine their concentration. Another approach to quantifying OH[•] radicals is to use the fluorescence-probe method, through the combination of a non-fluorescent probe with OH[•] radicals to form a stable adduct. Benzoic and terephthalic acids are examples of molecules that can scavenge OH[•] and form fluorescent compounds (Wang et al., 2020).

Quenching experiments can be used to determine the reactive species' contribution and indirectly identify the main species involved in the degradation process. It is fundamental to choose the appropriate scavenger agents to suppress the target reactions and thus allow an indirect identification of the reactive species. Furthermore, the scavenger concentration is also important and should be in large excess, with the molar ratio of the scavenger:reactive species being at least 500:1 (Wang and Wang, 2020). Some examples of reactive species and their usual scavenger agents include i) hydroxyl radicals: tertiary butanol, methanol, ethanol, n-butanol, isopropanol; ii) sulfate radicals: ethanol, methanol, 1-octanol; iii) superoxide radicals: benzoquinone, chloroform; iv) singlet oxygen: sodium azide; v) electron: potassium dichromate, silver nitrate; vi) electron-hole: EDTA, potassium iodine, ammonium oxalate (Diao et al., 2015; M. He et al., 2021; Wang and Wang, 2020; Wang et al., 2020).

Another fundamental study to evaluate the viability of a degradation process is the evolution of the solution's toxicity with time, or at least the toxicity of the final effluent (Brillas and Sirés, 2015). For this purpose, organisms from different trophic levels can be used, for instance, the crustacean *Daphnia magna*, the algae *Pseudokirchneriella subcapitata* and the bacteria *Vibrio fischeri*, which are the most used species for assessing the toxicity of pharmaceuticals (Desbiolles et al., 2018). Nonetheless, it is important to consider that different species could be more sensitive for acute or chronic exposure, according to the type of pharmaceutical. Thus, it is important to identify which organisms are the most relevant for specific pharmaceuticals. For anti-inflammatory drugs, such as ibuprofen and naproxen, crustaceans are reported to be the most sensitive organisms (Harada et al., 2008). Crustaceans are also reported to be sensitive to betablockers such as propranolol (Ferrari et al., 2004). While for antibiotics, like amoxicillin and clarithromycin,

Table 2
 HPCL operating conditions for monitoring pharmaceutical compounds during degradation processes for their removal.

Therapeutic class	Compound	Initial concentration and sample preparation	Degradation process	Analytical method/ Equipment	Operating conditions	LOD and LOQ	Ref.
Antibiotics	amoxicillin	10–30 mg L ⁻¹	Sonocatalysis/ electrolysis with magnesium oxide nanocatalyst	HPLC system coupled with a UV detector	Reversed-phase C18 column (250 × 4.6 mm, 5 μm); mobile phase of 40:60 methanol: phosphate buffer (pH 4.5) with flow rate of 1 mL/min; the detection wavelength was 254 nm	–	Darvishi Cheshmeh Soltani et al. (2018)
	azithromycin	20 mg L ⁻¹ ; Centrifugation to remove the photocatalyst	Photocatalysis with ZrO ₂ /Ag@TiO ₂ nanocomposite	HPLC system coupled with a UV detector (HPLC-UV)	Reversed-phase C18 column (150 × 4.6 mm, 5 μm); mobile phase of 0.1% of formic acid solutions in acetonitrile and water with flow rate of 0.8 mL/min in gradient mode; the detection wavelength was 274 nm	–	Naraginti et al. (2019)
	ciprofloxacin	~35 mg L ⁻¹	Fenton-like system	HPLC system coupled with a UV detector (HPLC-UV)	Reversed-phase C18 column (150 × 4.6 mm, 5 μm); mobile phase of water (containing 0.1% formic acid) and acetonitrile with flow rate of 0.5 mL/min at 30 °C; injection volume of 20 μL and detection wavelength at 278 nm	–	Diao et al. (2017)
	norfloxacin	20 mg L ⁻¹	Iron based reactions	HPLC system coupled with a UV detector (HPLC-UV)	Reversed-phase C18 column (150 × 4.6 mm, 5 μm); mobile phase of water (containing 0.1% formic acid) and acetonitrile with volume ratio 73:27 and flow rate of 0.8 mL/min at 30 °C; injection volume of 20 μL and detection wavelength at 278 nm	–	(J. J. Liu et al., 2018)
	oxytetracycline	20 mg L ⁻¹ ; Filtration with 0.45 μm nylon membrane filter	Photocatalysis with TiO ₂	HPLC equipped with a diode array detector (HPLC-DAD)	Reversed-phase C18 column (125 × 4 mm, 5 μm); mobile phase of mixture of acetonitrile/methanol/0.014 M oxalic acid in gradient mode; injection volume of 50 μL and flow rate of 0.8 mL/min. Retention time of 5.8 min the DAD detector was set at 354 nm	0.3 and 1.2 mg L ⁻¹ , respectively	Espindola et al. (2019)
Anti-cancer drugs	Anastrozole	50–500 mg L ⁻¹ ; Filtration with 0.22 μm PVDF membrane filter	Photo-Fenton	LC system coupled to QTOF mass spectrometer (LC-QTOF MS)	Reversed-phase C18 column (150 × 2.1 mm, 3 μm); mobile phase of acetonitrile and ultrapure water acidified with 0.1% formic acid at a flow rate of 0.5 mL/min; gradient mode; injection volume of 10 μL and retention time of 18.5 min. Detection with QTOF MS operated in positive ionization mode, with the following conditions: capillary at 4000 V, nebulizer at 4 bar, drying gas at 8 L min ⁻¹ , and gas temperature at 200 °C. Broadband collision-induced dissociation acquisition of 25 and 50 eV. MS information obtained in scan mode, in the m/z range 50–1200	–	Sanabria et al. (2021)
Psychotropic drugs	carbamazepine	Filtration with 0.45 μm membrane filter	UV/chlorine	LC coupled with triple quadrupole mass spectrometer (LC-MS-MS)	Reversed-phase C18 column (250 × 4.6 mm, 5 μm); mobile phase of aqueous and methanolic 5 mM ammonium acetate solutions at a flow rate of 0.6 mL/min; gradient mode; retention time of 18.5 min. Detection with the following settings for the ion source and mass spectrometer: curtain gas 25 psi, spraying gas 65 psi, drying gas 45 psi, temperature of 650 °C, collision gas value 7	LOQ of 10 ng L ⁻¹	(Seitz et al., 2006; Sichel et al., 2011)

(continued on next page)

Table 2 (continued)

Therapeutic class	Compound	Initial concentration and sample preparation	Degradation process	Analytical method/ Equipment	Operating conditions	LOD and LOQ	Ref.
	diazepam	10 mg L ⁻¹	Photo-Fenton	UPLC system coupled with a diode array detector (UPLC-DAD)	(range 1–12), and an ion spray voltage of 4500 V Reversed-phase C18 column (100 × 2.1 mm, 1.7 μm); mobile phase of aqueous and methanolic formic acid solutions (0.3% v/v) at a flow rate of 0.3 mL/min; gradient mode; retention time of 16.5 min. Injection volume of 20 μL and the analytical column was thermostated at 40 °C	–	Mitsika et al. (2021)
Analgesic anti-inflammatory drugs	diclofenac	5 mg L ⁻¹ ; Filtration with 0.23 μm membrane filter	Photoelectrocatalysis with TiO ₂ nanotube	HPLC system coupled with a UV detector (HPLC-UV)	Reversed-phase C18 column (250 × 4.6 mm, 5 μm); mobile phase of 75% of methanol and 25% of acetic acid aqueous solution (1%) at a flow rate of 1 mL/min; injection volume of 10 μL and detection at 276 nm	–	Cheng et al. (2016)
Beta-blockers	propranolol	Filtration with 0.45 μm membrane filter	Photocatalysis with TiO ₂ /ONLH	HPLC system coupled with a diode array detector (HPLC-DAD)	Reversed-phase C18 column (250 × 2.1 mm, 1.7 μm); mobile phase of 65% of water acidified phosphoric acid (pH = 3) and 35% acetonitrile at a flow rate of 1 mL/min; retention time of 16.5 min. Injection volume of 20 μL and detection at 213 nm	0.02 and 0.05 mg L ⁻¹ , respectively	(Q. Zhang et al., 2021)

growth inhibition on algae has shown high sensitivity (Andreozzi et al., 2004; Yamashita et al., 2006). Lastly, the determination of biological oxygen demand after a 5-day incubation (BOD5) is also useful for indicating effluent biodegradability (Brillas and Sirés, 2015).

Despite all the advances and possibilities with these analytical techniques, there is still a lack of studies that properly relate and discuss the effect of the by-products' formation with the radicals formed during the reaction and the toxicity of the final effluent. Many reported studies identify the by-products and even the radicals formed, but fail to properly evaluate the toxicity of the final effluent. The opposite is also common. Studies with a global evaluation, which take advantage of the analytical technology available, are fundamental in supporting real applications and ensuring the security of these treatment technologies.

3. Photocatalysis, electrocatalysis and photoelectrocatalysis

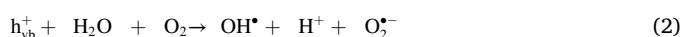
3.1. Photocatalysis

3.1.1. Fundamentals

Heterogeneous photocatalysis is an effective and promising technology based on the photo-activation of semiconductors (photocatalysts) such as TiO₂, ZnO, CeO₂, ZrO₂, WO₃, V₂O₅, CdS and ZnS, which act as active catalytic surfaces for the degradation and mineralization of persistent organic pollutants, including pharmaceuticals and their possible intermediate products in aqueous media (Bergamonti et al., 2019; Chaker et al., 2020). Among the cited semiconductors, TiO₂ is the most commonly used in photocatalysis (PC), since it has several advantages, such as chemical stability, resistance to acids and alkalis, large production, ability to use a small percentage of ultraviolet solar radiation for activation, possibility to be easily synthesized in laboratories as both colloidal dispersions and thin films deposited on inert supports (Antonopoulou et al., 2021). Recently, new metal-free photocatalysts, as the graphitic carbon nitride (g-C₃N₄), have been identified as favorable photocatalysts for environmental application on water and wastewater treatment. g-C₃N₄ presents good photochemical stability and appropriate bandgap energy (2.7 eV). However, it also presents the low-charge carrier mobility and low surface area, which limits its applications in PC (Ismael, 2020). To overcome these limitations, and

improve the charge separation, the majority of the works regarding g-C₃N₄ applications on PC take use of the synthesis of heterojunction composites, by coupling g-C₃N₄ with a large bandgap semiconductor. This approach for g-C₃N₄ and other photocatalysts modification is discussed in section "4.3. Heterostructured Materials".

In the degradation of pharmaceuticals, photocatalytic oxidation is the primary process. It is based on the non-selective production of highly reactive species, starting with the generation of electron (e_{cb}⁻) and hole (h_{vb}⁺) pairs (Eq. (1)), after the semiconductor absorbs a photon with equal (or higher) energy than the band gap (Fig. 3) (Mehrabadi and Faghihian, 2018). In the sequence, successive reactions can occur with the oxidizing holes and both the organic contaminants and the water/hydroxyl anion (Eqs. (2) and (3)), forming smaller fragments of the pollutants and the OH[•] radical, respectively (Marinho et al., 2019). When using semiconductors with a conduction band redox potential below that of O₂, the dissolved oxygen can act as an electron acceptor, forming superoxide radicals (O₂^{-•}, HO₂[•]) or other reactive species (Eqs. (4)–(8)) (Antonopoulou et al., 2021; Wang and Zhuan, 2020). The oxidation of pharmaceuticals can occur through a reaction with reactive oxygen radicals or by a direct reaction with the photohole (Eqs. (9) and (10)), eventually converting them to H₂O and CO₂ (Awfa et al., 2018; Mehrabadi and Faghihian, 2018). Fig. 2 shows a schematic representation of these reactions and the process flow diagram of PC.



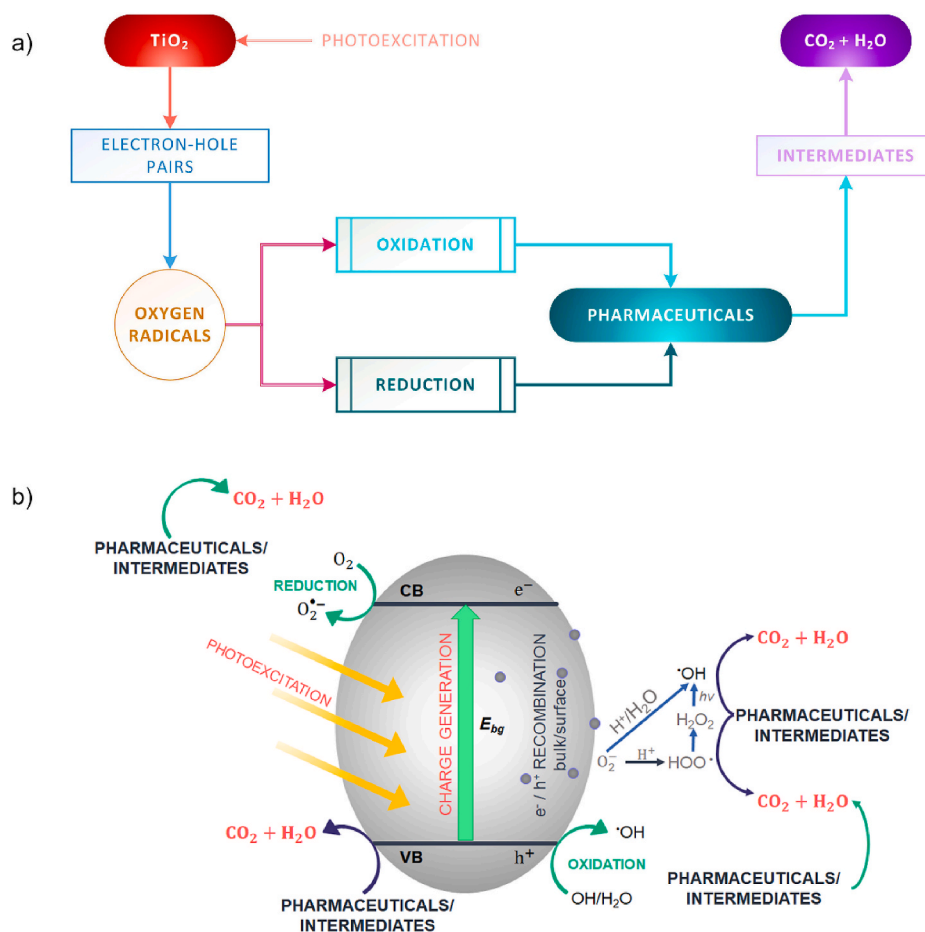
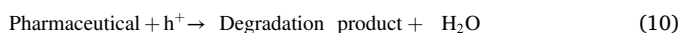


Fig. 2. Schematic of the photocatalysis process: a) process flow diagram; b) schematic representation PC reactions. Adapted from (Marinho et al., 2021) and (Cheng et al., 2016).



3.1.2. Affecting parameters

To scale up the photocatalytic process, it is important that visible light is used and absorbed by the photocatalyst. A crucial characteristic of the material is its band gap, which denotes the energy needed to promote an electron from the valence band to the conduction band. TiO_2 , the most widely used photocatalyst, has a band gap corresponding to UV light (~ 3.2 eV) (J. Zhang et al., 2021), which represents only 5% of the incident solar (Islam et al., 2021). Several strategies, which will be discussed later, have been proposed and tested to improve the performance of TiO_2 under visible light: doping, co-doping, the use of co-catalysts, the exploitation of defects and using different semi-conductors (Z-scheme).

The process efficiency is also controlled by several parameters, including the loading, particle size and surface area of the photocatalyst, the initial concentration of the contaminant, the type and intensity of the irradiation, the presence or absence of oxygen, the pH and the temperature (Attia and Mohamed, 2019; Bergamonti et al., 2019). Regarding the process kinetics, it is agreed that both the reaction constants and orders are apparent and that the heterogeneous photocatalysis usually follows a pseudo-first-order kinetics (Marinho et al., 2019). The kinetic studies are useful to understand the reaction mechanism and to the development of the reaction network, which is the first

step for simulation and design of commercial reactors. Furthermore, the reactions can be modeled using a reaction network and the kinetic parameters for each reaction can be obtained after the algorithm optimization with experimental data (Vafajoo et al., 2014).

The number of reactive sites driving the photocatalytic reactions is related to the particle size and the surface area: as the particle size is reduced and the surface area is increased, the photocatalytic efficiency is improved due to a more favorable area/size ratio, which justifies the use of nanocatalysts (Bergamonti et al., 2019). Another parameter that affects the number of reactive sites is the loading: as the concentration of the photocatalyst is increased, the reaction rate is also improved, up to a limit. For pharmaceuticals' degradation in slurry conditions, the optimum catalyst loading is usually between 250 mg L^{-1} (Achilleos et al., 2010) and 1000 mg L^{-1} (Marinho et al., 2017), depending on the reactor design and the working conditions. Higher catalyst loadings typically yield no additional efficiency gain or cause a decrease in efficiency since the excess catalyst (bulk) can block the photons from penetrating and/or cause shielding, reflection and scattering of light (Wang and Zhuan, 2020). In systems with supported photocatalysts, the increase of the loading is usually linked to the catalyst's film thickness. Thus, the enhancement of efficiency is limited to the point where the light is completely absorbed by the catalyst layer. Any further increase in the catalyst loading will not affect the process efficiency, since the diffusional length of the charge carrier to the catalyst-liquid interface remains constant (Marinho et al., 2017).

The intensity of the light and the photon flux are intimately related to the reactor geometry. For instance, with an increase in the number of photons that reaches the reactor, the photogeneration of the reactive species is usually increased. Nevertheless, after a limiting photon flux,

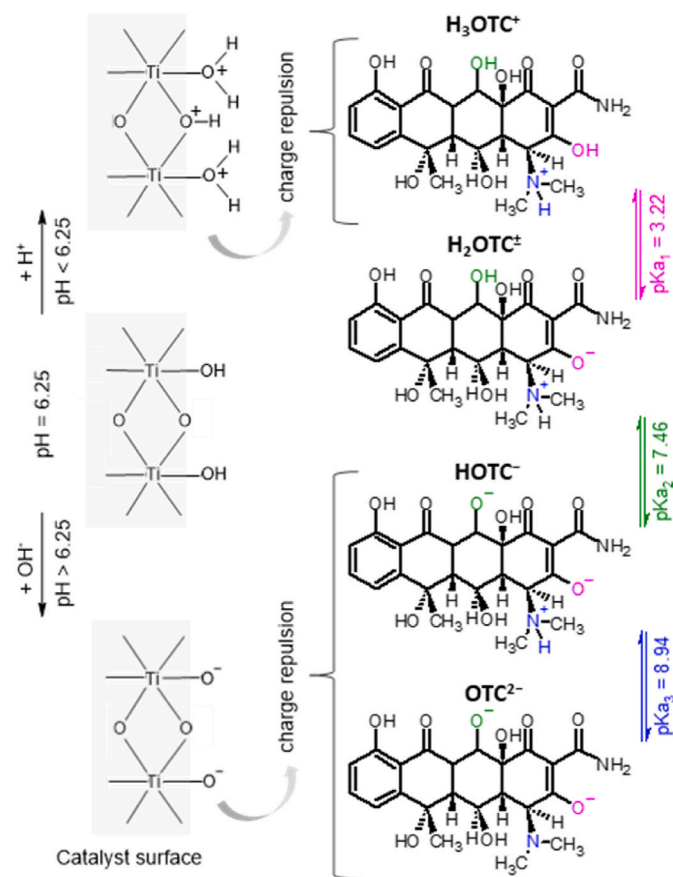


Fig. 3. Schematic of protonation/deprotonation of the TiO_2 surface and oxytetracycline molecule. Adapted from (Pereira et al., 2013) and (Bera-nek, 2011).

the photogenerated species will remain in excess and a high rate of e_{cb}^-/ h_{vb}^+ pairs' recombination will be observed. As a consequence, the reaction rate becomes constant even with the increased availability of photons (Marinho et al., 2019).

The pH of the solution is a crucial property of the aqueous system in heterogeneous photocatalysis, since the pH affects the semiconductor particles' charge as well as the protonation/deprotonation of the pharmaceuticals. When the pH of the solution is lower or higher than the pH of the zero point charge (pH_{zpc}), i.e., the pH where the photocatalyst surface is uncharged, the catalyst is positively or negatively charged, respectively (Fig. 3) (Marinho et al., 2021). Similarly, at pH values below or above the pK_a of the substrates, species with different charges are formed, which can facilitate or impede the reaction with the catalyst's surface (Wang and Zhuan, 2020). Fig. 3 highlights this behavior for oxytetracycline, which has three acidic hydrogens ($\text{pK}_{a1} = 3.22$, $\text{pK}_{a2} = 7.46$, $\text{pK}_{a3} = 8.94$) and can exist in four different forms (H_3OTC^+ , H_2OTC^\pm , HOTC^- , OTC^{2-}), depending on the pH of the solution. The H_3OTC^+ species is dominant under more acidic conditions and is electrostatically repelled by the positively charged TiO_2 surface. Similarly, under basic conditions, the dominant HOTC^- and OTC^{2-} species at equilibrium will be repelled from the negatively charged TiO_2 surface. Close to neutral pH values, the zwitterion H_2OTC^\pm species are dominant and can interact with the positive, negative and neutral TiO_2 surfaces, facilitating the oxidation process (Espíndola et al., 2019).

One of the main advantages of heterogenous photocatalysis is the possibility of working at room temperature. Since the irradiation activates the photocatalyst, it is not necessary to heat the system. It has been reported that the optimum temperature range is 20–80 °C; at lower temperatures, the adsorption of reactants can block the photocatalyst

surface, while at higher temperatures, the concentration of dissolved oxygen is diminished. Temperatures near the boiling point of water are also rate-limiting due to the increase of kinetic energy in the system, which hinders the reactions on the photocatalyst surface (Malato et al., 2016).

The stability of the catalyst, which is related to its capability of being reused, is an important aspect for industrial or commercial applications. Despite the existence of commercial catalysts with excellent photocatalytic efficiency, full-scale, heterogeneous, photocatalysis systems are still rare due to the aggregation during the operation and difficult recovery and reuse after the process. This also poses an environmental problem since the quality of the treated effluent might be compromised by the catalyst release (Linley et al., 2014; Paredes et al., 2019; Valério et al., 2020). In addition, commercial photocatalysts often have other shortcomings, such as a high rate of recombining electrons and holes as well as low efficiency for removing contaminants at low concentrations (Kim and Kan, 2016). To solve these problems, various techniques have been proposed to increase the process efficiency, including immobilization on appropriate supports, which facilitate the photocatalyst's recovery and reduce the costs of treatment. In addition, it can also contribute to minimizing the e_{cb}^-/ h_{vb}^+ pairs' recombination and enhance the activity of the photocatalyst in the UV–vis range (Savun-Hekimoğlu et al., 2020). Nevertheless, due to there being less active surface available, a reduction in the efficiency can occur when supported photocatalysts are used. As a result, the selection of appropriate support material is of fundamental importance for the fabrication of this type of photocatalysts (Paredes et al., 2019). The supports can be: i) a mechanically and chemically stable material, such as glass, alumina or stainless steel (Jayasree and Remya, 2020; Paredes et al., 2019); ii) an active support, such as activated carbon, biochar, zeolites, polymer beads, membranes, or magnetic nanoparticles (Behravesht et al., 2020; Bergamonti et al., 2019; Linley et al., 2014; C. M. Liu et al., 2018); or iii) floating supports, such as perlite and low-density polyethylene (Hartley et al., 2017). Various methods have been applied to immobilize the photocatalysts, including sol-gel processes, chemical vapor deposition, dip-coating, electron-beam evaporation, and sputtering (Katal et al., 2021). Consecutive cycles with immobilized catalysts are fundamental to evaluate the adhesion of the catalyst on the support and the potential reusability of the material, since the catalyst can leach from the support or can be poisoned by the sub-products generated during the reaction (Diao et al., 2020). Table 3 shows different support materials, immobilization methods and photocatalysts applied for the photocatalytic treatment of pharmaceuticals, as well as the evaluated reusability/durability.

Electrical energy is a significant fraction of the operating costs for heterogeneous photocatalysis. Its consumption is influenced by several experimental parameters, such as the type and concentration of the pollutant, the photocatalyst dosage, the reactor design, and the radiation source. For the removal of pharmaceuticals by photocatalysis, the Electrical Energy per Order (EEO) ranges from 25 to 13,000 kWh m^{-3} and indicates the amount of electrical energy (in kWh) necessary to degrade a pollutant by one order of magnitude per cubic meter of contaminated water (Durán et al., 2018). Note that the type of the irradiation source influences this value. For systems that use UVA lamps almost three times more electrical energy is required than for those that utilize UVC radiation. Nevertheless, natural solar UVA radiation can be an alternative that contributes substantially towards decreasing energy costs (Babić et al., 2015). In addition, the feasibility of the process at neutral pH is one of the major advantages of heterogeneous photocatalysis (Antonopoulou et al., 2021). After the optimization of the operating conditions, the values of the EEO can be significantly decreased (Durán et al., 2018). Nevertheless, few studies of the degradation of pharmaceuticals by photocatalysis evaluate the energetic consumption, and even fewer estimate the costs of the whole process. Since it is very difficult to compare studies with different photocatalysts,

Table 3
Supported photocatalysts for pharmaceuticals' degradation and reusability.

Pharmaceutical	Support	Photocatalyst	Immobilization method	Number of reuse cycles/hours of continuous use ^a	Removal of the starting compound	Ref.
Amoxicillin	Chitosan scaffolds	TiO ₂ P25	3D printing	3 cycles	From ~90 to ~80% in 180 min, after 3 cycles	Bergamonti et al. (2019)
Ibuprofen	Raschig rings	TiO ₂ anatase	Immersion in TiO ₂ -containing ink for 5 min and heating at 650 °C for 30 min	6 h	Unchanged 87%, after 6 h of continuous treatment	Cerrato et al. (2019)
Oxytetracycline	Kenics static mixer	Fe ₂ O ₃	Spray coating	3 cycles	The kinetic constant remained almost unchanged ($85 \times 10^{-3} \text{ min}^{-1}$), after 3 cycles	Dfez et al. (2018)
Tetracycline	Floating hollow acrylic spheres	TiO ₂ P25	Dip coating	35 days	The kinetic constant changed from 1.88×10^{-3} to $1.82 \times 10^{-3} \text{ min}^{-1}$, after 35 days of solar light exposition while floating in water	Hartley et al. (2017)
Oxytetracycline	Glass	TiO ₂ P25	Spray coating	4 cycles	The kinetic constant changed from 44×10^{-3} to $39 \times 10^{-3} \text{ min}^{-1}$, after 5 cycles	Espindola et al. (2019)
Paracetamol	Aluminosilicate	TiO ₂ (from titanium isopropoxide)	Sol-gel	3 cycles	From 99 to 94% in 30 min, after 3 cycles	Jayasree and Remya (2020)
Metronidazole	Chitosan (CS) and polyvinyl alcohol/chitosan blend (PVA-CS)	TiO ₂ P25	Sol-gel	15 cycles	98% using CS and 100% using PVA-CS in 90 min, after 15 cycles	Neghi et al. (2019)
Chlorhexidine digluconate	Alginate	TiO ₂ P25	Entrapping	5 cycles	From 99 to 85%, after 5 cycles	Sarkar et al. (2015)
Guaifenesin	Fumed silica	Catalyst residue from petrochemical plant containing Ti (2.5%)	Sol-gel	5 cycles	From 49 to 45% in 60 min, after 5 cycles	da Silva et al. (2015)
Tetracycline	Floating expanded perlite	z-scheme composite FeMo ₃ O _x /g-C ₃ N ₄	Dip-calcination method	5 cycles	From 98 to 85%, after 5 cycles	Liu et al. (2022)
Sulfamethoxazole	Biochar	TiO ₂ doped with zinc elements (Zn-TiO ₂ /pBC)	Sol-gel	5 cycles	From 81 to 77%, after 5 cycles	Xie et al. (2019)
Cefoperazone	Zeolite	CdS/g-C ₃ N ₄	Co-precipitation	3 cycles	From ~95 to ~80%, after 3 cycles	AttariKhasraghi et al. (2021)

^a Without significant efficiency lost.

reactor designs and sources of radiation, a cost analysis would be useful to enable this comparison and stimulate the implementation of this technology in real applications.

3.1.3. Degradation mechanisms - first-principles calculations

Electrons can be excited to any of the unoccupied energy states. However, in conventional photocatalysis, all the transitions from a

higher to the lowest excited state are considered fast and do not contribute significantly to the reaction rate (Fig. 4). This means that the molecules will spend most of their excited lifetime in the lowest excited state. This simplifies the catalyst design and reaction modeling considerably, necessitating that only the first excited states are considered when modeling reaction mechanism and molecule properties using density functional theory (DFT). Proposed by Michael Kasha in 1950,

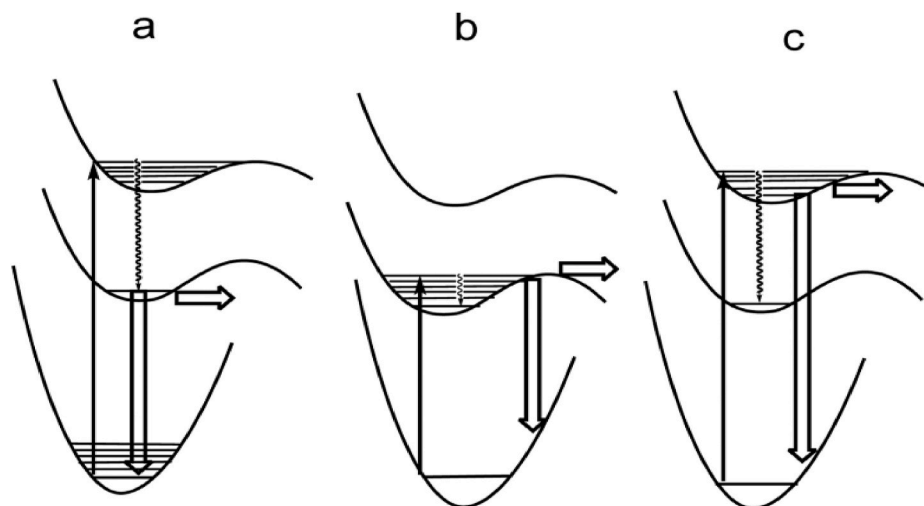


Fig. 4. Electronic states in reactions proceeding from (a) first excited state, (b) higher vibrational levels of the first excited state and (c) higher excited states. According to the Kasha rule, the contribution of (c) is negligible. Adapted from (Turro et al., 1978).

the eponymous rule, postulated with respect to emission and absorption spectra (Kasha, 1950), has only recently been circumvented, paving the way to the anti-Kasha approach (Demchenko et al., 2017; Shi et al., 2020).

While there is a vast body of research on the photo(electro)chemical degradation of pharmaceuticals, most focus either on the development of catalysts and associated techniques or on the performance. First-principles calculations, which can shed additional light on the processes by explaining the reaction steps and/or the catalyst structure, are rarely used. In degradation studies, DFT is generally employed in a supplementary fashion to calculate the band gap of the catalyst material, the Fukui function, work functions, or similar (Zhuangzhuang Wang et al., 2021). For the studies of photoactive catalytic materials, the band structure, densities of state and the electronic location function (ELF) are often calculated (Ding et al., 2019). Proper mechanistic studies are very rare. A common reaction pathway is the attack of the hydroxyl radical, which is formed upon irradiation in aqueous media. A typical reaction scheme involves decarboxylation, oxidation (dehydrogenation), C–C bond cleavage and addition to aromatic rings, as shown in Fig. 5.

The most often calculated Fukui functions are popular tools to predict the regioselectivity of the reactions with radicals (Li et al., 2021). The Fukui function ($f(r)$) is defined as a derivative of the electron density function with respect to a change in the number of electrons:

$$f(r) = \left[\frac{\partial \mu}{\partial v(\mathbf{r})} \right]_N = \left[\frac{\partial \rho(\mathbf{r})}{\partial N} \right]_v$$

where μ is the electronic chemical potential, $\rho(\mathbf{r})$ is the electron density at \mathbf{r} , N is the number of electrons and v is the constant external potential. The first equality gives the formal definition of the Fukui function (Fukui, 2006). As it is an exact differential, this definition lends itself to be rewritten as the second equality following the Maxwell relations between derivatives. Two finite versions, corresponding to the addition or removal of one electron, are most easily calculated and describe the susceptibility of a particular site to nucleophilic or electrophilic attack. The electronic band structure is commonly calculated as it gives the band gap value and other useful information stemming from the arrangement of the energy levels that the electrons can occupy. The band gap, being the difference between the valence and conduction bands, is intimately connected to the photo-activity of the material. Only photons with an energy greater than the band gap can be absorbed. The work function is sometimes calculated. It describes the work required to remove an electron from a solid material to a point adjacent to the surface.

Very few studies try to computationally elucidate the reaction

mechanism of the photodegradation of pharmaceuticals. Even those that attempt this, often fail to include the effect of irradiation or excited sites instead of simulating the process after the OH^\bullet has been formed. Wang et al. (2021b) studied the photochemical degradation of ibuprofen (IBP) with experiments and DFT. However, the authors performed conventional thermocatalytic DFT calculations at the B3LYP-D3/6-31G(d,p) level with the integral equation formalism version of the polarizable continuum model (IEFPCM) solvation and did not model the photocatalytic effects explicitly. Instead, they assumed that OH^\bullet and NO_2^\bullet form and then modeled their reactions with IBP. They showed that OH^\bullet plays a crucial role in the process, calculating the second-order kinetic constant for IBP degradation with OH^\bullet as $3.93 \times 10^6 \text{ m}^3 \text{ mol}^{-1} \text{ s}^{-1}$ using the transition state theory. NO_2^\bullet was found to be a potent inhibitor, as its addition lowered the overall reaction rate. The second-order kinetic constant for the reaction with NO_2^\bullet was found to be $5.59 \times 10^{-6} \text{ m}^3 \text{ mol}^{-1} \text{ s}^{-1}$. The reactivity of $\text{O}_2^{\bullet-}$ was smaller than that of OH^\bullet .

One of very few fully mechanistic studies was focused on the oxidation of phenazopyridine (PhP) over iron(III) oxyhydroxide structures in a $\text{O}_3^+/\text{PTNL}/\text{N}_2$ process. Using the M062X/6-31 + G(d) DFT approach, Pelalak et al. (2021) proposed a full reaction mechanism to support their experimental data. They calculated the Fukui functions for a radical attack on PhP and showed the most reactive site in the molecule, the intermediates and transition states for an OH^\bullet -mediated degradation, ultimately causing the breakup of the azo bond. The activation barrier for the initial attack is 28 kcal mol^{-1} . A frontier molecular orbital (FMO) analysis of different intermediate structures and transition states of PhP and OH^\bullet confirmed that the azo nitrogen is the most susceptible to attack. Lastly, other chemical parameters of the structures were calculated: global hardness, ionization potential and electron affinity (EA), and electrophilicity index.

A complex mechanistic study of carbamazepine (CBZ) degradation using a biosource composite by El Mouchtari et al. (2021) featured DFT calculations heavily. At the B3LYP/6-31G (d,p) level with the conductor-like polarizable continuum model (CPCM), the authors calculated the structures of the CBZ and all the intermediates/products in a OH^\bullet -mediated degradation. The Fukui functions were also calculated. A comprehensive study of pindolol (PIN) photodegradation by Armaković et al. (2020) also relied heavily on theory. After identifying all the possible conformers of PIN at a force-field level (OPLS3e) and optimizing them at a B3LYP level, the bond-dissociation energies (BDEs) of the cleavage of single acyclic bonds and hydrogen abstraction were calculated using the LACV3P basis set. As PIN has a HOMO-LUMO gap of 5.2 eV, which is indicative of a stable molecule, the molecular electrostatic potential (MEP) and the average local ionization energy (ALIE)

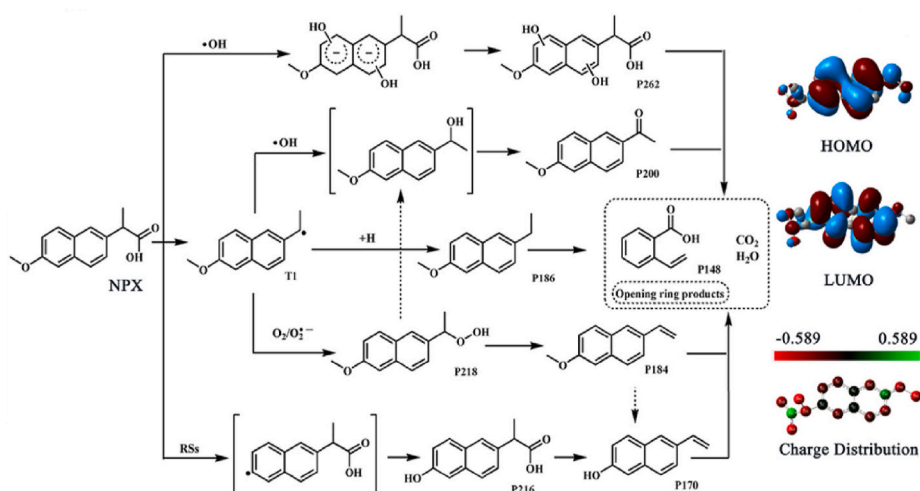


Fig. 5. A degradation pathway of naproxen (NPX) by crystalline carbon nitride (CCN) upon irradiation. Reprinted from Wang et al., 2020. Copyright© (2020), with permission from Elsevier.

were used as proxies to estimate the most susceptible part of the molecule to an attack. High values for H-BDE show that the molecule does not readily undergo auto-oxidation. Instead, cleavage of the C–O bond is the most probable site of attack. Molecular dynamic simulations showed that the molecule is stable in aqueous solutions. For an insight into the photodegradation route, the Fukui functions were calculated.

Gurkan et al. (2012) used DFT to predict the degradation pathway of cefazolin over N-doped TiO₂ under UV and visible light. Assuming that the OH[•] is formed under the irradiation conditions, they calculated the reaction network for the interaction of cefazolin with OH[•] at the B3LYP/6-31G* level. Additionally, reactivity parameters such as the global hardness and the Fukui function were obtained. Being a β-lactam antibiotic, cefazolin was predicted to degrade via the intramolecular β-lactam, thiadiazole, tetrazole and dihydrothiazin ring cleavages, which further on react with the OH[•].

Wang et al. (2020e) studied the photodegradation of pharmaceuticals and personal-care products (PRCP) on bulk and crystalline carbon nitrides (BCNs and CCNs, respectively) and showed that the crystalline structure is more effective. Theoretical calculations at the PBE level were used to underpin the experiments. The authors focused on the mechanism of active-species generation, i.e., the oxygen-reduction reaction (ORR) pathway. They calculated the reaction energies on BCNs and CCNs for the adsorption of O₂ (−0.10 and −0.44 eV), the transformation to OOH (−0.31 eV and −0.73 eV) and the formation of H₂O₂ (+0.01 eV and +0.50 eV). The reaction is much more exothermic on CCNs. A projected density-of-state analysis of the adsorbed HO₂[•] was used to show that a BCN is a poorer electron acceptor, while O₂ is crucial to the degradation process.

Tang et al. (2017) investigated the mechanism for the photocatalytic degradation of carbamazepine (CBZ) on BiVO₄ with graphene quantum dots. The calculations were performed at the B3LYP/6-31 + G(d,p) level with water as the solvent. The active species was modeled as OH[•]. The calculations of its reaction with CBZ showed that it preferentially attacks the heterocyclic (azepine) ring rather than the aromatic ring.

TiO₂–SnS₂ was evaluated as a photocatalyst for the degradation of a polar and non-polar pharmaceutical compound: diclofenac (DCF) and memantine (MEM) (Kovacic et al., 2020). The SnS₂ decoration on the TiO₂ lowered the band gap and improved the photo-oxidation of the DCF, while the MEM remained stable. Theoretical calculations performed on a 4 × 4 supercell of a SnS₂ monolayer showed that the DCF adsorbs about three times more strongly than the MEM because of the interaction of the π-electrons of the DCF's phenyl group and the negatively charged S surface atoms. The MEM binds solely through the amine group. The solvation effect was checked on a Sn₃₆S₇₂ finite section using a continuum water model and found to be < 1 kcal mol^{−1}.

3.1.3.1. Fukui-function calculations. In many studies, first-principles calculations are employed solely to provide the Fukui functions or other similar descriptors, which are used to postulate a probable reaction mechanism. Huang et al. (2021) studied the photocatalytic degradation of amoxicillin (AMX) on carbon-rich g-C₃N₄. They used DFT to calculate the natural population analysis (NPA) charge distribution and the Fukui functions of AMX, which were then used to postulate the degradation pathway. The Fukui functions were calculated for the photocatalytic degradation of diclofenac (DCF) on quantum-dots-modified g-C₃N₄ (W. Liu et al., 2019), for amoxicillin and cefotaxime degradation under visible light over g-C₃N₄ (Dou et al., 2020), for carbamazepine photodegradation over g-C₃N₄ (Zhao et al., 2020) and for meropenem degradation over g-C₃N₄ nanosheets with nitrogen defects (Wang et al., 2020).

F. Liu et al. (2019) investigated the photocatalytic removal of diclofenac using a Ti-doped BiOI microsphere. They established that h⁺, O₂^{•−} and H₂O₂ play crucial roles in the reaction. The Fukui functions were also calculated in a study of naproxen degradation over a Bi₂MoO₆/g-C₃N₄ heterojunction under visible light (Fu et al., 2021),

diclofenac degradation over activated carbon-fiber-supported titanate nanotubes (Dang et al., 2020), and for the photodegradation of ofloxacin by perovskite-type NaNbO₃ nanorods modified g-C₃N₄ heterojunction (D. Zhang et al., 2020). X. Liu et al. (2019) showed that graphene modifications of anatase/titanate nanosheets improve their photocatalytic activity in the photodegradation of sulfamethazine using the Fukui functions.

3.1.3.2. Other electronic properties. When Yin et al. (2020) showed that peroxymonosulfate enhances the photocatalytic ability of Pd/g-C₃N₄ in bezafibrate degradation, the DFT calculations were used to ascribe the electron transfer to the chemical bond between the Pd and the g-C₃N₄. In the plane-wave approach, the electronic band structure, density of state, electronic location function and charge-difference function were calculated for g-C₃N₄ and Pd/g-C₃N₄.

Regmi et al. (2019a) showed that phosphate-doped BiVO₄ is an effective photocatalyst for degrading IBP and *p*-amino salicylic acid. They used DFT (in the PBE + U approach) to calculate the density of states of the catalyst, the band gap (2.11 eV vs. experimental 2.4 eV), the charge-density difference and the bond lengths. They showed that phosphate doping increases the electron density of states in the valence band, improves the carrier mobility and thus enhances the photocatalytic efficiency. They also studied the N-doped catalyst. The presence of nitrogen in the catalyst led to an increase in ibuprofen degradation from 71 (undoped catalyst) to 90% in 150 min (Regmi et al., 2019b).

Z. Yang et al. (2021) used DFT to elucidate the photocatalytic degradation pathway of tetracycline (TC) over Z-scheme Ag₃PO₄/mixed-valence MIL-88A(Fe) heterojunctions. They used the periodic approach with the Perdew–Burke–Ernzerhof (PBE) functional and Hubbard corrections (DFT + U) to calculate the catalyst's band structure and charge-density difference. For calculating the Fukui functions of TC, an atomic-orbital approach at the B3LYP/6–31(d,p) with solvation (IEFPCM) was employed. Huang et al. (2015) showed that Bi₂O₂(OH) (NO₃) works as a [Bi₂O₂]²⁺ layered catalyst for the photo-oxidation of phenol, bisphenol A, 2,4-dichlorophenol and tetracycline hydrochloride. They used DFT to investigate the electronic band structure and dipole moment at the local-density approximation (LDA) level of theory. In a study of ciprofloxacin photodegradation in aqueous bismuth oxybromide by photohole oxidation, Zhang et al. (2015) used theory to pinpoint the active sites with a spin-distribution analysis on the ciprofloxacin radical. Similarly, Zhang et al. (2019) calculated the highest occupied and lowest unoccupied molecular orbitals for a polymeric O and N co-linked carbon nitride framework with carbon dots, which was 11.6 times more active in the photodegradation activity of diclofenac than g-C₃N₄.

Armaković et al. (2019) studied La-doped TiO₂ as a photocatalyst for the degradation of metoprolol tartrate (MET) and propranolol hydrochloride (PRO). The authors calculated the opto-electronic properties, the e[−] and h⁺ reorganization energies (ERE and HRE), the hydrophobic areas, the HOMO–LUMO gap, the chemical hardness, the chemical potential and the electrophilicity index.

Xing et al. (2018) tested the photoelectrochemical properties of a bismuth oxybromide heterostructure and employed DFT as a supporting technique for determining the band gap energy, the conduction band minimum and the valence band maximum. The photodegradation of levofloxacin by Fe-doped BiOCl nanosheets was studied by Zhong et al. (2020), who used DFT to prove the shrinkage of the unit cell upon Fe substitution and to calculate the band gap structure and the density of states of the undoped and Fe-doped BiOCl.

3.2. Electrocatalysis

3.2.1. Fundamentals

Instead of light, electricity can be used to guide the desired chemical

reaction. In this context, electrochemical advanced oxidation processes (EAOPs) have emerged as a promising alternative for treating and remediating water streams. Conceptually, electrocatalysis is a way to convert electrical energy into chemical energy. In practice, the EAOPs are based on the electrochemical generation of oxidizing species, mainly the hydroxyl radical (OH^\bullet). Since electrical energy can be obtained from renewable sources, this technique can be considered as a green oxidation process (Suhadolnik et al., 2019a).

The EAOPs can be divided in homogeneous (electroFenton, photoelectroFenton and sonoelectrolysis) and heterogeneous processes (anodic oxidation and photoelectrocatalysis), in the function of the OH^\bullet generation in the bulk solution or at the anode surface, respectively (Sirés et al., 2014).

In heterogeneous electrocatalysis, the electrode is a solid conductive material, usually a metal. This is one of the main reasons for the overpotential, which depends on the reactants and the products at the interphase, the electrolyte and the electrode material. The overpotential is the potential required in excess of the thermodynamic minimum and represents the kinetic barrier for the reaction. Thus, the aim of electrocatalysts' development is to lower the overpotential for the desired reaction.

3.2.2. Anodic oxidation

Anodic oxidation (AO) is one of the most common electrocatalytic processes among EAOPs to remove organic pollutants from water (Martínez-Huitle et al., 2015). This section will deal with the treatment of water and wastewater containing pharmaceuticals by applying AO, as well as a discussion of its fundamentals and the main parameters that affect this process.

AO's advantages include high efficiency, the possibility of automation, the simple equipment required, the mild operating conditions (room temperature and pressure), and versatility, since it can be used for effluents with up to 100 g L^{-1} of COD. Nevertheless, there are still some drawbacks that limit the industrial applications, such as the high costs of electricity and some electrode materials, the mass-transfer limitations, foam formation, the temperature increase during the process, the need to add electrolytes to wastewaters with low conductance, and the deposition of organic material on the electrode's surface, so shortening its lifetime (Martínez-Huitle et al., 2015; Sirés et al., 2014).

Pharmaceuticals and organic pollutants in general can be degraded by AO using direct AO when there is a direct electron transfer to the anode, or indirect reactions with the electrogenerated species in the bulk

solution (Fig. 6). The most relevant species generated are the hydroxyl radicals and active chlorine (when the electrolyte contains chlorine) (Suhadolnik et al., 2019a). In both cases the type of electrode is of fundamental importance and directly influences the efficiency of the process. Actually, the Gibbs free energy of any reaction is also a function of the electric potential, which is non-zero at the electrodes in electrocatalysis. This means that the electrode does not act merely as an acceptor or donor of electrons, but actively modifies the reaction rates.

An ideal electrode should have a high surface area and current efficiency as well as a long lifetime and low cost. Several types of electrode materials have already been reported for the electrocatalytic degradation of pharmaceuticals, among which boron-doped diamond (BDD) (Lan et al., 2018), platinum (Guitaya et al., 2017) and metal oxides (e.g., TiO_2) (Arredondo Valdez et al., 2012) are the most common. However, an electrode that has all the desired characteristics remains to be found.

The formation of radical species that are able to react in the bulk solution occurs first through the direct oxidation of these species on the anode surface. It depends on the anode material and the electrolyte type. When using anode materials like BDD and PbO_2 coatings, the formation of radicals from anions such as sulfate, phosphate, carbonate and chloride are explained by Eqs. (11)–(14) (Sirés et al., 2014). The formation of OH^\bullet occurs during the anodic oxidation of water (Eq. (15)). However, due to its high reactivity, it can rapidly react to form H_2O_2 and/or HO_2^\bullet (Eqs. (16) and (17)) (Oturán et al., 2012). Since the oxidation of organic compounds to CO_2 is favored by the reaction with OH^\bullet , anodes with a high O_2 -evolution overpotential (such as BDD) are preferable to anodes with a low O_2 -evolution overpotential for the removal of pharmaceuticals (Martínez-Huitle et al., 2015).

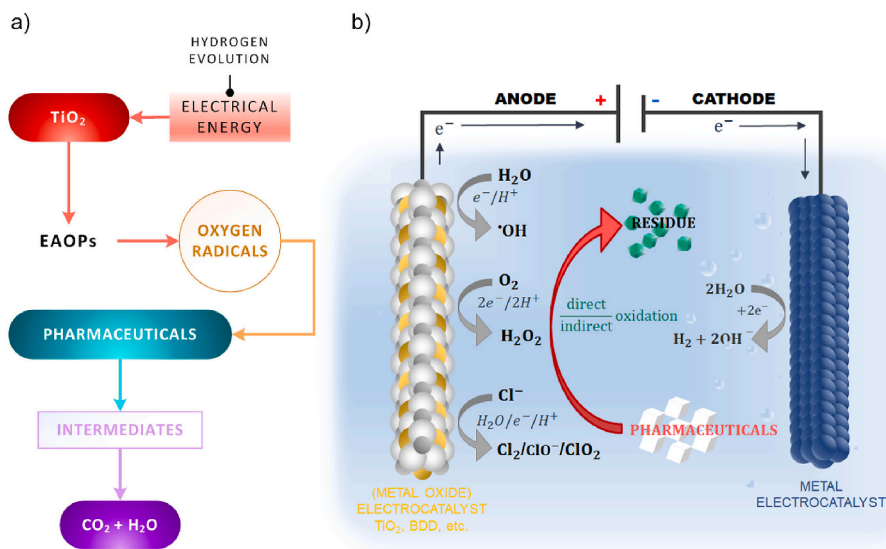


Fig. 6. Schematic of the electrocatalysis process (anodic oxidation): a) process flow diagram; b) schematic representation EC reactions. Adapted from (Lan et al., 2018) and (Feier et al., 2018).

Another important reaction that should be considered is the production of H_2O_2 by reducing oxygen on the cathode surface. Thus, a strong oxidant can be produced instead of other unproductive reactions at the cathode. It can occur in most cathode materials when dissolved oxygen is available; however, it demands a large contact area, which is usually found with porous cathodes (Zhou et al., 2012).

3.2.2.1. Affecting parameters. Some figures of merit that are important to evaluate the AO performance from the electrochemical point of view, such as the current efficiency (the ratio of the charge needed to oxidize the pollutant to the total charge required in the process), the space-time yield (electrochemical oxidation capacity), the specific energy consumption (the energy used to remove a unit mass of COD) and the limiting current density (for maximum production rate), can be found in detail elsewhere (Panizza and Cerisola, 2009).

Other parameters such as the current density and the stirring rate, the effluent conductivity, the pollutant type and concentration, the pH and the temperature, can also influence the process performance and sometimes are not fully evaluated in all reports.

The operating current density is a parameter of fundamental importance in the AO process, since the distance between the electrodes is fixed and the current is continuously supplied. This is the one parameter that can be directly controlled during the process (Martínez-Huitle et al., 2015). Typically, when the current density is increased, the rate of pollutant removal also rises; however, it is often followed by a fall in the current efficiency. Despite the simplicity, undesirable reactions can also occur and affect the performance of the process. Sopaj et al. (2015) reported the influence of the current density for different anode materials during the EC treatment of amoxicillin. For almost all the materials tested (Pt, PbO_2 , DSA, carbon-fiber and carbon-graphite) a weak influence of the current density was observed in the range 2–20 mA/cm^2 . The exceptions were BDD and carbon-felt anodes, which exhibited higher efficiencies when using current densities of 20 and 15 mA/cm^2 , respectively. The current density applied for the EC degradation of pharmaceuticals normally remains between 1 and 50 mA/cm^2 , and the best condition depends on the materials and the reactor design. However, it is important to ensure appropriate stirring of the system, to minimize the mass-transfer limitations and to ensure homogeneous conditions (Macpherson, 2015). In an experimental set-up with a recirculation system (10 L capacity), the limited influence of the flow rate in the range 125–500 L/h was reported (Loos et al., 2018). Since the mass-transfer coefficient's enhancement affects the reaction rate to a limited extent, even for the minimum flow rate tested, the system was adequately homogenized and the reaction was not mass-transfer limited.

The electrolyte concentration determines the solution's conductivity, while its type is related to the reactive species formed, with both being very significant for the AO efficiency. Normally, NaCl or Na_2SO_4 are used as electrolytes, but ideally the wastewater itself should be the electrolyte. It is worth noting that chloride-mediated reactions are favored in the presence of NaCl, while in the presence of Na_2SO_4 , persulfates can be produced (Cheng et al., 2003). Y. J. Liu et al. (2019) evaluated the influence of the electrolyte type (NaCl and Na_2SO_4) at different current intensities (0.1–0.5 A) for the EC degradation of acetaminophen, diclofenac and sulfamethoxazole. The results showed there was little influence of the current intensities when using Na_2SO_4 , reaching degradations of about 80% for all the pharmaceuticals in 60 min at all the current intensities tested. On the other hand, when using NaCl the EC efficiency was greatly improved by increasing the current intensity from 0.1 to 0.5 A, increasing the pharmaceuticals' removal from 50 to 60% to more than 90% in 20 min (Y. J. Liu et al., 2019). These results indicate that for the reaction with Na_2SO_4 as the electrolyte, the oxidation mainly occurs on the anode surface, while in the system with NaCl indirect reactions also occur, promoting the synergy between the hydroxyl radicals and the active chlorine. Nevertheless, the presence of chlorine must be cautiously monitored since there is the possibility of

toxic by-products being formed (Lan et al., 2017). Longer reaction times can be an alternative to ensure the mineralization of the organic species and avoid the residual presence of organochlorine species. Furthermore, to confirm that the final effluent is not dangerous, toxicity tests and TOC analysis should be performed.

Welter et al. (2020) studied the influence of the electrolyte in the EC degradation of prednisone by comparing the efficiencies when using synthetic and real matrices. The EC was able to oxidize the prednisone in all the tested conditions. When using a synthetic solution with 1 g L^{-1} of Na_2SO_4 as the electrolyte, it was possible to achieve a degradation of 78% and a mineralization of 42%. However, the results were improved when the process was applied to a real wastewater matrix spiked with the same amount of prednisone, which can be attributed to the different ions in the real wastewater matrix that allow the greater electro-generation of oxidizing agents. In fact, the presence of different ions seems to be more important for the EC efficiency than the single electrolyte concentration since the efficiency in the unmodified wastewater matrix (84% of prednisone removal and 63% of TOC removal) was higher than the one with the addition of 1 g L^{-1} Na_2SO_4 matrix (82% of prednisone removal and 55% of TOC removal). Furthermore, excess sulfate ions at high concentrations of Na_2SO_4 can lead to a decrease in the pharmaceuticals' removal efficiency, since the adsorption of the excess ions at the anode surface reduces the number of accessible active sites for the generation of OH^\bullet (Samarghandi et al., 2021).

The effect of the pH on the AO process is related to the pollutant type, which is sometimes easily oxidized in an alkaline or acidic medium, depending on its pK_a . Furthermore, pollutants can preferentially adsorb/desorb on the surface of the electrodes at different pH values. In addition, the pH can also influence the availability of the OH^\bullet and other oxidants in the bulk solution (Macpherson, 2015). Despite the inexistence of a general rule for the influence of pH, the AO process generally has an optimum pH value for its maximum efficiency, which must be experimentally determined. For the EC removal of antibiotics from the fluoroquinolone family, different studies with different electrodes have found a diversity of optimum pH values. For ciprofloxacin the best pH evaluated was 4 (C. Yang et al., 2021), while for ofloxacin (Xie et al., 2017) and levofloxacin (Meng et al., 2021), high efficiencies were found in more basic conditions, at pH values of 11 and 10, respectively.

Regarding the pollutant's initial concentration, for higher initial concentrations, greater current efficiencies are usually observed; however, longer reaction times are required. On the other hand, the temperature has a minimum influence on the AO efficiency when oxidation by OH^\bullet is the primary reaction for the pollutants' removal (Martínez-Huitle et al., 2015).

Despite the promising results obtained in AO laboratory-scale tests and its feasibility to be utilized in small-scale decentralized treatment plants, its practical application for treating real pharmaceutical effluents is still limited. This behavior can be attributed to its high energy consumption (50–1000 kWh kg^{-1} COD) when compared to the aerobic biological treatment (3 kWh kg^{-1} COD) (Yang and Hoffmann, 2016), as well as to the need for more information about the by-products formed during the process and the theoretical description of the systems.

3.2.2.2. Degradation mechanisms. While the theoretical description of thermocatalytic reactions at solid-vacuum or solid-gas interfaces has traditionally shown good agreement with experiments, electrocatalytic-reaction modeling suffers from three drawbacks: (i) the processes are influenced by the electrode potential, (ii) the description of liquid electrolytes is computationally expensive and imprecise, and (iii) the density functional theory's description of the transition states involved falls short of the elusive chemical accuracy ($<1 \text{ kcal mol}^{-1}$). These shortcomings have prevented researchers from developing a universal or generally accepted approach to modeling electrocatalysis.

While thorough theoretical studies of electrochemical reaction mechanisms exist, they are limited to smaller molecules or industrially

relevant processes. For the degradation of pharmaceuticals, theoretical calculations are used as a supporting technique with limited predictive power. Some authors used DFT to calculate adsorption energies and use them to infer the reaction mechanism. Zichen Wang et al. (2021) used waste 1D-FeOOH as an electrocatalyst for peroxymonosulfate (PMS) activation and metronidazole degradation. First-principle calculations were used to calculate the adsorption energy of PMS on 1D-FeOOH and 1D-FeOOH@Mo and the surface-electron density, relating the superior activity of FeOOH@Mo to its strong interaction with PMS. Meng et al. (2021) synthesized FeOOH nanoneedles with quantum carbon dots (CQDs@FeOOH) for the electrodegradation of levofloxacin and then calculated the adsorption energies of OH on (221), (111) and (110) facets. The oxygen-reduction reaction (ORR), which is instrumental in the electro-Fenton degradation of sulfonamides on N,S co-doped cathodes, was explored by calculating the adsorption energy of O₂ over graphene in pure, N-doped, S-doped and co-doped forms, finding the strongest interaction in the last of these (Zhu et al., 2021).

Even more often, the use of DFT is relegated to calculations of the principal electronic properties of the materials and substrates involved. The HOMO-LUMO gap is important for activity and was calculated for Turkey et al. (2018) in a study of its electro-oxidation over several Ti-containing electrodes and boron-doped diamond. Acetaminophen and its analogs are common substrates for testing electrocatalysts and mechanism investigations. Q. Zhang et al. (2020a) focused on sulfur-doped graphene (SGN), which has edge and thiophene structured sulfur species. The authors used DFT to help postulate a reaction mechanism by calculating the HOMO and LUMO and the electron-density difference upon Cl⁻ adsorption, concluding that the thiophene structure S catalyzes the reaction. When using a boron-doped graphene electrode, boron was found to slightly change the charge density, the HOMO-LUMO gap and the magnetic moment, as confirmed by DFT calculations on six different models (Q. Zhang et al., 2020b). The same properties were calculated in a study of N-(4-hydroxyphenyl) ethanamide electrodegradation on phosphorus-graphene (Yu et al., 2021), acetaminophen degradation on S-doped graphene/Pt/TiO₂.

3.3. Photoelectrocatalysis

3.3.1. Fundamentals

The combination of photocatalysis and electrochemistry emerged at the beginning of this century, leading to photoelectrocatalysis (PEC) technology, which finds extensive use in environmental applications as a promising alternative for degrading refractory organic pollutants in water and wastewater as well as water splitting (Garcia-Segura and Brillas, 2017; D. Liu et al., 2017; S. Liu et al., 2017). The electrical potential is used to make the desired reaction exothermic (a negative Gibbs free-energy change) and irradiation then increases the reaction rate further. Artificial photosynthesis (solar fuel production) is an example of a photo-electrocatalytic system. Photo-electrocatalysis has numerous advantages, such as better performance over refractory contaminants and a faster mineralization of organic pollutants, the possibility of automation, modularity and portability, as well as a small footprint (Ghasemian et al., 2017; Suhadolnik et al., 2019b). However, since PEC is a relatively new technology, most of its reported applications relate to synthetic wastewater that had the electrolytes added. Nonetheless, it is important to mention that urban and industrial wastewaters generally already contain electrolytes such as sulfate, chloride and carbonate salts, which guarantee enough conductivity to effectively perform the PEC treatment, making this technology more attractive for the treatment of real wastewater.

This technique is based on the use of a semiconductor photo-anode, which is composed of a semiconductor photocatalyst (commonly TiO₂ or ZnO) supported on a conductive substrate, and a cathode with an active metal surface that allows the desired reactions (Fig. 6) (Jaramillo-Gutiérrez et al., 2016). When the anode is irradiated by light with an energy equal to or higher than the semiconductor's band gap,

electrons and holes are photogenerated. This system is simultaneously biased by a gradient of potential, which drives the electrons from the anode to the cathode, preventing electron-hole recombination, while additional reactions on the cathode can help the oxidation of the pollutants and enhance the photocatalytic efficiency (Liu et al., 2017; Suhadolnik et al., 2019b). In fact, although the reduction of water to produce H₂ is the conventional reaction on the cathode (Fig. 7), the use of carbonaceous cathodes can lead to the formation of H₂O₂ by reducing the O₂ in accordance with Eq. (18) (Brillas and Martínez-Huitle, 2015). The formed H₂O₂ is able to react with e_{cb}⁻ and contributes to the formation of additional OH[•] radicals (Eq. (19)) (Garcia-Segura and Brillas, 2017). Furthermore, when an anodic potential (E_{anod}) is applied over the semiconductor, anodic oxidation (AO) is also feasible since the water can be oxidized with the subsequent formation of a hydroxyl radical (OH[•]), as exemplified in Eq. (20) (Cavalcanti et al., 2013).



Since the recombination of the electron/hole is suppressed in PEC, the hole's lifetime is increased, readily oxidizing the pharmaceutical compounds directly (Eq. (10)), as well as reacting with water, producing a hydroxyl radical by conventional PC (Eq. (2)) (Garcia-Segura and Brillas, 2017). With all possible reactions that can occur in the PEC process, it is challenging to determine the contribution of every individual process. Nevertheless, the greater efficiency of PEC over conventional EC can be explained by the photocatalytic reactions that take place only in PEC systems (Garcia-Segura et al., 2013). The choice of appropriate anode materials is a fundamental step that strongly influences the process efficiency, cost and selectivity (Ghasemian et al., 2017). The most suitable electrode should exhibit a high catalytic activity and stability, facilitating its recovery and recycling along successive treatments, without losing its efficiency (Garcia-Segura and Brillas, 2017). Consequentially, a key aspect of a successful PEC system is a strong adhesion of the photocatalyst to the conductive support (anode) (Suhadolnik et al., 2019b). Several immobilization techniques can be used to prepare anodes, such as sol-gel, thermal, chemical vapor deposition, electrodeposition and anodization methods (Garcia-Segura et al., 2013). Each method leads to different characteristics of the anodes, such as a high catalytic activity or strong adherence.

3.3.2. Affecting parameters

The use of PEC systems for the treatment of pharmaceuticals and organic pollutants at low concentrations usually follows pseudo-first-order kinetics and the global efficiency is influenced by other operational variables, such as current voltage and intensity, catalyst layer thickness, electrolyte types and concentration, effluent/solution pH, light intensity and pollutant concentration (Zanoni et al., 2003).

The efficiency of the PEC process is enhanced by an anodic potential increase, since it slows down the electron-hole recombination and allows for the formation of additional reactive species on the cathode. Nevertheless, this enhancement is observed only until a certain anodic potential value, at which the maximum amounts of photoexcited electrons are driven to the cathode and the reaction becomes dependent only on the photon flux. With a further increase in the anodic potential, the space-charge layer can exceed the thickness of the photocatalyst, leading to a redistribution of the charges, reducing the PEC efficiency and increasing the energy consumption (Yang et al., 2016). This behaviour was observed by Wang et al. (2021) during the photo-electrocatalytic degradation of carbamazepine. With an increase of the bias voltage from 0.5 to 1.5 V, the carbamazepine degradation rate increased from 47 to 73%. Nevertheless, with a further increase up to 2.0 V, only 63% of the initial carbamazepine concentration was degraded. The authors

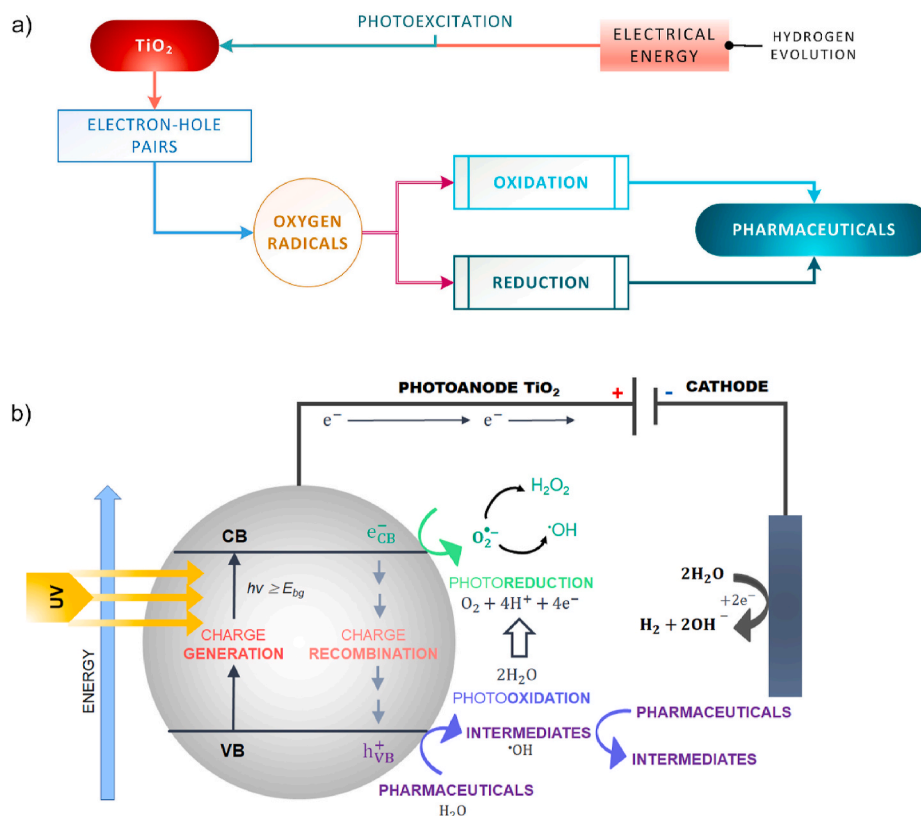


Fig. 7. Schematic of the photo-electrocatalysis process: a) process flow diagram; b) schematic representation PEC reactions. Adapted from (Jeon et al., 2018) and (Divyapriya et al., 2021).

attributed this reduced efficiency at a bias voltage of 2.0 V to the oxygen-evolution reaction at an elevated overpotential. On the other hand, if the catalyst layer thickness is too large, the material resistivity will rise, making the charge carriers moving to the catalyst surface more difficult and facilitating the charge recombination (Chaplin, 2014).

In addition to influencing the material conductivity, the catalyst thickness is also related to the light penetration into the film. Therefore, the catalyst thickness increases will enhance the process efficiency up to a limit, and a further increase will diminish the PEC performance (Garcia-Segura and Brillas, 2017). It is worth to mention that the incident radiation with a certain wavelength presents a maximum penetration depth into TiO_2 film according to the relation $1/\alpha$, where α is the TiO_2 absorption coefficient at the light wavelength (Hitchman and Tian, 2002). Furthermore, the surface area also plays an important role in PEC efficiency. While the reduction in the grain size increase of the active surface area, it also increases the grain boundaries and the defects associated with small grains. These boundaries and defects can act as trapping sites for electrons and holes, which slow down the charge carriers transport to the film active surface, and consequentially decrease the photocatalytic activity (Jelovica Badovinac et al., 2020).

The mass transfer between the catalyst surface and the bulk solution is directly related to the reactor geometry and flow profiles. It is expected that the system design is projected to minimize the resistance in the mass transfer. However, even in small scale reactors, deviations from the ideal mix configuration may happen. Computational fluid dynamics (CFD) is a tool that can consider these deviations in the models and provides information that helps to understand these complexities (Ješić et al., 2021).

The electrolyte type and concentration can strongly influence the PEC efficiency as they affect the solution's conductivity and can contribute to the formation of strong oxidant species (such as active chlorine species), the scavenging of OH^\bullet (by inorganic anions, Eqs. (21)–(24)), and lead to the production of recalcitrant and toxic by-products

(chlorine derivatives) (Moreira et al., 2017). The common electrolytes applied in PEC systems include sodium and potassium salts like Na_2SO_4 , NaCl , KCl , NaClO_4 , NaNO_3 , and Na_2CO_3 . Of these, sodium sulfate (Na_2SO_4) is the most commonly used.



Jia et al. (2020) evaluated the effect of Na_2SO_4 concentration in a PEC system on the degradation of sulfamethazine. An increase in the pharmaceutical degradation rate from 60 to 82% in 180 min was observed when the electrolyte concentration increased from 0.1 to 0.5 mol/L. With a further increase of the electrolyte concentration to 1 mol/L, no significant improvement in the degradation rate was observed. The authors also evaluated the effect of the presence of inorganic anions (Cl^- , CO_3^{2-} , PO_4^{3-}) and humic acid (HA) in the same PEC system. The sulfamethazine degradation rate was decreased with the ionic strength increase in all cases, with the lowest efficiency being observed in the system with HA. The interference in the sulfamethazine degradation was $\text{HA} > \text{PO}_4^{3-} > \text{CO}_3^{2-} > \text{Cl}^-$. The authors attributed the adverse impact of the inorganic anions and HA on the sulfamethazine degradation to the scavenging of active oxidants (h_{ν}^+ and OH^\bullet).

The light intensity (a photon flux with sufficient energy to promote the band gap) and the stirring rate influence the amount of photo-generated electrons and the mass transfer, respectively, in a PEC system. However, both parameters are not usually evaluated in most studies. Researchers normally use irradiation sources of high intensity and high stirring rates to ensure the maximum efficiency. The same behavior is observed for the influence of temperature, which is typically kept at

20–25 °C (Garcia-Segura and Brillas, 2017; Moreira et al., 2017). Nonetheless, it is important to mention that by optimizing the light intensity and the stirring rate, it is possible to achieve higher PEC efficiencies and reduce the operational costs.

The pH value influences the PEC efficiency. However, the best condition has to be determined experimentally, since this influence cannot be explained by PZC (as in photocatalysis) and depends on the interactions of the pollutant molecule and the photocatalyst surface, which will be positively charged at the anodic potential (Garcia-Segura and Brillas, 2017). Different optimum pH values were reported for different PEC systems during the degradation of target pharmaceuticals, such as pH 2.7 for sulfamethoxazole (TiO₂/Ti photoanode) (Su et al., 2016), pH 3.5 for sulfamethazine (zeolitic imidazolate frameworks with N and F co-doped TiO₂ nanotubes photoanode) (Jia et al., 2020), pH 5.4 for ciprofloxacin (expanded graphite supported p-n MoS₂-SnO₂ photoanode) (Umukoro et al., 2018), pH 5.6 for diclofenac (γ -Bi₂MoO₆ photoanode) (S. Liu et al., 2017) and pH 9.0 for tetracycline (K₂Ti₆O₁₃ nanobelt/TiO₂ microflower - ITO photoanode) (Wang et al., 2019). In PEC system where the anodic and cathodic reactions take place in separated tanks, the pH in the anode tank may decrease during the reaction. To solve this problem, the conventional salt bridge can be replaced by a cation exchange membrane, which allows the transport of H⁺ generated in the anode tank to the cathode tank (Diao et al., 2013).

Regarding the initial pollutant concentration, the usual observation is that for high initial concentrations longer treatment times are required. This is the case for sulfamethoxazole photoelectrocatalytic degradation, reported by Su et al. (2016), where it was necessary to increase the reaction time from 50 to 250 min for the complete degradation when the initial concentration was increased from 0.7 to 13 mg L⁻¹. However, R. Dagherir et al. (2013) reported similar degradation rates (97–92%) for the degradation of chlortetracycline with initial concentrations ranging from 32 to 230 µg/L, indicating that for low pharmaceutical concentrations, the PEC efficiency can be maintained.

Since the degradation kinetics typically follows pseudo first order, the initial concentration should not influence the kinetic constant values. Nevertheless, lower pseudo-first-order kinetic constants for higher pollutant concentrations are often observed. This behavior can be attributed to a possible shift from the pseudo-first-order kinetic to the zero-order kinetic or limitations of this kinetic model to precisely describe the decay, since it simplifies the many reactions that occur simultaneously in a PEC system (Moreira et al., 2017).

3.3.3. Degradation mechanisms

First-principle theoretical methods already struggle to describe photo-induced processes and electrochemical reactions, which is in no small part due to the enormous computational cost. Since a theoretical description of photoelectrocatalysis compounds presents difficulties, few papers on this topic employ any first-principle calculations.

When DFT is employed, it does not account for the photo-activation and the electric field. When investigating water splitting and the photoelectrochemical degradation of tetracycline over a F-BiVO₄@NiFe-LDH photoanode, Liu et al. (2020) used DFT to study the structure-property relations. They focused on calculating the binding energies between F⁻ doped and undoped BiVO₄, and NiFe-LDH, showing that F⁻ increases the interaction. The band structure calculations, band gap, density of states and work function confirmed that F⁻ increases the range of the light absorption and improves the function of the catalyst. Similarly, Ma et al. (2021) calculated the band structure, density of state and work function for p-chloronitrobenzene photodegradation by BiO-Br/TiO₂ nanotube arrays. Sometimes, DFT is used to calculate the charge distribution and bond orders, such as in a study of sulfamethoxazole degradation in plasma (Zheng et al., 2019).

3.3.3.1. Chemical micro-kinetics or Monte Carlo at mesoscale. Understanding the mechanisms on the mesoscale is vital to link the atomic-

scale, first-principles catalysis to continuum-based reactor unit operation design or optimization. The mesoscale thus calls for the integration of adsorption, desorption, kinetics, diffusion and/or convection, or at least a comparison of these in terms of the assessment of process-rate-determining steps, simplifying it enough for control later. Indeed, looking at the literature, little has been completed in this specific direction, highlighting the opportunity and necessity to develop an integrated understanding of both (photo)(electro)catalytic degradation mechanisms and reactor unit design.

Manassero et al. (2015) were the first to apply a Monte Carlo methodology to the photocatalytic degradation reactions of a drug, focusing on the modeling of radiation itself. Pharmaceutical clofibrac acid was subjected to detailed kinetic modeling in a reactor. Manassero et al. (2017) later advanced this by implementing the Monte Carlo simulations to optimize the conditions under photocatalytic degradation reactions, immobilizing TiO₂ on packing to provide a continuous process operation. Jalali and Dezhampannah (2021) applied a genuine kinetic Monte Carlo model simulation so as to describe the catalytic surface photodegradation of amoxicillin, ampicillin and cloxacillin, tackling the complexity of the intermediates as well.

As photo-, electro- and photo-electro-catalysis bring about an increase in complexity, the latter is an emerging research field, while in thermo-catalysis such a methodology is much more common to date. However, model integration is still performed intuitively.

In our recent work (Suhadolnik et al., 2019a) we demonstrated how micro-kinetics could be usefully put to work to understand, predict, and optimize reactions as complex as the electro-catalytic phenol degradation, which proceeds through various intermediate/product steps. The concentrations of all bulk/surface intermediates or products can thus be simulated for multiple process times, reactor positions, as well as operating process conditions (Fig. 8).

4. Catalytic materials

The development of new materials for applications in water and wastewater treatment is growing fast in recent years. The need for efficient and at the same time low-cost materials is an issue for the removal of different water contaminants, including pharmaceuticals as well as heavy metals (Khandaker et al., 2021), endocrine disruptors (Diao et al., 2018), rare earths (Kubra et al., 2021), nitrate reduction (Diao et al., 2019b), dyes (Katheresan et al., 2018), algae inactivation (Diao et al., 2019a), among others. Furthermore, many reviews on catalytic materials were published (Atkinson et al., 2019; Gadipelly et al., 2014; Khetan and Collins, 2007; Kitano et al., 2018; Patel et al., 2019; Singh et al., 2018). They focus on synthesis methods and characterization of various groups of materials that can be used for the degradation of pharmaceuticals. They include non-metal materials, metals on in/organic supports, metal-organic frameworks, bulk metals, metal hydroxides, metal nanoparticles and surfactant-based catalysts. This section of the review will focus on titanium dioxide (TiO₂) as a catalytic material for photocatalysis, electrocatalysis and photo-electrocatalysis, as well as on boron-doped diamond (BDD) and heterostructured materials. They are among the most promising materials for the photo-electro-catalytic oxidation of pharmaceuticals or their conversion into biocompatible compounds.

It is important to mention that many catalyst properties can influence photo(electro)catalytic performance, such as size, specific surface area, pore volume, pore structure, crystalline phase, and exposed surface facets. Thus, a precise characterization of the catalyst materials is crucial for comprehending the photocatalytic mechanism and enabling the synthesis of enhanced photo(electro)catalysts (Luo et al., 2017; Nakata and Fujishima, 2012). Fig. 9 summarizes the techniques most utilized for the characterization of photo(electro)catalysts.

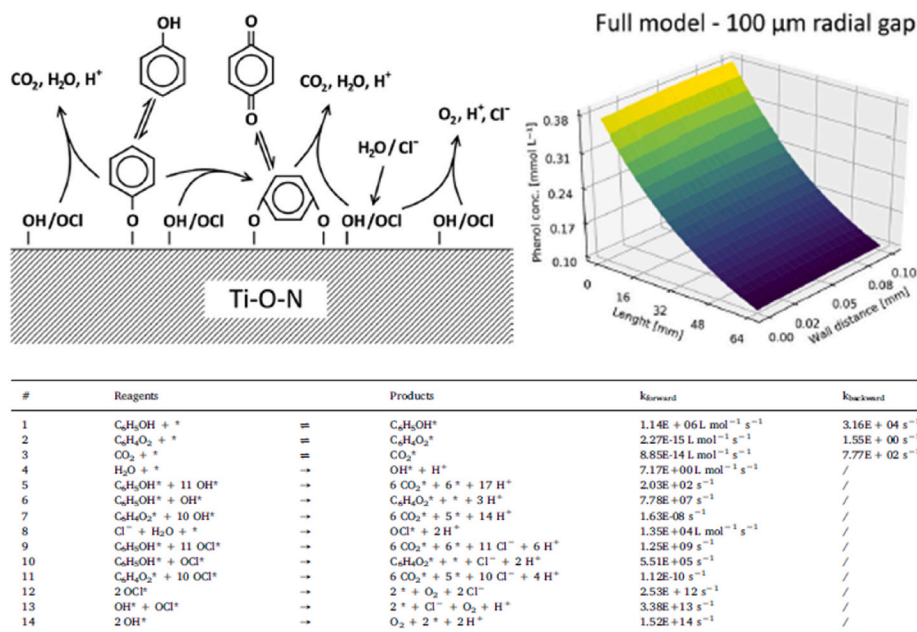


Fig. 8. Example of mechanism (top left), the reactions with constants (below) and the predictions of the process of degradation (top right), applying chemical microkinetics; results are reproduced from our previous work (Suhadolnik et al., 2019a), taking phenol as a model compound. Copyright© (2019), with permission from Elsevier.

SEM & TEM	XRD	PHOTOLUMINESCENCE SPECTROSCOPY	UV-VIS DRS
<ul style="list-style-type: none"> Surface morphology Grain size Crystal structure and interface Specific surface area Microstructural evolution and morphology transformation during the preparation process TEM can be equipped with EELS <ul style="list-style-type: none"> Chemical composition, lattice and crystal structure, band-gap, oxidation state 	<ul style="list-style-type: none"> Structural identification of atomic and molecular structures of crystals Crystal structures and crystallographic phases <ul style="list-style-type: none"> Crystallite size Size distribution Morphology Crystal structure Orientation of exposed crystal facets The effect of dopants 	<ul style="list-style-type: none"> Electronic structures Defects Separation and recombination of photoinduced carriers Studying the oxygen vacancies in TiO₂ Characterizing photocatalytic activity based on morphology, contact environment, hydrogen-treatment surface capping Investigation of the production of active •OH 	<ul style="list-style-type: none"> Light absorption properties
			XPS
			<ul style="list-style-type: none"> Surface chemical composition and chemical status
			ELECTROCHEMICAL IMPEDANCE SPECTRE
			<ul style="list-style-type: none"> Charge transfer ability between the electrode and electrolyte interface Matt-Schottky plots Transient photocurrent densities Linear sweep voltammetry <ul style="list-style-type: none"> Explore charge transport at the interface of semiconductor and electrolyte, which is reflected by photocurrent density Open circuit potential <ul style="list-style-type: none"> Also reflect the electron transport between electrode and electrolyte
			PHOTOVOLTAMMETRY MEASUREMENTS
			<ul style="list-style-type: none"> Similar to the photocurrent; current signal is collected under applied potential
			TIME-RESOLVED SPECTROSCOPY
			<ul style="list-style-type: none"> Useful to study fast or ultrafast charge separation, recombination and transfer process Time-resolved photoluminescence spectroscopy <ul style="list-style-type: none"> Radiation recombination of photoinduced carriers Time-resolved transient absorption spectroscopy <ul style="list-style-type: none"> Separate absorption signals for the photoinduced e⁻/h⁺ Time-resolved IR <ul style="list-style-type: none"> Study the excited status of electrons
			FTIR
			<ul style="list-style-type: none"> Monitoring the evolution of initial compounds and the transformation of functional groups Monitoring the adsorption and degradation of organics on catalyst surface Investigating the surface state of the photocatalyst after adsorption and splitting of water radicals
			PHOTOCURRENT MEASUREMENTS
			<ul style="list-style-type: none"> Useful for measuring the separation of photoinduced carriers

Fig. 9. Characterization techniques used for photo(electro)catalysts.

4.1. Titanium dioxide (TiO₂)

TiO₂ is the most widely studied photocatalyst, since it combines important physical-chemical properties such as chemical stability, long durability, and transparency to visible light, with the advantage of low cost and high photocatalytic activity (Luo et al., 2017; Nakata and Fujishima, 2012). Crystalline TiO₂ can exist in three different phases: anatase, rutile, and brookite. The first two can be easily synthesized in the laboratory and are widely used in photocatalytic studies. Rutile is the most stable form, while anatase exhibits better photocatalytic activity (Pelaez et al., 2012). Meanwhile, there is a lack of studies using

brookite for the degradation of pharmaceuticals. Table 4 shows some physical and structural properties of the anatase and rutile phases.

The high photocatalytic activity of anatase, when compared to rutile, is related to characteristics that include: i) lower packing density (~3.8 g/cm³) (Liu et al., 2010); ii) presence of [0 0 1] facets with remarkable photocatalytic activity due to the abundance of under-bonded Ti atoms as well as large Ti–O–Ti bond angles (Gong and Selloni, 2005); iii) longer recombination lifetimes and, iv) photocarriers with faster migrations to the catalyst surface (Zhang et al., 2014). The combination of two different phases produces a synergistic effect in photocatalysis, as is the case for the most common TiO₂ commercial powder, P25 (80% anatase,

Table 4

Physical and structural properties of TiO₂ (anatase and rutile) (Burnside et al., 1999; Luo et al., 2017; Pelaez et al., 2012).

Property	Crystalline phases	
	Anatase	Rutile
Band gap (eV)	3.2	3.0
Valence band (eV)	-2.8	-2.4
Conduction band (eV)	0.4	0.6
pH _{ZPC}	6.4	5.8
Density (g/cm ³)	3.79	4.13
Light absorption (nm)	<390	<415
Dielectric constant	31	114
Refractive index	2.55	2.75
Crystal structure	Tetragonal	Tetragonal
Mohr's Hardness	5.5	6.5–7.0
Melting point	1825	1825
Boiling point	2500–3000	2500–3000
Lattice constants (Å)	a = 3.78 c = 9.52	a = 4.59 c = 2.96
Ti–O bond length (Å)	1.94 (4)	1.95 (4)
	1.97 (2)	1.98 (2)
Electron mobility (cm ² /V s)	10	1

20% rutile). It was also found that the optimum mixture rate is up to 60% anatase and 40% rutile, and that this approach can also be applied to the anatase and brookite mixtures (Luo et al., 2017).

TiO₂ nanoparticles can be produced by different synthesis techniques, including sol-gel (Dolatbadi et al., 2021), hydrothermal (Li et al., 2020), solvothermal (Das et al., 2008), anodic oxidation (Marinko et al., 2021), chemical vapor deposition (Khanna et al., 2020), electrospinning (Marinho et al., 2021), etc. Depending on the methodology utilized for TiO₂ production, the nanoparticles can present different structural dimensionalities, such as powders and 1 to 3D, which imparts different properties to the produced material (Fig. 10). Furthermore, a significant enhancement of the photocatalytic performance of TiO₂ can be achieved with strategies like surface modification and doping (Luo et al., 2017).

The nanostructured TiO₂ powders are the most widely studied and used in TiO₂-related materials. Commercial TiO₂ powders include P25,

which is composed of a mixture of anatase and rutile phases, and PC105, PC500, which are pure anatase (Marinho et al., 2018). The main advantage of this type of structure is a larger specific surface area and the high pore volume and size, which facilitates the rate of mass transfer and the pollutants' adsorption (Nakata and Fujishima, 2012). Using these materials in slurry systems brings about the need for a post-step (such as filtration) to remove the photocatalysts or a previous immobilization of the nanoparticles in inert supports. The same behavior occurs with 2D nanosheets and 3D nanostructured TiO₂ materials.

This could be avoided with the use of TiO₂ 1D structures, such as fibers and tubes, which can be synthesized with electrospinning and anodization methods, respectively. Electrospinning is a simple and effective method of producing nanofibers through a high-voltage electric field, in which the TiO₂ can be electrospun with a polymer solution (Marinho et al., 2021). Anodization is a useful tool for producing nanotubes in which TiO₂ structures are grown directly in an electrode foil/mesh (Nakata et al., 2011). In both cases the TiO₂ is already strongly attached to the produced material, eliminating the need for nanoparticle immobilization or a post-step to remove the nanoparticles from the solution/effluent.

The structural characteristics of these 1D materials result in superior photocatalytic activity since they enable a facile diffusion of organic pollutants over the TiO₂ nanofibers/nanotubes. Furthermore, for TiO₂ nanotubes, a reduction in the electron/hole recombination is also observed since the thickness of the nanotube walls is smaller than the TiO₂ carriers' diffusion length (Almquist and Biswas, 2002).

Doping is an attractive strategy to overcome the limitations of TiO₂ related to the need for irradiation with wavelengths below 385 nm to promote its activation. Doping or co-doping TiO₂ with non-metals (N, F, C, S, B) (Dozzi and Selli, 2013; Li et al., 2005; H. Yu et al., 2021), transition metals (Cu, Ni, Cr, Fe) (A. S. Chen et al., 2021; Ferreira et al., 2021; Lee et al., 2021; Mancuso et al., 2021), noble metals (Pt, Ag, Au) (J. He et al., 2021; Komaraiah et al., 2020; Mohammed, 2020) and rare earths (La, Ce, Eu) (Chaker et al., 2020; Prakash et al., 2021), are approaches that change the crystalline structure and significantly improve the TiO₂'s photocatalytic activity by shorting the band gap and expanding the absorption wavelength to visible light. The synthesis of

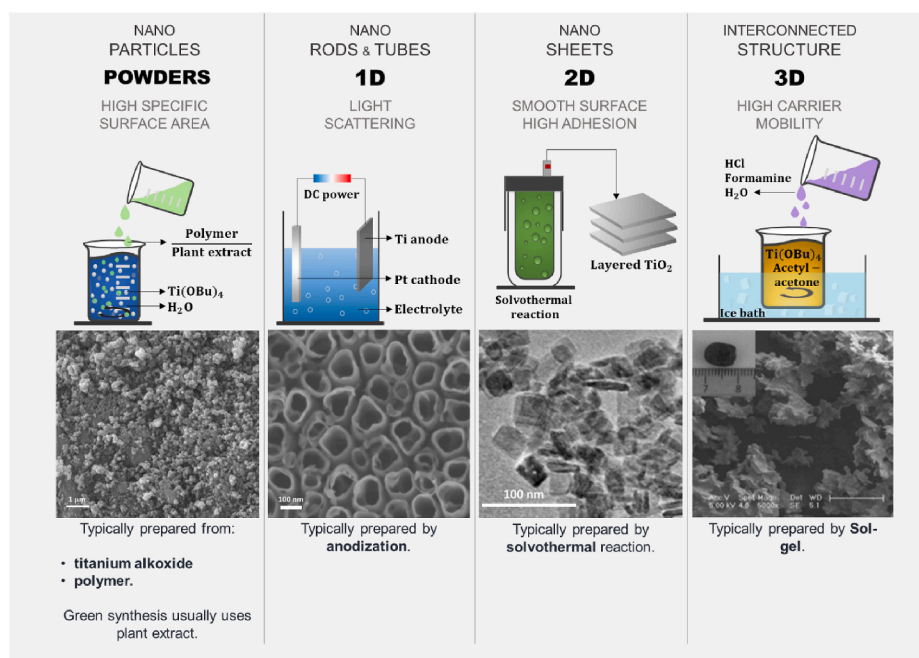


Fig. 10. Schematic of the structural dimensionality of materials with the expected properties. SEM/TEM images reprinted from: powders – Nabi et al., 2021, Copyright© (2021), with permission from Elsevier; 1D – Koiki et al., 2020, Copyright© (2020), with permission from Elsevier; 2D – Qu et al., 2021, Copyright© (2021), with permission from Elsevier; Chen et al., 2010, Copyright© (2010), with permission from Elsevier.

TiO₂ composites can also contribute to the enhancement of the photo (electro)catalytic efficiency. As an example, the GO/TiO₂ composite is generally more efficient than pure TiO₂, since the GO sheets can accept and transport the photo-generated electrons, reducing the electron/hole recombination (Garmroudi et al., 2020). Xie et al. (2019) evaluated the efficiency of titanium dioxide doped with zinc, fixed on reed straw biochar (Zn–TiO₂/pBC), for the degradation of sulfamethoxazole (SMX). The material showed visible light response due to the presence of zinc, which also hindered the combination of photogenerated electrons and holes. The biochar proved to be a suitable support, facilitating the adsorption of the SMX and its by-products. Fig. 11 shows a schematic diagram of the mechanism of Zn–TiO₂/pBC photocatalytic activity and SMX degradation. The removal rate of SMX was increased from 50%, when using only TiO₂, to 81%, when using Zn–TiO₂/pBC (Xie et al., 2019). It is clear that these improvements provide beneficial effects for the photodegradation of pharmaceuticals; however, it is necessary to evaluate whether the oxidative strength of photogenerated holes is lower than in undoped TiO₂ or if the use of expensive or potentially toxic materials could hamper the use of these new materials.

4.2. Boron-doped diamond (BDD)

BDD is a material that combines diamond-like properties like chemical inertness, extreme hardness, thermal conductivity, low friction, high charge-carrier mobilities and versatility with boron's electrical conductivity due to its incorporation into the diamond lattice (Guillery, 1993). Other electrochemical characteristics that increase the material's popularity are a wide solvent window, low capacitance, reduced resistance to fouling and mechanical robustness (Cobb et al., 2018). When synthesizing a diamond electrode, four different thin-diamond-electrode outcomes can be fabricated. They are presented in Fig. 12 (Luong et al., 2009).

There are many diamond thin-film syntheses procedures and post modifications, such as etching/shaping (Yang et al., 2005), high-pressure, high-temperature (Ekimov and Kondrin, 2020), vacuum annealing (Watanabe et al., 2002), surface transfer doping (Strobel et al., 2004) and chemical vapor deposition (CVD). Of these, CVD is the most favored and widely used due to the possibility of the film growing on any substrate geometry (May, 2000). However, the harsh conditions limit the substrates that can be used for diamond-film synthesis. The most suitable are niobium (Jum'h et al., 2017), tungsten (Vokhmyanin and Oglezneva, 2019), silicon (May, 2000) and titanium (Askari, 2012). Interestingly, more flexible substrates, such as polymers (Parylene-C

(Fan et al., 2017)), can be used if the film is transferred to the substrate.

The CVD synthesis of a thin diamond film is schematically presented in Fig. 13 and can be described as a four-step sequence. First, a mixture of hydrogen/hydrocarbon gas (usually methane and hydrogen (Butler et al., 2009)) is activated via hot-filament CVD (HF-CVD) or a microwave plasma CVD (MW-CVD). Second, hydrogen atoms react with the hydrocarbon and create a mixture of hydrocarbon species. The hydrogen atoms also create radical surface sites for the adsorption of carbon species and the recombination of hydrogen atoms. In the last step, the hydrogen atoms and other gaseous species react with sp² carbon sites and convert them into sp³ carbon. The hydrogen-terminated surface drives the carbon to incorporate into the diamond lattice (Butler et al., 2009; Srikanth et al., 2012). Competition between the surface-activation reaction and hydrogen-atom recombination with the radical surface site is linked to the number of nucleation sites. The growth continues as the carbon diffuses over the surface until the diamond seeds eventually merge and form a highly controlled thin film.

Regardless of the crystallinity, a diamond has a wide band gap of 5.47 eV. As diamond is inherently an insulator, the conductivity is achieved with doping. One possible route is the so-called surface-transfer doping. In this case, dopant atoms are not incorporated into the diamond lattice. Instead, they are evaporated and adsorbed onto the hydrogen-terminated surface (Strobel et al., 2004). Another possibility is annealing in different atmospheres (Seshan et al., 2013), high-temperature diffusion (Seo et al., 2014), and ion implantation with heteroatoms (Prawer and Kalish, 1995). Depending on the dopant, new energy levels are formed, forming a *n*- or *p*-type semiconductor. However, the method is invasive and demands harsh conditions, often leading to a resistive material (Goss et al., 2008). The possibility of damaging the substrate is high, but if the ion implantation is controlled, the controlled growth of a doped diamond film is possible (Achard and Tallaire, 2018).

By far the most popular method is doping with gas during the CVD synthesis of the diamond thin film. Besides the typical CVD setting for a diamond-film synthesis, the addition of boron in gaseous form is needed (Macpherson, 2015). The substitution of the sp³ hybridized carbon atoms in a tetrahedral diamond lattice with boron atoms occurs during the process, which results in the formation of a BDD film (Luong et al., 2009). The boron atom is the most favorable for diamond doping since i) it can easily incorporate into the packed lattice due to its small size, ii) it acts as an electron acceptor, iii) it modifies the material electrical properties (Yang et al., 2005), and iv) it has a small activation energy (0.37 eV) (Macpherson, 2015). Doping diamonds with boron introduces holes into the lattice and makes the diamond film a *p*-type semiconductor. Time, pressure, gas ratio, the addition of other gases and other parameters influence the grain size of BDD films. An important characteristic is that the crystalline facets will increase with the growth period or the film thickness.

According to Macpherson (2015), the following issues must be considered when working with BDD: i) surface morphology, ii) amount of boron that contributes to the conductivity, and iii) surface termination. Because the surface morphology has a considerable impact on the electrochemical behavior, a complete surface characterization must be performed before analyzing results, emphasizing the crystallinity, the surface roughness and the grain size (Selesovská et al., 2016; Zhao et al., 2010). Understanding the material properties and electrode characteristics is vital for achieving the maximum growth of the material. The boron concentration can be determined with the methods mentioned in Table 5; its values are usually expressed in ppm, % or the number of atoms per cm³. Approximately one boron atom per 1000 carbon atoms must be placed to ensure optimal semiconductor properties (Macpherson, 2015). Lastly, the BDD surface can be oxygen-terminated (*hydrophilic, positive electron affinity*) or hydrogen-terminated (*hydrophobicity, negative electron affinity*). Surface termination has a considerable impact on the electron transfer, wettability and electrostatic interactions (Bhardwaj et al., 2020; Hoffmann et al., 2010). Immediately after the synthesis, the

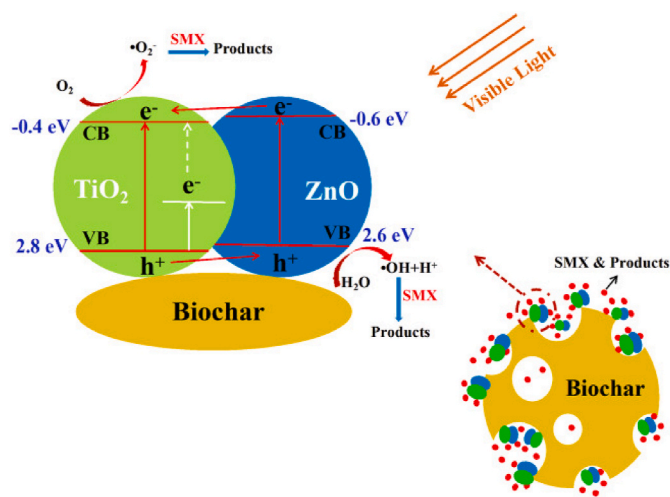


Fig. 11. Mechanism of photocatalytic activity of Zn–TiO₂/pBC under visible light irradiation. Reprinted from (Xie et al., 2019). Copyright© (2019), with permission from Elsevier.

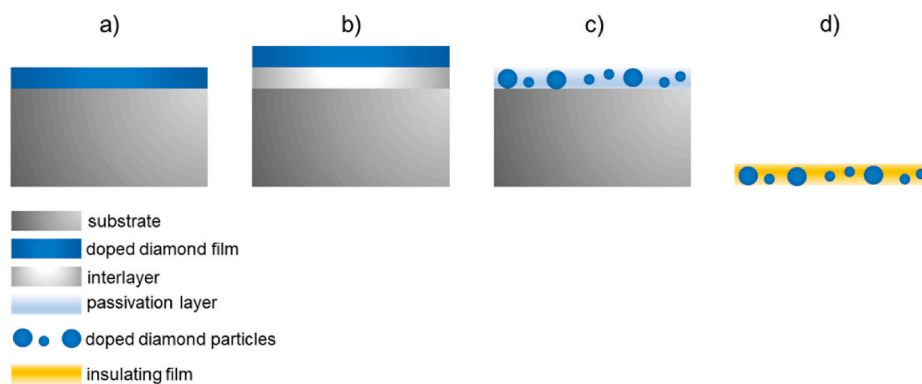


Fig. 12. Four different thin-diamond-electrode outcomes.

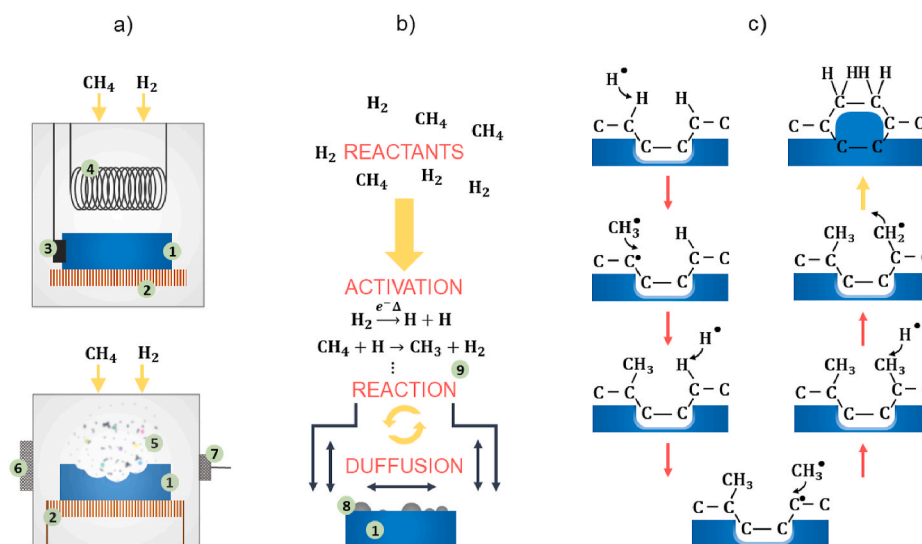


Fig. 13. Schematic of processes occurring during diamond CVD. a) overview of the process. 1-Substrate, 2-substrate heater, 3-thermocouple, 4-filament, 5-plasma, 6-microwave generator, 7-tuner. b) details of the process. 1-substrate, 8-diffusion layer, 9-generation of free radicals.

BDD electrode is hydrogen terminated. However, the oxygen-terminated surface possesses better electrochemical characteristics (Hutton et al., 2013). Therefore, the surface termination needs to be checked periodically and acted upon if a change is needed.

BDD's popularity for wastewater treatment is attributed to the absence of hydrogen and oxygen evolution reactions that could interfere with the degradation and analysis. This is a consequence of the very low capacitance, the absence of surface oxide, the high overpotential and the reduced reactions between oxygen and hydrogen evolution (Santana et al., 2005). Moreover, its use allows the rapid production of hydroxyl radicals with a high standard reduction potential ($E^\circ \text{OH}^\bullet/\text{H}_2\text{O}$, 2.8 V), contributing to a significant unselective reactivity with organic contaminants. However, if the electrochemical conditions during degradation are severe, delamination of diamond film from the BDD electrode can occur (Chaplin et al., 2011, 2013). This can result in lower efficiency and, possibly, electrode failure. Delamination results from etching the sp^2 carbon that acts as a deactivation site for the OH^\bullet radicals (Wang et al., 2014). If the phenomenon is detected in time, it can be slowed by changing the electrochemical conditions.

Li et al. (2019) investigated the degradation of 300 mL of an aqueous solution of ciprofloxacin in a differential column batch reactor where the BDD anode was 15 mm from the titanium foil cathode. Different concentrations (1, 5, 10, 20 mg L^{-1}), process times (5, 25, 30, 50 min), current densities (5, 10, 20, 30, 40 mA cm^{-2}), supporting electrolyte concentrations (5, 50, 100, 500 mmol L^{-1}), pHs (3, 4.5, 7, 9) and

voltages (between 3.5 and 8.6 V) were monitored, and the best degradation conditions determined.

4.3. Heterostructured materials

The construction of heterojunctions based on coupling two different semiconductors is an efficient strategy to reduce the recombination of electron-hole pairs and to overcome one of the main drawbacks in photocatalytic applications. When semiconductors have different Fermi energy levels (E_F), the electrons of the semiconductor with higher E_F are spontaneously diffused to the one with the lower E_F , forming an electric field at the heterojunction interface, which inhibits the recombination of the carriers (Yang, 2021). It is important to mention that this electric field depends on many factors, such as the semiconductor (*p*-type or *n*-type), the Fermi level, and the conduction and valence band potentials of the semiconductors. Heterojunction photocatalysts can be divided into four types: i) semiconductor-semiconductor (S-S); ii) semiconductor-metal (S-M); iii) semiconductor-carbon (S-C); and iv) tandem heterojunctions (Xue and Bao, 2021). Low et al. (2017) presented a detailed review of the basic principles of various heterojunction photocatalysts.

An important example of a heterostructured material for photoelectrocatalytic processes is the combination of the *p*-type BDD with the *n*-type TiO_2 . This makes it possible to enhance the material's quantum yield by reducing the recombination of electron-holes (photogenerated

Table 5
Experimental parameters of BDD film synthesis.

	SUBSTRATE	SYNTHESIS CONDITIONS	ANALYSIS	REF.
HF-CVD	Silicon wafers (100), niobium-coated under diamond seeds.	Filaments: 16 kW, 12 pcs of 32 cm long tantalum filament Time: 12 and 60 h Temperature: 0 °C Pressure: 4000 Pa Gas flux: (CH ₃) ₂ CO 90 sccm, B(OCH ₃) ₃ 6 sccm (7902 ppm of B) and H 400 sccm	FE-SEM RAMAN XRD CV	(Song et al., 2020)
	<ul style="list-style-type: none"> After 12 h the film resulted in 1.22 μm thickness and 5.91 μm after 60 h of the The electrochemical performance was influenced by the intrinsic properties of the Silicon wafers (single-crystal), polished with 1 μm diamond paste	particles exposed and not by the density and thickness of the BDD film. deposition. Filaments: Helical-shaped filaments, 0.127 mm diameter tungsten wire, operated at 1800 °C Time: 20–90 h Temperature: 750–800 °C Pressure: 5300 Pa Gas flux: H 100 sccm, Ar 2–10 sccm and B 200–6300 ppm. Feed gas was a mixture of argon, bubbled through a solution of B ₂ O ₃ in C ₂ H ₆ O, and H. The B ₂ O ₃ /C ₂ H ₆ O ratios ranged from 10 g L ⁻¹ for the lowest doping level to 50 g L ⁻¹ for the highest doping level.	SEM RAMAN XRD TGA SIMS AES	Farabaugh et al. (1995)
MW-CVD	<ul style="list-style-type: none"> The following parameters had the most significant influence on the growth rate: argon flow rate between 8 and 10 sccm, a substrate temperature of 800 °C, increased amount of carbon and hydrogen flow rate of 100 sccm. Silicon wafers (<i>p</i> -type <111> oriented single-crystalline), polished with 0.25 μm diamond paste for 1 h	Time: 7 h Temperature: 800 °C Pressure: 35 Torr Gas flux: B ₂ H ₆ 0, 0.005, 0.01, 0.1, 0.5, 1 ppm, CH ₄ and H, B/C ratios were 0, 2, 4, 40, 200, 400 ppm, CH ₄ to H volumetric ratio 0.5%, gas flow rate 100 cm ³ min ⁻¹	SIMS SEM STM TEM EELS RAMAN	Wang et al. (1992)
	<ul style="list-style-type: none"> With a growth rate of 0.15 μm h⁻¹, the film resulted in 1.1 μm thickness. Boron increased structural perfection but reduced diamond grain size. Oriented diamond films (001), etched <i>in situ</i> in hydrogen microwave plasma for 20 min to remove the surface contamination	Time: 4–6 h Temperature: 770 °C Pressure: 1.3–5 bar Gas flux: CH ₄ 0.5% (2 sccm), H 99.5% (498 sccm), trimethylborate (TMB)/triethylborate (TEB)/tripropylborate (TPB) 93 ppm (up to 550 ppm), B/H ratios were 1–10 sccm	SEM AFM RAMAN SIMS EPMA ERD	Jiang et al. (1999)
	<ul style="list-style-type: none"> <i>In situ</i> doping. Silicon wafers (100) coated with silicon dioxide grown via a thermal growth process. Surfaces were seeded with nanocrystalline diamond particles via immersion in an ultrasonic system and grown in plasma	Thermal diffusion: Diffusion was carried on 3 samples of ultra-nanocrystalline diamond films grown on a silicon substrate. Annealing at low oxygen atmosphere at 800, 900, 1000 °C for 180 s for inducing the process of boron diffusion inside the diamond film	RAMAN XRD SEM SIMS XPS UPS	Tirado et al. (2018)
	<ul style="list-style-type: none"> An approximately 200 nm thick boron coating was deposited on the surface of ultra-nanocrystalline diamond films using the spin-on-dopant solution. Nanodiamond with a diameter of 4.7 nm and specific surface area of 270 m ² g ⁻¹	Post - heat treatment: air at 425 °C for 8 h to minimize the amount of sp ² carbon impurities Time: 8 h Temperature: 800 °C Gas flux: 70% B(OCH ₃) ₃ /CH ₄ and acetone (the B/C atomic concentration ratio was 20,000 ppm)	RAMAN TEM BET CV	Miyashita et al. (2019)
<ul style="list-style-type: none"> Post - heat treatment was necessary to minimize the amount of sp² carbon impurities. Polypyrrole films (<i>coral-like polypyrrole</i>), coated with a dense layer of diamond nanoparticles using an electrostatic grafting process	Time: Until a continuous boron doped nanocrystalline diamond layer was obtained (6 and 12 h) Temperature: seeds grown at a temperature below 450 °C Pressure: 20 Torr Gas: CH ₄ 1%, B(OCH ₃) ₃ 2.4%	SEM RAMAN EIS CV	Hébert et al. (2015)	
<ul style="list-style-type: none"> The thickness of a diamond layer is 90 and 170 nm. Incredible electrochemical performances, porous diamond material and no limitation for the process to reach larger surface areas. Silicon pillar array 10 μm diameter and 50 μm height, silicon wafer as a blank	Special: Photolithography Gas: B(OCH ₃) ₃ , CH ₄ and (CH ₃) ₂ CO 70%. B/C atomic concentration ratio of 20,000 ppm	SEM RAMAN CV EIS	Kondo et al. (2017)	
	<ul style="list-style-type: none"> CV measurements indicated successful enhancement of the double-layer current up to 2800 μF cm⁻², maintaining a wide potential window and short time constant (18 ms). The use of photolithography increased the specific surface area of BDD (use of silicon pillar array). 			

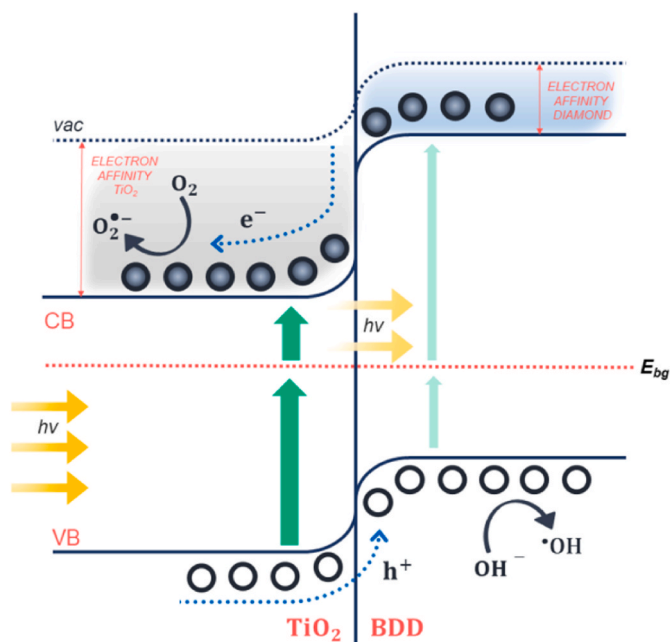


Fig. 14. Schematic band diagram of the *n*-type TiO₂ nanotubes and *p*-type BDD heterojunction.

charge carriers), making it more efficient for the degradation process. BDD can be used directly or as a substrate for other materials. By immobilizing the TiO₂ on a conductive material, it is possible to suppress the electron-hole recombination and, consequently, improve the photocatalytic efficiency by forming a heterojunction. This type of structure acts as an internal electrostatic potential in the space-charge region, allowing for an efficient separation of the photo-induced charge carriers (Fig. 14).

There are three possibilities for electrodes: i) separate TiO₂ and BDD electrode; ii) TiO₂ films on the BDD electrode where the morphology of the deposition of TiO₂ films can vary (nanocrystals, nanosheets, nanorods, etc.), and iii) BDD on the TiO₂ electrode. Han et al. (2011) reported that the p-n junction elevates the photoelectrocatalytic activity over the oxidation of organic compounds in wastewaters. Additionally, the heterostructure electrode has an excellent resistance to acids (due to the BDD). Yuan et al. (2010) also reported that the heterojunction shows no loss of activity in the recycling experiments. Han et al. (2013) also reported on a very high chemical stability.

The evidence of the heterojunction formation can be observed by TEM and HRTEM micrographs. As an example, in Fig. 15 it is possible to observe the heterojunction between the rGO, g-C₃N₄ and CoFe₂O₄

nanoparticles (rGO/g-CN/CFO). In Fig. 15a it is highlighted the g-CN/CFO composite is well attached on rGO nanosheet, which is fundamental to the heterojunction formation. In Fig. 15b it can be noted d-spacing of CFO nanoparticle (0.239 nm, (311) plane), which makes the interface formation with g-CN and rGO nanosheets (Palanivel et al., 2021).

Graphitic carbon nitride (g-C₃N₄) has low-charge carrier mobility and low surface area, which limits its application in photocatalysis. However, it has a unique band structure, capable of coupling it with a large bandgap semiconductor to produce Z-scheme heterojunction composites (Ismael, 2020). Wu et al. (2022) have evaluated the tetracycline degradation using a floral and lamellar interlaced double Z-scheme ternary heterojunction Bi₂O₂CO₃/g-C₃N₄/Bi₂O₃ (CNBB-5). The synthesized heterostructured material showed enhanced photocatalytic than the single catalysts, under simulated solar irradiation. All individual catalysts presented less than 50% of TC degradation, while the ternary heterojunction material was capable to degrade up to 100% of TC in the same reaction time. In this dual Z-scheme structure (Fig. 16), the photogenerated (e_{cb}⁻) of Bi₂O₂CO₃ and Bi₂O₃ can be transmitted to the VB of g-C₃N₄ so that photogenerated electrons can reduce O₂ to produce O₂⁻ in the CB of g-C₃N₄. At the same time, the (h_{vb}⁺) of Bi₂O₂CO₃ and Bi₂O₃, are able to oxidize TC to small molecules, while (h_{vb}⁺) of Bi₂O₂CO₃ can also react with water to produce OH[•] (Wu et al., 2022).

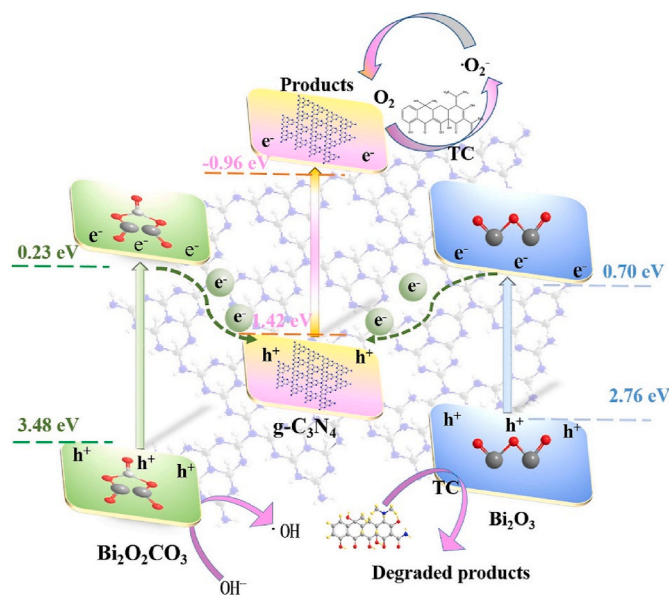


Fig. 16. Schematic heterojunction mechanism of CNBB-5. Reprinted from (Wu et al., 2022). Copyright© (2022), with permission from Elsevier.

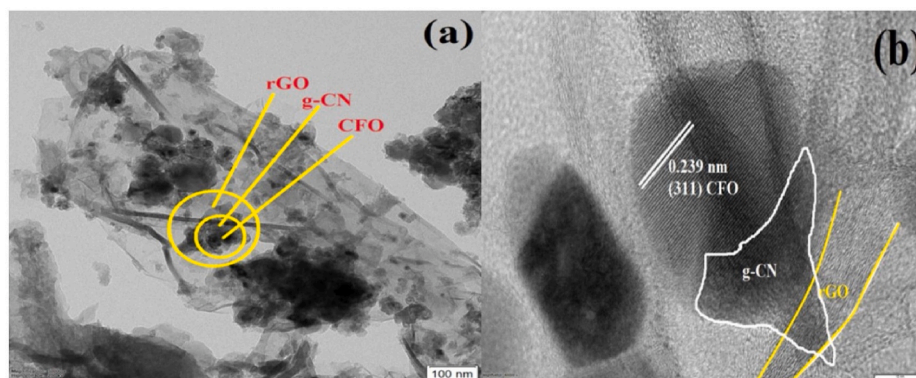


Fig. 15. Evidence of heterojunction formation on rGO/g-C₃N₄/CoFe₂O₄ (rGO/g-CN/CFO) photocatalyst confirmed by a) TEM and b) HRTEM images. Reprinted from (Palanivel et al., 2021). Copyright© (2021), with permission from Elsevier.

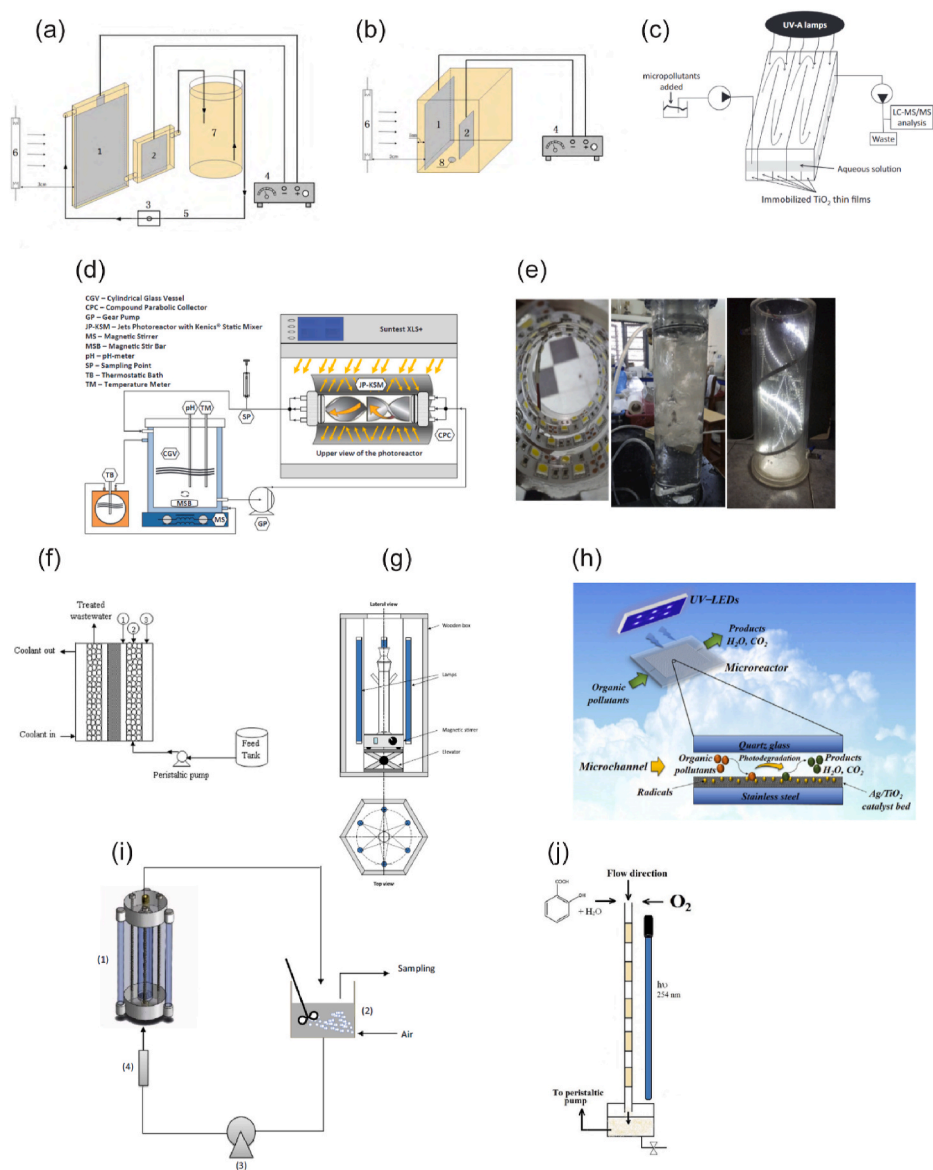


Fig. 17. The most common types of catalytic reactors. a) TNAs based thin-layer PEC reactor (Bai et al., 2010), Copyright© (2010), with permission from Elsevier; b) conventional PEC reactor (for both a and b: 1-double-faced TNAs electrode, 2-Pt electrode, 3-peristaltic pump, 4-DC power supply, 5-hose, 6-UV lamp, 7-solution container, 8-magnetic stirrer) (Bai et al., 2010), Copyright© (2010), with permission from Elsevier; c) continuous-flow reactor (Carbonaro et al., 2013), Copyright© (2013), with permission from Elsevier; d) low system equipped with two Kenics® static mixing elements (Díez et al., 2018), Copyright© (2018), with permission from Elsevier; e) fluidized bed type LED reactor with immobilized catalyst on MBBR media (Surenjan et al., 2019), Copyright© (2019), with permission from Elsevier; f) packed bed photoreactor (PBPR) (Sarkar et al., 2015), Copyright© (2015), with permission from Elsevier; g) cylindrical batch photoreactor (Palmisano et al., 2015), Copyright© (2015), with permission from Elsevier; h) microchannels microreactor (Eskandarloo et al., 2015), Copyright© (2015), with permission from Elsevier; i) fluidized bed photocatalytic reactor (FBPR) (1-FBPR, 2-storage tank, 3-pump, 4-flowmeter) (Rezaei and Mohseni, 2017), Copyright© (2017), with permission from Elsevier; j) quartz capillaries as multiphase photocatalytic reactors (Hurtado et al., 2016), Copyright© (2016), with permission from Elsevier.

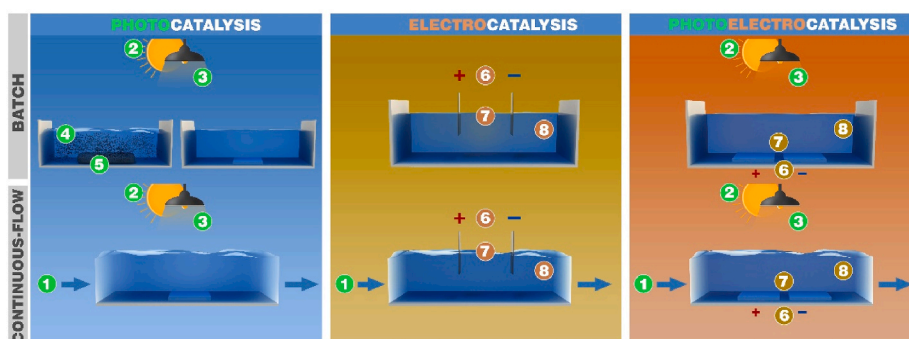


Fig. 18. Parameters of photocatalytic, electrocatalytic and photoelectrocatalytic degradation. 1-flow rate, 2-light source, 3-light intensity, 4-surface-to-volume ratio, 5-mixing, 6-applied potential, 7-distance between electrodes, 8-solution conductivity.

5. Design of laboratory reactors

Photocatalytic, electrocatalytic or photoelectrocatalytic reactor is a device where the conversion of pharmaceuticals occurs. Depending on the process being used to degrade organic contaminants, there are

several different reactor types. While a photoelectrocatalytic reactor can also be used for a photocatalytic or electrocatalytic process, this is not the case with the other two reactor types, which significantly differ in terms of device design and operation. Electrocatalytic reactors require electrically conductive electrodes positioned parallel to one another

Table 6
Results of the degradation of pharmaceuticals published in the literature.

Degradation process and catalyst	Pharmaceutical compound(s)	Initial concentration	Reactor type	Experimental conditions	Removal of the starting compound [%]	Ref.
Photocatalysis Three forms of TiO ₂	Ibuprofen	10 mg L ⁻¹	Batch photoreactor	10 mg of photocatalyst 250 mL aqueous suspension UV light source (60 W, 370–400 nm) Reaction time: 5 h	97	Tran et al. (2017)
Photocatalysis TiO ₂ /Fe ₂ O ₃ core-shell nanostructures	Paracetamol	50 mg L ⁻¹	Batch photoreactor	2.5 mg of photocatalyst 50 mL aqueous suspension 450W medium-pressure mercury vapor lamp Reaction time: 90 min	100	Abdel-Wahab et al. (2017)
Photocatalysis TiO ₂	Ibuprofen	6 mg L ⁻¹ , 60 mg L ⁻¹ or 213 mg L ⁻¹	Batch photoreactor	0.5, 1.0 or 1.5 g L ⁻¹ photocatalyst 250 mL of aqueous suspension 40 W UV LEDs with peak intensity at 382 nm Reaction time: 90 min	70% dissolved organic carbon	Jallouli et al. (2018)
Photocatalysis C-doped TiO ₂	Tetracycline hydrochloride	5 mg L ⁻¹	Batch photoreactor	300 mg L ⁻¹ photocatalyst 200 mL aqueous suspension 25 W visible-light LED strip with peak intensity at 450 nm Reaction time: 2 h	83% after 4 cycles	Oseghe and Ofomaja (2018)
Photocatalysis TiO ₂	Sulfamethoxazole	1 mg L ⁻¹	Recirculating photoreactor	100 mg of photocatalyst 1 L of solution with simulated seawater or deionized water Illuminated volume: 77 mL 1500 W Xenon lamp with solar spectrum Reaction time: 6 h	100% in deionized water and 91% for seawater	Porcar-Santos et al. (2020)
Photocatalysis TiO ₂ and oxidized multi-walled carbon nanotube/anatase	Diclofenac	8 mg L ⁻¹	Batch photoreactor under O ₂ /Ar atmosphere	50 mg–1000 mg of photocatalyst 500 mL aqueous suspension UV light with intensity of 8.33 × 10 ⁻⁶ E s ⁻¹ at peak wavelength of 254 nm or NUV-vis with photon flux at 366 nm of 2.38 × 10 ⁻⁶ E s ⁻¹ 200 mL/min O ₂ /Ar (50% vol. of oxygen) stream was continuously supplied to the reactor Reaction time: 1 h	100%	Martínez et al. (2011)
Photocatalysis Whey stabilized TiO ₂ and ZnO	Carbamazepine	295 ng L ⁻¹	Batch photoreactor with immobilized film	Photocatalytic geometric surface: 1 cm ² UV light with intensity of 6.9 mW cm ⁻² at peak wavelength of 254 nm Reaction time: 2 h	100% for TiO ₂ and 92% for ZnO after 55 min	Mohapatra et al. (2014a)
Photocatalysis TiO ₂	Sulfamethoxazole	10–50 mg L ⁻¹	Fixed-bed recirculating photoreactor	Photocatalytic geometric surface: 190 cm ² 250 mL aqueous solution Flow rate: 0.11–0.48 L min ⁻¹ 18 W UV lamp (peak intensity at 365 nm) or 18 W white lamp (400–600 nm and insignificant amount of 365 nm) Reaction time: 7.5 h	100% for 10 ppm of SFX	Ahmed et al. (2014)
Photocatalysis TiO ₂ and Fe ₂ O ₃	Oxytetracycline	20 mg L ⁻¹	Fixed-bed recirculating photoreactor	Photocatalytic geometric surface: 190 cm ² 1.8 L aqueous solution Flow rate: 0.42–1.67 L min ⁻¹ 1700 W Xenon lamp with solar spectrum (radiation intensity at the	100% for TiO ₂ and >90% for Fe ₂ O ₃	Díez et al. (2018)

(continued on next page)

Table 6 (continued)

Degradation process and catalyst	Pharmaceutical compound(s)	Initial concentration	Reactor type	Experimental conditions	Removal of the starting compound [%]	Ref.
Photocatalysis TiO ₂	Iopromide acetaminophen sulfamethoxazole carbamazepine	50 µg L ⁻¹ each	Fixed-bed continuous-flow photoreactor	photoreactor surface of 44 W m ⁻²) 77 mg L ⁻¹ H ₂ O ₂ for TiO ₂ and 154 mg L ⁻¹ H ₂ O ₂ for Fe ₂ O ₃ Reaction time: 180 min for TiO ₂ and 40 min for Fe ₂ O ₃ Photocatalytic geometric surface: 469 cm ² 325 mL reactor volume Flow rate: 2.7 mL/min 5–15 W UV-A lamps with spectrum centered at ~365 nm pH 8.2 Reaction time: 7 days	In the continuous-flow mode only the overall reactor and photocatalyst stability was evaluated. App. 60–90% of pharmaceuticals were degraded 99%	Carbonaro et al. (2013)
Photocatalysis TiO ₂ @nZVI/persulfate	Amoxicillin	20 mg L ⁻¹	Batch photoreactor	1000 mg L ⁻¹ of photocatalyst 50 mL aqueous solution containing 0.5 mM of persulfate 10 W UV lamp (peak intensity at 254 nm) pH 5.0 Reaction time: 1 h		Diao et al. (2021)
Photocatalysis TiO ₂	Diclofenac	2.37 mg L ⁻¹	Batch photoreactor	105 mg of photocatalyst 80 mL aqueous suspension UV light with intensity of 3.04 × 10 ⁻⁷ E s ⁻¹ at peak wavelength of 365 nm pH 6.0 Reaction time: 3 h	100% in 156 min	Perisic et al. (2016)
Photocatalysis TiO ₂	Diclofenac	5–20 mg L ⁻¹	Batch photoreactor	17.5 mg of photocatalyst 350 mL aqueous suspension 9 W UVA (350–400 nm) light with intensity of 3.37 × 10 ⁻⁶ E s ⁻¹ pH 6.0 Reaction time: 4 h	85%	Achilleos et al. (2010)
Photocatalysis TiO ₂	Sulfamethoxazole	10 mg L ⁻¹	Batch photoreactor	500 mg of biochar supported TiO ₂ 100 mL aqueous suspension 15 W UV lamp (peak intensity at 254 nm) pH 4 Reaction time: 6 h	91%	Kim and Kan (2016)
Photocatalysis TiO ₂	Sulfamethoxazole trimethoprim	0.4 mg L ⁻¹ of each	Continuous photoreactor with air purging	0.05 mg L ⁻¹ of photocatalyst 500 mL reactor volume Flow rate: 8 mL/min 32 W UV light with intensity of 4.32 × 10 ³ mW cm ⁻² at peak wavelength of 365 nm Reaction time: 5 h	90% in 20 min	Cai and Hu (2017)
Photocatalysis TiO ₂ /Fe ⁰	Ciprofloxacin (simultaneously with Cr(VI) reduction)	30 mg L ⁻¹ of ciprofloxacin and 20 mg L ⁻¹ of Cr(VI)	Batch photoreactor	1000 mg L ⁻¹ of photocatalyst 10 W UV lamp (peak intensity at 254 nm) pH 3.0 Reaction time: 1 h	95% of ciprofloxacin and 98% of Cr(VI)	Diao et al. (2017)
Electrocatalysis BDD anode Zr cathode	Ciprofloxacin sulfamethoxazole salbutamol	69 µmol L ⁻¹	Recirculating electrocatalytic reactor	BDD anode geometric surface: 69 cm ² Distance between the electrodes: 10 mm 1 L aqueous solution 0.1 M (pH 4, adjusted with H ₂ SO ₄) or 0.02 M K ₂ SO ₄ Applied current density: 0.72–7.24 mA/cm ² Flow rate: 6 L min ⁻¹ Reaction time: 5 h	100%	Lan et al. (2018)
Electrocatalysis Ti/Pt or Ti/PbO ₂ anodes and carbon felt	Carbamazepine	4.5 µg L ⁻¹	Recirculating electrocatalytic reactor	Anode geometric surface area: 130 cm ² Distance between the electrodes: 10 mm	75% for Ti/PbO ₂ anodes	Guitaya et al. (2017)

(continued on next page)

Table 6 (continued)

Degradation process and catalyst	Pharmaceutical compound(s)	Initial concentration	Reactor type	Experimental conditions	Removal of the starting compound [%]	Ref.
covered with titanium cathode				Anode surface area to reactor volume: 1.9 m ² /m ³ 500 mg L ⁻¹ Na ₂ SO ₄ Flow rate: 1–6 L min ⁻¹ Applied current: 1–3 A Reaction time: 100 min		
Electrocatalysis BDD anode and stainless-steel cathode	Amoxicillin	1000 or 2000 mg L ⁻¹	Batch electrocatalytic reactor	BDD anode geometric surface: 10 cm ² Distance between the electrodes: 15 mm 0.2 L aqueous solution with 2–4 g L ⁻¹ NaCl Applied current density: 30–50 mA/cm ² Reaction time: 1.5 h	84.1%	Frontistis et al. (2017)
Electrocatalysis Nb/BDD or Ti/IrO ₂ anode and Ti mesh cathode	Carbamazepine	10 mg L ⁻¹	Recirculating electrocatalytic reactor	Anode geometric surface area: 62 cm ² Distance between the electrodes: 5 mm 2 L aqueous solution with 7 or 14 mM NaCl Flow rate: 0.8 L min ⁻¹ Applied current: 0.5–1.5 A Reaction time: 30 min	88.7%	García-Espinoza et al. (2018)
Electrocatalysis BDD anode and cathode	Iopromide, sulfamethoxazole, 17- α -ethinyloestradiol, diclofenac	0.5 or 10 mg L ⁻¹ of each component	Recirculating electrocatalytic reactor	Electrodes geometric surface area: 189 cm ² 10 L of simulated or real waste water Flow rate: 250 L min ⁻¹ Applied current: 0.9 A Reaction time: 180 min	32.3%–73.7%	Loos et al. (2018)
Electrocatalysis BDD anode and stainless-steel cathode	Losartan	377 mol/L	Batch electrocatalytic reactor	Anode geometric surface area: 5 cm ² Distance between the electrodes: 10 mm 100 mL aqueous solution with 0.05 M Na ₂ SO ₄ Applied current density: 10 mA cm ⁻² pH 7 Reaction time: 360 min	100%	Salazar et al. (2016)
Electrocatalysis CuO/TiO ₂ /Al ₂ O ₃ /RVC anode and RVC cathode	Paracetamol	96 mg L ⁻¹	Batch electrocatalytic reactor	Anode geometric surface area: 3 cm ² Ag/AgCl reference electrode 150 mL aqueous solution with 10 mM H ₂ O ₂ and 0.5 M Na ₂ SO ₄ Electrode potential of 1.3 V vs. SCE pH 5 Reaction time: 1 h	98%	Arredondo Valdez et al. (2012)
Electrocatalysis Boron doped graphene anode and Cu cathode	Acetaminophen	10 mg L ⁻¹	Batch electrocatalytic reactor	Anode geometric surface area: 2.5 cm ² Distance between the electrodes: 15 mm 200 mL aqueous solution with 17 mM NaCl Applied current: 20 mA Reaction time: 90 min	100%	(Q. Zhang et al., 2020b)
Electrocatalysis g-C ₃ N ₄ /Ti/PbO ₂ anode and Ti cathode	Acetaminophen	100 mg L ⁻¹	Batch electrocatalytic reactor	Anode geometric surface area: 15 cm ² Distance between the electrodes: 20 mm 1 L aqueous solution with 6 g L ⁻¹ Na ₂ SO ₄ Current density: 15 mA cm ⁻² pH 7 Reaction time: 3 h	83%	(S. Chen et al., 2021)
Photoelectrocatalysis TiO ₂ anode, Pt cathode	Tetracycline	10 mg L ⁻¹	Batch photoelectrocatalytic reactor	Catalyst (anode) geometric surface area: less than 10 cm ² Ag/AgCl reference electrode 20 mL aqueous solution with 20 mM Na ₂ SO ₄	80%	Liu et al. (2009)

(continued on next page)

Table 6 (continued)

Degradation process and catalyst	Pharmaceutical compound(s)	Initial concentration	Reactor type	Experimental conditions	Removal of the starting compound [%]	Ref.
Photoelectrocatalysis Reduced TiO ₂ anode, Pt cathode	Diclofenac	5 mg L ⁻¹	Batch photoelectrocatalytic reactor with air purging	Electric bias: 0.5 V 4 W UV light with intensity of 2.5 mW cm ⁻² and peak wavelength of 254 nm pH 5.5 Reaction time: 3 h Catalyst (anode) geometric surface area: 4 cm ² SCE reference electrode 80 mL aqueous solution with 0.1 M Na ₂ SO ₄ Electric bias: 0.4 V 35 W Xenon lamp Reaction time: 12 h	100% in 8 h	Cheng et al. (2016)
Photoelectrocatalysis TiO ₂ anode, Pt cathode	Tetracycline	20–120 mg L ⁻¹	Fixed-bed recirculating photoelectrocatalytic reactor	Catalyst (anode) geometric surface area: less than 20 cm ² Ag/AgCl reference electrode 50 mL aqueous solution with 0.1 M Na ₂ SO ₄ Flow rate: 10 mL/min Electric bias: 2 V 4 W UV light with intensity of 5 mW cm ⁻² and peak wavelength of 254 nm pH 8 Reaction time: 1 h	96.4% for 20 mg L ⁻¹ and 54.8% for 120 mg L ⁻¹	Bai et al. (2010)
Photoelectrocatalysis N-doped TiO ₂ anode, 2 vitreous carbon plates cathodes	Chlortetracycline	100 µg L ⁻¹	Fixed-bed recirculating photoelectrocatalytic reactor	Catalyst (anode) geometric surface area: 24 cm ² 1 L aqueous solution with 0.07 M Na ₂ SO ₄ Flow rate: 250 mL/min Applied electric current: 0.1–0.8 A AM 1.5 solar illumination conditions (150 W xenon lamp) Reaction time: 20–240 min	99.6% in 180 min	(Rimeh Dagherir et al., 2013)
Photoelectrocatalysis TiO ₂ anode, Pt cathode	Acyclovir	20 mg L ⁻¹	Continuous-flow photoelectrocatalytic reactor	Catalyst (anode) geometric surface area: less than 0.785 cm ² Ag/AgCl reference electrode 100 µL aqueous solution with 0.2 M NaNO ₃ Electric bias: 1 V UV light with intensity of 10 mW cm ⁻² and peak wavelength of 365 nm Reaction time: 0–370 s	97.1% at 370 s residence time	Nie et al. (2013)
Photoelectrocatalysis TiO ₂ anode, Pt cathode	Tetracycline	120 mg L ⁻¹	Fixed-bed recirculating photoelectrocatalytic reactor	Catalyst (anode) geometric surface area: 40 cm ² 50 mL aqueous solution with 0.1 M Na ₂ SO ₄ Electric bias: 2 V UV light with intensity of 5 mW cm ⁻² and peak wavelength of 355 nm Reaction time: 2 h	54.8% in 1 h	Bai et al. (2010)
Photoelectrocatalysis Sb-doped Sn80%- W20%-oxide anode, Stainless-steel cathode	Carbamazepine	0.2 mg L ⁻¹	Batch photoelectrocatalytic reactor	Catalyst (anode) geometric surface area: less than 50 cm ² 550 mL aqueous solution with 0.1 M KH ₂ PO ₄ Current densities of 1, 2, 4, 6 and 10 mA/cm ² 10 W UV lamp with peak wavelength of 254 nm pH 7 Reaction time: 1 h	100%	Ghasemian et al. (2017)

(continued on next page)

Table 6 (continued)

Degradation process and catalyst	Pharmaceutical compound(s)	Initial concentration	Reactor type	Experimental conditions	Removal of the starting compound [%]	Ref.
Photoelectrocatalysis BiVO ₄ /Ag ₂ S anode, Pt cathode	Ciprofloxacin sulfamethoxazole	10 mg L ⁻¹	Batch photoelectrocatalytic reactor	Catalyst (anode) geometric surface area: less than 6.5 cm ² Ag/AgCl reference electrode 70 mL aqueous solution with 0.1 M Na ₂ SO ₄ Electric bias: 0.2–1.5 V Solar illumination conditions (100 W xenon lamp) pH 7 Reaction time: 2 h	80% for ciprofloxacin and 86% for sulfamethoxazole at 1.2 V	Orimolade and Arotiba (2020)
Photoelectrocatalysis Cu ₂ O/TiO ₂ anode, Pt cathode	Ibuprofen	10 mg L ⁻¹	Batch photoelectrocatalytic reactor	Catalyst (anode) geometric surface area: 2 cm ² Ag/AgCl reference electrode Electric bias: 0.5 V 100 W Hg lamp Reaction time: 4 h	100% of ibuprofen removal after 1.5 h and ~50 of mineralization (TOC decay) after 4 h	Chang et al. (2016)
Photoelectrocatalysis I and P co-doped TiO ₂ anode and stainless steel cathode	Tetracycline	10 mg L ⁻¹	Batch photoelectrocatalytic reactor	Catalyst (anode) geometric surface area: 30 cm ² 100 mL aqueous solution with 0.1 M Na ₂ SO ₄ Electric bias: 1.4 V Metal halide lamp with 420 nm cut-off filter (average light intensity: 30 mW cm ⁻²) pH 7 Reaction time: 3 h	100%	Liu et al., 2021
Photoelectrocatalysis Cu/TiO ₂ anode, Pt cathode	Diclofenac	5 mg L ⁻¹	Batch photoelectrocatalytic reactor	Catalyst (anode) geometric surface area: 1 cm ² Ag/AgCl reference electrode 50 mL aqueous solution with 0.1 M Na ₂ SO ₄ Electric bias: 0.5 V 300 W xenon arc lamp with intensity on the photoanode surface of 100 mW cm ⁻² pH 6.2 Reaction time: 6 h	71%	Hua et al. (2016)
Photoelectrocatalysis TiO ₂ /Ti anode and Pt cathode	Sulfamethoxazole	2 mg L ⁻¹	Batch photoelectrocatalytic reactor	Catalyst (anode) geometric surface area: 4 cm ² Ag/AgCl reference electrode 50 mL aqueous solution with 0.01 M NaCl 4 W UVA lamp pH 5.4 Reaction time: 70 min	100%	Su et al., 2016
Photoelectrocatalysis g- C ₃ N ₄ /TiO ₂ anode and Pt cathode	Tetracycline	10 mg L ⁻¹	Batch photoelectrocatalytic reactor	Catalyst (anode) geometric surface area: 4 cm ² Ag/AgCl reference electrode 50 mL aqueous solution with 0.5 M Na ₂ SO ₄ Electric bias: 1 V 300 W Xe lamp (200–800 nm) Reaction time: 2 h	100%	Tang et al. (2020)
Photoelectrocatalysis Cu ₂ O/TiO ₂ anode, Pt cathode	Ciprofloxacin	10 mg L ⁻¹	Batch photoelectrocatalytic reactor	Catalyst (anode) geometric surface area: 15 cm ² Ag/AgCl reference electrode 50 mL aqueous solution with 0.1 M Na ₂ SO ₄ Electric bias: 1.5 V Solar simulator with a 400 nm cut-off filter pH 6 Reaction time: 4 h	73%	Koiki et al. (2020)

(continued on next page)

Table 6 (continued)

Degradation process and catalyst	Pharmaceutical compound(s)	Initial concentration	Reactor type	Experimental conditions	Removal of the starting compound [%]	Ref.
Photoelectrocatalysis TiO ₂ /Ti anode stainless steel cathode	5-fluorouracil	~5 mg L ⁻¹	Batch photoelectrocatalytic reactor	Catalyst (anode) geometric surface area: 4 cm ² Ag/AgCl reference electrode 80 mL aqueous solution with 42 mM Na ₂ SO ₄ Electric bias: 1 V Solar simulator equipped with a xenon lamp with irradiation intensity 4.5 mW cm ⁻² pH 6.4 Reaction time: 3 h	100%	Mazierski et al. (2019)
Photoelectrocatalysis CuS/TiO ₂ anode and Pt cathode	Penicillin G	5 mg L ⁻¹	Batch photoelectrocatalytic reactor	Catalyst (anode) geometric surface area: 4 cm ² SCE reference electrode 80 mL aqueous solution with 0.1 M Na ₂ SO ₄ Electric bias: 0.4 V Xenon lamp (35 W) with a 420 nm cut-off filter Reaction time: 2.5 h	99%	Ma et al. (2018)

with a small gap in between where the generated reactive oxygen species degrade the pollutants when a potential bias is applied. On the other hand, photocatalytic reactors require a light source that has to illuminate the largest possible area of a photocatalyst with light of sufficient energy to excite the electrons in the photocatalyst in use. Due to the light illumination requirement, photocatalytic reactors have to be at least in part made of a transparent material. In general, photocatalytic reactors can be classified based on the photocatalyst form. Slurry reactors have suspended photocatalytic nanoparticles, whereas photocatalytic reactors with immobilized photocatalysts have the catalyst attached to the support via physical surface forces or chemical bonds. Immobilized photocatalytic reactors can be further divided into different types of fixed-bed reactors like monolith reactors, thin-film reactors and packed-bed reactors. Both main photocatalytic reactor types possess certain advantages and/or disadvantages. Slurry reactors provide a high surface area of photocatalyst per unit volume and therefore exhibit a larger photocatalytic activity than the immobilized photocatalyst reactors. However, the most important advantage of the latter reactor types is that they do not require catalyst recovery and permit the continuous use of the photocatalyst. Furthermore, immobilized photocatalysts can also be used for photoelectrocatalytic degradation if they are incorporated into a photoelectrocatalytic reactor. This reactor type is the most difficult to design since an effective photoelectrocatalytic reactor has to ensure an efficient exposure of the photocatalyst to irradiation, good contact between the illuminated catalyst and water, the optimal position and relative surface area of anode(s) and cathode(s) as well as optimal photocatalytic surface-to-volume ratio. In the case of a large-scale reactor, mixing and mass-transfer limitations also need to be considered.

Regardless of the degradation process and the catalyst form, various catalytic reactors can be operated in a continuous-flow or batch mode. The most common types of catalytic reactors used for the degradation of pharmaceuticals are shown in Fig. 17.

Regardless of the degradation process, catalytic reactors can be operated in a continuous-flow or batch mode. A degradation reaction inside a continuous-flow reactor can be efficiently controlled by the flow rate of the treated fluid, whereas in batch mode the reaction time is the parameter mostly used to control the degradation process. In Fig. 18, all the most important parameters for the photocatalytic, electrocatalytic and photoelectrocatalytic degradation of pharmaceuticals are shown together with the most frequently used values. As is clear from Fig. 18, the photoelectrocatalytic process is the most complicated one, which is why there are the fewest reactor-design variations developed for this

type of process.

Finally, Table 6 shows the results of the degradation of pharmaceuticals by photocatalysis, electrocatalysis and photoelectrocatalysis published in the literature. The degradation of pharmaceutical compounds with different initial concentrations was performed in many reactor types with one of the three degradation processes covered in this review paper. The operating conditions influencing the degradation process are also listed. Based on the published literature, it can be concluded that all the photocatalytic experiments were carried out at 20–25 °C and mixing in the reactor is usually achieved with a Teflon-covered stirring bar when needed. In the case of the flow reactors, the mixing is achieved with the flow of the treated water. If recirculating conditions are used, the flow rate does not influence the degradation rate (Ahmed et al., 2014). On the other hand, the degradation rate strongly depends on the flow rate in the case of a continuous-flow reactor. However, when studying the degradation process, the residence time is commonly selected so that 50–90% degradation of the target micropollutants is achieved, since this range of micropollutant degradation permits better quantification of the matrix effects than if the design was based on a higher level of treatment where changes in catalyst activity would be more difficult to quantify (Carbonaro et al., 2013). The use of UVC light significantly increases the degradation rate, when compared to the degradation rate when UVA or solar light is used. Furthermore, the degradation under UV irradiation is more effective than under near-UV-Vis (Martínez et al., 2011). The reason for the better results achieved using UVC irradiation is the high degradation rate achieved with direct photolysis alone (Kim and Kan, 2016). In any case, it can be seen in Table 4 that although a 100% degradation of the starting pharmaceutical compounds can be achieved, this does not indicate the overall quality of the degradation process. More attention should be paid to the formation of intermediate products, which can be even more harmful and resistant to different subsequent water treatments. A study by Porcar-Santos et al. (2020) shows that reactive halogen species can form from chlorine and bromine radicals when using TiO₂ to treat pharmaceuticals in seawater. The generation of reactive halogen species resulted in the formation and accumulation of harmful halogenated organic byproducts. For identification purposes, the photocatalytic decomposition of pharmaceuticals is usually conducted in batch mode with optimal catalyst loading and sufficient reaction time to ensure the amount of intermediates generated is above the LC-MS-MS and GC-MS detection limit (Cai and Hu, 2017). The working conditions where enough intermediate products are formed depend on

the photoreactor's geometry and the amount of catalyst. However, the degradation rate is generally found to increase with the photocatalyst concentration towards a limiting value at relatively high concentrations.

Electrocatalytic degradation studies mainly use the BDD electrodes as anodes and titanium or stainless steel as cathodes for the degradation of pharmaceuticals. When simulated or real wastewater is not used as the matrix solution, NaCl or Na₂SO₄ are used as supporting electrolytes. NaCl increases the degradation rate through the indirect oxidation by electro-generated active chlorine, which is accelerated in acidic media in comparison to alkaline media (Brillas and Sirés, 2015). Guitaya et al. (2017) determined that the anode type is the most important parameter affecting the pharmaceutical degradation rate followed by the treatment time, the applied current, and then the recirculation flow rate.

Few papers have reported the treatment of pharmaceuticals solutions by photoelectrocatalysis. All of them report on the better performance of photoelectrocatalytic process when compared to photocatalytic and electrocatalytic processes. A significant synergetic effect usually results in at least a five-times higher degradation-rate constant than the one of the photocatalytic process using the same catalytic material. Studies also show that the photoelectrocatalytic method results in lower levels of intermediate transformation products than the photolytic and photocatalytic methods. This suggests a potentially lower overall toxicity of the final solution when treated by the photoelectrocatalytic method. Furthermore, the photoelectrocatalytic process was determined to be the most energy efficient (Ghasemian et al., 2017). However, similar to the results of the photocatalytic degradation, continuous-flow reactors are very rarely used for the photoelectrocatalytic degradation of pharmaceuticals since one pass of the treated pharmaceutical solution through the reactor is not enough to degrade a relatively high concentration of pharmaceuticals at low retention times/high flow rates with the catalysts and reactor designs developed so far. Therefore, continuous-flow reactors (also listed in Table 6) have a very small volume of less than 1 mL to intensify the degradation reaction of the pharmaceuticals (Nie et al., 2013). It can be concluded that the currently developed catalysts and reactors are not applicable yet for the treatment of large wastewater volumes existing in sewage treatment plants.

6. Prospects

In this review major aspects involving the degradation of pharmaceuticals by photocatalysis, electrocatalysis and photoelectrocatalysis are discussed and the main challenges were indicated. Based on the information reported, the following can be prospect:

- Since the analytical methods to determine pharmaceuticals concentration in aquatic media are already well established, regulation limits should be addressed by environmental agencies to regulate the discharge of these compounds in the aquatic environment. However, the lack of techniques capable of efficiently treating these compounds in large scale still limits this regulation. For now, the analytical techniques are utilized for scientists to monitor the presence of pharmaceuticals in the environment. They are also a powerful instrument to evaluate the efficiency of new treatment techniques.
- Theoretical modeling of PC, EC and PEC from first principles remains limited to small molecules; instead, the theory is used solely to provide partial insights into the catalyst or substrate structure (such as HOMO/LUMO) but not their interplay. The studies regarding theoretical calculations and modeling methods should attract much more attention. These tools are useful for a deeper understanding of the mechanism and charge-migration kinetics in the catalysts. Further advances in theoretical calculations are highly desirable to understand more complex systems, such as water and wastewater contaminated with pharmaceuticals.
- The existing photocatalytic materials feature various drawbacks such as high cost, large bandgaps, low active surface area, limited

reusability, etc. Significant challenges still remain in the development of new, efficient and low cost catalysts, capable to be applied and produced on large scale for practical applications, is one of the key research goals.

- Future research directions in this field should be focused on cost-effective systems for treating large amounts of effluents in studies using more complex matrices (and not pure aqueous solutions), to enable scaling-up of this technology.

7. Conclusions

Based on the information reported in this review, it can be concluded that water and wastewater containing pharmaceuticals can be effectively treated by photocatalysis, electrocatalysis and photoelectrocatalysis. These processes have been extensively studied by several researcher groups and evaluated for the treatment of a wide range of pharmaceuticals compounds. The analytical tools necessary for the evaluation of the processes are well developed and the HPLC analysis is the most common one to determine pharmaceuticals concentration decay during the treatment. The toxicity tests are also well established; however, they are not present in great part of the revised works. The evaluation of oxidative and reductive species formed during the catalytic reaction and theoretical modeling, help to provide a full view of the degradation process and become more popular in recent years. There is a wide variety of catalyst materials already synthesized and well characterized, but only a few are available on commercial scale. Among them TiO₂ and BDD are the most utilized catalysts for photocatalysis and electrocatalysis, respectively. Furthermore, the development of strongly attached photocatalysts, such as TiO₂ nanotubes, on conductive materials, as BDD, forming heterostructured materials, seems to be a good way to overcome some limitations of these treatment technologies. Different reactor designs can be chosen for applications in PC, EC and PEC, however, the great majority of the studied reactors are capable to treat only a few milliliters of simulated effluent (or pure aqueous solutions), posing a major challenge for applications in larger and real scale. In conclusion, we have summarized recent work related to PC, EC and PEC and their application of pharmaceuticals in aqueous media. The studies in this field provide a meritorious platform for accelerating the practical applications of these techniques. We hope that this review can stimulate further exploration of these techniques to fulfill the present challenges.

Declaration of competing interest

The authors declare that they have no known competing financial interests or personal relationships that could have appeared to influence the work reported in this paper.

Acknowledgements

The authors gratefully acknowledge the Slovenian Research Agency (ARRS) for financial support within the research program P2-0084 and project L2-2614. B.L. and M.H. appreciate ARRS core funding (P2-0152) and ARRS infrastructure funding (I0-0039).

Nomenclature

1D	One-dimensional shape
2D	Two-dimensional shape
3D	Three-dimensional shape
ADWG	Australian drinking water guidelines
AES	Auger electron spectroscopy
AFM	Atomic force microscopy
ALIE	Average local ionization energy
AMX	Amoxicillin
AO	Anodic oxidation

AOPs	Advanced oxidation processes	MEP	Molecular electrostatic potential
B3LYP	Becke, 3-parameter, Lee–Yang–Parr	MET	Metoprolol tartrate
BC	Biochar	MW-CVD	Microwave plasma chemical vapor deposition
BCN	Bulk carbon nitride	N	Number of electrons
BDD	Boron-doped diamond	NPA	Natural population analysis
BDEs	Bond-dissociation energies	NPX	Naproxen
BET	Brunauer-Emmett-Teller surface area analysis	nZVI	Nano zerovalent iron
CBZ	Carbamazepine	ORR	Oxygen-reduction reaction
CCN	Crystalline carbon nitride	OTC	Oxytetracycline
CFO	Cofe ₂ O ₄	PBE	Perdew–Burke–Ernzerhof functional
CN	G-C ₃ N ₄	PC	Photocatalysis
CNBB-5	Bi ₂ O ₂ CO ₃ /g-C ₃ N ₄ /Bi ₂ O ₃	PEC	Photoelectrocatalysis
COD	Chemical oxygen demand (mg L ⁻¹)	PhP	Phenazopyridine
CPCM	Conductor-like polarizable continuum model	pH _{pzc}	Ph of the zero point charge
CV	Capacitance–voltage profiling	PIN	Pindolol
CVD	Chemical vapor deposition	pKa	Negative log base ten of the acid dissociation constant value
DCF	Diclofenac	PMS	Peroxymonosulfate
DFT	Density functional theory	ppb	Parts per billion
DMPO	5,5-Dimethyl-1-pyrroline N-oxide	ppm	Parts per million
DRS	Diffuse reflectance spectroscopy	PRCP	Pharmaceuticals and personal-care products
E _{anod}	Anodic potential	PRO	Propranolol hydrochloride
EAOPs	Electrochemical advanced oxidation processes	PZC	Point of zero charge
EC	Electrocatalysis	rGO	Reduced graphene oxide
EC	European commission	RVC	Reticulated vitreous carbon
EDTA	Ethylenediamine tetraacetic acid	SCE	Saturated calomel electrode
EELS	Electron energy loss spectroscopy	SEM	Scanning electron microscope
EEO	Electrical Energy per Order	SGN	Sulfur-doped graphene
E _F	Fermi energy levels	SIMS	Secondary ion mass spectrometry
EIS	Electrochemical impedance spectroscopy	SPE	Solid-phase extraction
ELF	Electronic location function	SPME	Solid-phase microextraction
E°	Standard reduction potential	STM	Scanning tunneling microscopy
EPMA	Electron probe microanalysis	TC	Tetracycline
EPR	Electron paramagnetic resonance	TEB	Triethylborate
ERD	Elastic recoil detection	TEM	Transmission electron microscopy
ERE	Electron reorganization energy	TEMP	2,2,6,6-tetramethylpiperidine
EU	European union	TGA	Thermogravimetric analysis
f(r)	Fukui function	TMB	Trimethylborate
FMO	Frontier molecular orbital	TOC	Total organic carbon (mg L ⁻¹)
FTIR	Fourier-transform infrared spectroscopy	TPB	Tripropylborate
GC	Gas chromatography	TRL	Technology readiness level
GO	Graphene oxide	UCMR	Unregulated contaminant monitoring rule (usa)
HA	Humic acid	UPLC	Ultra performance liquid chromatography
HF-CVD	Hot-filament chemical vapor deposition	UPS	Ultraviolet photoelectron spectroscopy
HOMO	Highest occupied molecular orbital	UV	Ultraviolet
HPLC	High performance liquid chromatography	UVA	Ultraviolet A
HPLC-DAD	High performance liquid chromatography with diode-array detection	UVC	Ultraviolet C
HPLC-UV	High performance liquid chromatography with UV detector	Vis	Visible
HRE	Hole reorganization energy	WWTPs	Water- and wastewater-treatment plants
HRTEM	High resolution transmission electron microscopy	XPS	X-ray photoelectron spectroscopy
IBP	Ibuprofen	XRD	X-ray diffraction analysis
IEFPCM	Integral equation formalism version of the polarizable continuum model	μ	Electronic chemical potential
LC/MS/MS	Liquid chromatography tandem mass spectrometry	ν	Constant external potential
LC-MS	Liquid chromatography mass spectrometry	ρ(r)	Electron density
LC-QTOF MS	Liquid chromatography quadrupole time-of-flight mass spectrometry		
LC-QTOF-MS-MS	Liquid chromatography tandem quadrupole time-of-flight mass spectrometry		
LDA	Local-density approximations		
LDH	Layered double hydroxide		
LED	Light-emitting diode		
LLE	Liquid-liquid extraction		
LLME	Liquid-liquid micro-extraction		
LUMO	Lowest unoccupied molecular orbital		
MEM	Memantine		

References

- Abdel-Wahab, A.M., Al-Shirbini, A.S., Mohamed, O., Nasr, O., 2017. Photocatalytic degradation of paracetamol over magnetic flower-like TiO₂/Fe₂O₃ core-shell nanostructures. *J. Photochem. Photobiol. Chem.* 347, 186–198. <https://doi.org/10.1016/j.jphotochem.2017.07.030>.
- Abdurahman, M.H., Abdullah, A.Z., 2020. Mechanism and reaction kinetic of hybrid ozonation-ultrasonication treatment for intensified degradation of emerging organic contaminants in water: a critical review. *Chem. Eng. Process. - Process Intensif.* 154, 108047. <https://doi.org/10.1016/j.cep.2020.108047>.
- Achard, J., Tallaire, A., 2018. Diamond wafer technologies for semiconductor device applications. In: Koizumi, S., Umezawa, H., Pernot, J., Suzuki, M. (Eds.), *Power Electronics Device Applications of Diamond Semiconductors*. Elsevier Ltd., pp. 1–97. <https://doi.org/10.1016/b978-0-08-102183-5.00001-7>

- Achilleos, A., Hapeshi, E., Xekoukoulotakis, N.P., Mantzavinos, D., Fatta-Kassinos, D., 2010. Factors affecting diclofenac decomposition in water by UV-A/TiO₂ photocatalysis. *Chem. Eng. J.* 161, 53–59. <https://doi.org/10.1016/j.cej.2010.04.020>.
- Ahmed, O., Pons, M.N., Lachheb, H., Houas, A., Zahraa, O., 2014. Degradation of sulfamethoxazole by photocatalysis using supported TiO₂. *Sustain. Environ. Res.* 24, 381–387.
- Alharbi, S.K., Price, W.E., 2017. Degradation and fate of pharmaceutically active contaminants by advanced oxidation processes. *Curr. Pollut. Reports* 3, 268–280. <https://doi.org/10.1007/s40726-017-0072-6>.
- Almquist, C.B., Biswas, P., 2002. Role of synthesis method and particle size of nanostructured TiO₂ on its photoactivity. *J. Catal.* 212, 145–156. <https://doi.org/10.1006/jcat.2002.3783>.
- Andreozzi, R., Caprio, V., Ciniglia, C., De Champdoré, M., Lo Giudice, R., Marotta, R., Zuccato, E., 2004. Antibiotics in the environment: occurrence in Italian STPs, fate, and preliminary assessment on algal toxicity of amoxicillin. *Environ. Sci. Technol.* 38, 6832–6838. <https://doi.org/10.1021/es049509a>.
- Antonopoulou, M., Kosma, C., Albanis, T., Konstantinou, I., 2021. An overview of homogeneous and heterogeneous photocatalysis applications for the removal of pharmaceutical compounds from real or synthetic hospital wastewaters under lab or pilot scale. *Sci. Total Environ.* <https://doi.org/10.1016/j.scitotenv.2020.144163>.
- Armaković, S.J., Armaković, S., Sibul, F., Cetojević-Simin, D.D., Tubić, A., Abramović, B. F., 2020. Kinetics, mechanism and toxicity of intermediates of solar light induced photocatalytic degradation of pindolol: experimental and computational modeling approach. *J. Hazard Mater.* 393, 122490. <https://doi.org/10.1016/j.jhazmat.2020.122490>.
- Armaković, S.J., Grujić-Brojin, M., Šćepanović, M., Armaković, S., Golubović, A., Babić, B., Abramović, B.F., 2019. Efficiency of La-doped TiO₂ calcined at different temperatures in photocatalytic degradation of β-blockers. *Arab. J. Chem.* 12, 5355–5369. <https://doi.org/10.1016/j.arabj.2017.01.001>.
- Arredondo Valdez, H.C., García Jiménez, G., Gutiérrez Granados, S., Ponce de León, C., 2012. Degradation of paracetamol by advance oxidation processes using modified reticulated vitreous carbon electrodes with TiO₂ and CuO/TiO₂/Al₂O₃. *Chemosphere* 89, 1195–1201. <https://doi.org/10.1016/j.chemosphere.2012.07.020>.
- Askari, S.J., 2012. Development of CVD diamond thin films on titanium substrate and study their tribological behavior. In: *Advanced Materials Research*, pp. 1994–1997. <https://doi.org/10.4028/www.scientific.net/AMR.399-401.1994>.
- Atkinson, A.J., Apul, O.G., Schneider, O., Garcia-Segura, S., Westerhoff, P., 2019. Nanobubble technologies offer opportunities to improve water treatment. *Acc. Chem. Res.* <https://doi.org/10.1021/acs.accounts.8b00606>.
- AttariKhasraghi, N., Zare, K., Mehrizad, A., Modirshahla, N., Behnadjy, M.A., 2021. Zeolite 4A supported CdS/g-C₃N₄ type-II heterojunction: a novel visible-light-active ternary nanocomposite for potential photocatalytic degradation of cefoperazone. *J. Mol. Liq.* 342, 117479. <https://doi.org/10.1016/j.molliq.2021.117479>.
- Attia, Y.A., Mohamed, Y.M.A., 2019. Silicon-grafted Ag/AgX/rGO nanomaterials (X = Cl or Br) as dip-photocatalysts for highly efficient p-nitrophenol reduction and paracetamol production. *Appl. Organomet. Chem.* 33, e4757. <https://doi.org/10.1002/aoc.4757>.
- Awfa, D., Ateia, M., Fujii, M., Johnson, M.S., Yoshimura, C., 2018. Photodegradation of pharmaceuticals and personal care products in water treatment using carbonaceous-TiO₂ composites: a critical review of recent literature. *Water Res.* <https://doi.org/10.1016/j.watres.2018.05.036>.
- Awofiranye, O.S., Modise, S.J., Naidoo, E.B., 2020. Overview of polymer-TiO₂ catalyst for aqueous degradation of pharmaceuticals in heterogeneous photocatalytic process. *J. Nanoparticle Res.* 22 <https://doi.org/10.1007/s11051-020-04877-9>.
- Babić, S., Zrnić, M., Ljubas, D., Čurković, L., Škorić, I., 2015. Photolytic and thin TiO₂ film assisted photocatalytic degradation of sulfamethazine in aqueous solution. *Environ. Sci. Pollut. Res.* 22, 11372–11386. <https://doi.org/10.1007/S11356-015-4338-5/FIGURES/8>.
- Bai, J., Liu, Y., Li, J., Zhou, B., Zheng, Q., Cai, W., 2010. A novel thin-layer photoelectrocatalytic (PEC) reactor with double-faced titania nanotube arrays electrode for effective degradation of tetracycline. *Appl. Catal. B Environ.* 98, 154–160. <https://doi.org/10.1016/j.apcatb.2010.05.024>.
- Behraves, S., Mirghaffari, N., Alemrajabi, A.A., Davar, F., Soleimani, M., 2020. Photocatalytic degradation of acetaminophen and codeine medicines using a novel zeolite-supported TiO₂ and ZnO under UV and sunlight irradiation. *Environ. Sci. Pollut. Res.* 27, 26929–26942. <https://doi.org/10.1007/s11356-020-09038-y>.
- Beranek, R., 2011. (Photo)electrochemical methods for the determination of the band edge positions of TiO₂-based nanomaterials. *Adv. Phys. Chem.* <https://doi.org/10.1155/2011/786759>.
- Bergamonti, L., Bergonzi, C., Graiff, C., Lottici, P.P., Bettini, R., Elviri, L., 2019. 3D printed chitosan scaffolds: a new TiO₂ support for the photocatalytic degradation of amoxicillin in water. *Water Res.* 163, 114841. <https://doi.org/10.1016/j.watres.2019.07.008>.
- Bhardwaj, K., Bhardwaj, K., Parvis, F.S., Wang, Y., Blanchard, G.J., Swain, G.M., Swain, G.M., 2020. Effect of surface oxygen on the wettability and electrochemical properties of boron-doped nanocrystalline diamond electrodes in room-temperature ionic liquids. *Langmuir* 36, 5717–5729. <https://doi.org/10.1021/acs.langmuir.0c00294>.
- Bhattacharya, P., Mukherjee, D., Deb, N., Swarnakar, S., Banerjee, S., 2020. Application of green synthesized ZnO nanoparticle coated ceramic ultrafiltration membrane for remediation of pharmaceutical components from synthetic water: reusability assay of treated water on seed germination. *J. Environ. Chem. Eng.* 8, 103803. <https://doi.org/10.1016/j.jece.2020.103803>.
- Bourgin, M., Beck, B., Boehler, M., Borowska, E., Fleiner, J., Salhi, E., Teichler, R., von Gunten, U., Siegrist, H., McArdell, C.S., 2018. Evaluation of a full-scale wastewater treatment plant upgraded with ozonation and biological post-treatments: abatement of micropollutants, formation of transformation products and oxidation by-products. *Water Res.* 129, 486–498. <https://doi.org/10.1016/j.watres.2017.10.036>.
- Brillas, E., 2020. A review on the photoelectro-Fenton process as efficient electrochemical advanced oxidation for wastewater remediation. Treatment with UV light, sunlight, and coupling with conventional and other photo-assisted advanced technologies. *Chemosphere.* <https://doi.org/10.1016/j.chemosphere.2020.126198>.
- Brillas, E., Martínez-Huitle, C.A., 2015. Decontamination of wastewaters containing synthetic organic dyes by electrochemical methods. An updated review. *Appl. Catal. B Environ.* <https://doi.org/10.1016/j.apcatb.2014.11.016>.
- Brillas, E., Sirés, I., 2015. Electrochemical removal of pharmaceuticals from water streams: reactivity elucidation by mass spectrometry. *TRAC Trends Anal. Chem.* (Reference Ed.) 70, 112–121. <https://doi.org/10.1016/j.trac.2015.01.013>.
- Burnside, S., Moser, J.E., Brooks, K., Grätzel, M., Cahen, D., 1999. Nanocrystalline mesoporous strontium titanate as photoelectrode material for photosensitized solar devices: increasing photovoltage through flatband potential engineering. *J. Phys. Chem. B* 103, 9328–9332. <https://doi.org/10.1021/jp9913867>.
- Butler, J.E., Mankelevich, Y.A., Cheesman, A., Ma, J., Ashfold, M.N.R., 2009. Understanding the chemical vapor deposition of diamond: recent progress. *J. Phys. Condens. Matter* 21. <https://doi.org/10.1088/0953-8984/21/36/364201>.
- Cai, Q., Hu, J., 2017. Decomposition of sulfamethoxazole and trimethoprim by continuous UVA/LED/TiO₂ photocatalysis: decomposition pathways, residual antibacterial activity and toxicity. *J. Hazard Mater.* 323, 527–536. <https://doi.org/10.1016/j.jhazmat.2016.06.006>.
- Carbonaro, S., Sugihara, M.N., Strathmann, T.J., 2013. Continuous-flow photocatalytic treatment of pharmaceutical micropollutants: activity, inhibition, and deactivation of TiO₂ photocatalysts in wastewater effluent. *Appl. Catal. B Environ.* 129, 1–12. <https://doi.org/10.1016/j.apcatb.2012.09.014>.
- Cavalcanti, E.B., Garcia-Segura, S., Centellas, F., Brillas, E., 2013. Electrochemical incineration of omeprazole in neutral aqueous medium using a platinum or boron-doped diamond anode: degradation kinetics and oxidation products. *Water Res.* 47, 1803–1815. <https://doi.org/10.1016/j.watres.2013.01.002>.
- Cerrato, G., Bianchi, C.L., Galli, F., Pirola, C., Morandi, S., Capucci, V., 2019. Micro-TiO₂ coated glass surfaces safely abate drugs in surface water. *J. Hazard Mater.* 363, 328–334. <https://doi.org/10.1016/j.jhazmat.2018.09.057>.
- Chaker, H., Fourmentin, S., Chérif-Aouali, L., 2020. Efficient photocatalytic degradation of ibuprofen under visible light irradiation using silver and cerium Co-doped mesoporous TiO₂. *ChemistrySelect* 5, 11787–11796. <https://doi.org/10.1002/slct.202002730>.
- Chang, K.L., Sun, Q., Peng, Y.P., Lai, S.W., Sung, M., Huang, C.Y., Kuo, H.W., Sun, J., Lin, Y.C., 2016. Cu₂O loaded titanate nanotube arrays for simultaneously photoelectrochemical ibuprofen oxidation and hydrogen generation. *Chemosphere* 150, 605–614. <https://doi.org/10.1016/j.chemosphere.2016.02.016>.
- Chaplin, B.P., 2014. Critical review of electrochemical advanced oxidation processes for water treatment applications. *Environ. Sci. Process. Impacts.* <https://doi.org/10.1039/c3em00679d>.
- Chaplin, B.P., Hubler, D.K., Farrell, J., 2013. Understanding anodic wear at boron doped diamond film electrodes. *Electrochim. Acta* 89, 122–131. <https://doi.org/10.1016/j.electacta.2012.10.166>.
- Chaplin, B.P., Wyle, I., Zeng, H., Carlisle, J.A., Farrell, J., 2011. Characterization of the performance and failure mechanisms of boron-doped ultrananocrystalline diamond electrodes. *J. Appl. Electrochem.* 41, 1329–1340. <https://doi.org/10.1007/s10800-011-0351-7>.
- Chen, A., Chen, W.F., Majidi, T., Pudadera, B., Atanacio, A., Manohar, M., Sheppard, L. R., Liu, R., Sorrell, C.C., Koshy, P., 2021. Mo-doped, Cr-Doped, and Mo-Cr codoped TiO₂ thin-film photocatalysts by comparative sol-gel spin coating and ion implantation. *Int. J. Hydrogen Energy* 46, 12961–12980. <https://doi.org/10.1016/j.ijhydene.2021.01.136>.
- Chen, C., Cai, W., Long, M., Zhang, J., Zhou, B., Wu, Y., Wu, D., 2010. Template-free sol-gel preparation and characterization of free-standing visible light responsive C₃N₄-modified porous monolithic TiO₂. *J. Hazard Mater.* 178, 560–565. <https://doi.org/10.1016/j.jhazmat.2010.01.121>.
- Chen, S., He, P., Zhou, P., Wang, X., Xiao, F., He, Q., Li, J., Jia, L., Zhang, H., Jia, B., Tang, B., 2021. Development of a novel graphitic carbon nitride and multiwall carbon nanotube co-doped Ti/PbO₂ anode for electrocatalytic degradation of acetaminophen. *Chemosphere* 271. <https://doi.org/10.1016/j.chemosphere.2021.129830>.
- Cheng, H., Scott, K., Christensen, P.A., 2003. Electrochemical hydrodehalogenation of chlorinated phenols in aqueous solutions. *J. Electrochem. Soc.* 150, D25. <https://doi.org/10.1149/1.1531972>.
- Cheng, X., Cheng, Q., Deng, X., Wang, P., Liu, H., 2016. A facile and novel strategy to synthesize reduced TiO₂ nanotubes photoelectrode for photoelectrocatalytic degradation of diclofenac. *Chemosphere* 144, 888–894. <https://doi.org/10.1016/j.chemosphere.2015.09.070>.
- Cobb, S.J., Ayres, Z.J., Macpherson, J.V., 2018. Boron doped diamond: a designer electrode material for the twenty-first century. *Annu. Rev. Anal. Chem.* <https://doi.org/10.1146/annurev-anchem-061417-010107>.
- da Silva, W.L., Lansarin, M.A., Livotto, P.R., dos Santos, J.H.Z., 2015. Photocatalytic degradation of drugs by supported titania-based catalysts produced from petrochemical plant residue. *Powder Technol.* 279, 166–172. <https://doi.org/10.1016/j.powtec.2015.03.045>.
- Daghrir, Rimeh, Drogui, P., Deegan, N., El Khakani, M.A., 2013. Electrochemical degradation of chlortetracycline using N-doped Ti/TiO₂ photoanode under sunlight irradiations. *Water Res.* 47, 6801–6810. <https://doi.org/10.1016/j.watres.2013.09.011>.

- Daghrir, R., Drogui, P., El Khakani, M.A., 2013. Photoelectrocatalytic oxidation of chlortetracycline using Ti/TiO₂ photo-anode with simultaneous H₂O₂ production. *Electrochim. Acta* 87, 18–31. <https://doi.org/10.1016/j.electacta.2012.09.020>.
- Dang, C., Sun, F., Jiang, H., Huang, T., Liu, W., Chen, X., Ji, H., 2020. Pre-accumulation and in-situ destruction of diclofenac by a photo-regenerable activated carbon fiber supported titanate nanotubes composite material: intermediates, DFT calculation, and ecotoxicity. *J. Hazard Mater.* 400, 123225. <https://doi.org/10.1016/j.jhazmat.2020.123225>.
- Darvishi, A., Davand, R., Khorasheh, F., Fattahi, M., 2016. Modeling-based optimization of a fixed-bed industrial reactor for oxidative dehydrogenation of propane. *Chin. J. Chem. Eng.* 24, 612–622. <https://doi.org/10.1016/j.cjche.2015.12.018>.
- Darvishi Cheshmeh Soltani, R., Mashayekhi, M., Khataee, A., Ghanadzadeh, M.J., Sillanpää, M., 2018. Hybrid sonocatalysis/electrolysis process for intensified decomposition of amoxicillin in aqueous solution in the presence of magnesium oxide nanocatalyst. *J. Ind. Eng. Chem.* 64, 373–382. <https://doi.org/10.1016/j.jiec.2018.03.038>.
- Das, K., Panda, S.K., Chaudhuri, S., 2008. Solvent-controlled synthesis of TiO₂ 1D nanostructures: growth mechanism and characterization. *J. Cryst. Growth* 310, 3792–3799. <https://doi.org/10.1016/j.jcrysgro.2008.05.039>.
- de Oliveira, M., Frihling, B.E.F., Velasques, J., Filho, F.J.C.M., Cavalheri, P.S., Miglioli, L., 2020. Pharmaceuticals residues and xenobiotics contaminants: occurrence, analytical techniques and sustainable alternatives for wastewater treatment. *Sci. Total Environ.* 705, 135568. <https://doi.org/10.1016/j.scitotenv.2019.135568>.
- Demchenko, A.P., Tomin, V.I., Chou, P.T., 2017. Breaking the Kasha rule for more efficient photochemistry. *Chem. Rev.* 117, 13353–13381. <https://doi.org/10.1021/acs.chemrev.7b00110>.
- Desbiolles, F., Malleret, L., Tiliacos, C., Wong-Wah-Chung, P., Laffont-Schwob, I., 2018. Occurrence and ecotoxicological assessment of pharmaceuticals: is there a risk for the Mediterranean aquatic environment? *Sci. Total Environ.* 639, 1334–1348. <https://doi.org/10.1016/j.scitotenv.2018.04.351>.
- Dhangar, K., Kumar, M., 2020. Tricks and tracks in removal of emerging contaminants from the wastewater through hybrid treatment systems: a review. *Sci. Total Environ.* 738, 140320. <https://doi.org/10.1016/j.scitotenv.2020.140320>.
- Diao, Z., Li, M., Zeng, F., Song, L., Qiu, R., 2013. Degradation pathway of malachite green in a novel dual-tank photoelectrochemical catalytic reactor. *J. Hazard Mater.* 260, 585–592. <https://doi.org/10.1016/j.jhazmat.2013.05.037>.
- Diao, Z.H., Dong, F.X., Yan, L., Chen, Z.L., Qian, W., Kong, L.J., Zhang, Z.W., Zhang, T., Tao, X.Q., Du, J.J., Jiang, D., Chu, W., 2020. Synergistic oxidation of Bisphenol A in a heterogeneous ultrasound-enhanced sludge biochar catalyst/persulfate process: reactivity and mechanism. *J. Hazard Mater.* 384, 121385. <https://doi.org/10.1016/j.jhazmat.2019.121385>.
- Diao, Z.H., Jin, J.C., Zou, M.Y., Liu, H., Qin, J.Q., Zhou, X.H., Qian, W., Guo, P.R., Kong, L.J., Chu, W., 2021. Simultaneous degradation of amoxicillin and norfloxacin by TiO₂@nZVI composites coupling with persulfate: synergistic effect, products and mechanism. *Separ. Purif. Technol.* 278, 119620. <https://doi.org/10.1016/j.seppur.2021.119620>.
- Diao, Z.H., Pu, S.Y., Qian, W., Liang, S., Kong, L.J., Xia, D.H., Lei, Z.X., Du, J.J., Liu, H., Yang, J.W., 2019a. Photocatalytic removal of phenanthrene and algae by a novel Ca-Ag₃PO₄ composite under visible light: reactivity and coexisting effect. *Chemosphere* 221, 511–518. <https://doi.org/10.1016/j.chemosphere.2019.01.044>.
- Diao, Z.H., Qian, W., Lei, Z.X., Kong, L.J., Du, J.J., Liu, H., Yang, J.W., Pu, S.Y., 2019b. Insights on the nitrate reduction and norfloxacin oxidation over a novel nanoscale zero valent iron particle: reactivity, products, and mechanism. *Sci. Total Environ.* 660, 541–549. <https://doi.org/10.1016/j.scitotenv.2019.01.037>.
- Diao, Z.H., Wei-Qian, Guo, P.R., Kong, L.J., Pu, S.Y., 2018. Photo-assisted degradation of bisphenol A by a novel FeS₂@SiO₂ microspheres activated persulfate process: synergistic effect, pathway and mechanism. *Chem. Eng. J.* 349, 683–693. <https://doi.org/10.1016/j.cej.2018.05.132>.
- Diao, Z.H., Xu, X.R., Jiang, D., Liu, J.J., Kong, L.J., Li, G., Zuo, L.Z., Wu, Q.H., 2017. Simultaneous photocatalytic Cr(VI) reduction and ciprofloxacin oxidation over TiO₂/Fe⁰ composite under aerobic conditions: performance, durability, pathway and mechanism. *Chem. Eng. J.* 315, 167–176. <https://doi.org/10.1016/j.cej.2017.01.006>.
- Diao, Z.H., Xu, X.R., Liu, F.M., Sun, Y.X., Zhang, Z.W., Sun, K.F., Wang, S.Z., Cheng, H., 2015. Photocatalytic degradation of malachite green by pyrite and its synergism with Cr(VI) reduction: performance and reaction mechanism. *Separ. Purif. Technol.* 154, 168–175. <https://doi.org/10.1016/j.seppur.2015.09.027>.
- Díez, A.M., Moreira, F.C., Marinho, B.A., Espíndola, J.C.A., Paulista, L.O., Sanromán, M.A., Pazos, M., Boaventura, R.A.R., Vilar, V.J.P., 2018. A step forward in heterogeneous photocatalysis: process intensification by using a static mixer as catalyst support. *Chem. Eng. J.* 343, 597–606. <https://doi.org/10.1016/j.cej.2018.03.041>.
- Ding, W., Wu, X., Lu, Q., 2019. Structure and photocatalytic activity of thin-walled CuWO₄ nanotubes: an experimental and DFT study. *Mater. Lett.* 253, 323–326. <https://doi.org/10.1016/j.matlet.2019.06.109>.
- Divyapriya, G., Singh, S., Martínez-Huitle, C.A., Scaria, J., Karim, A.V., Nidheesh, P.V., 2021. Treatment of real wastewater by photoelectrochemical methods: an overview. *Chemosphere* 276, 130188. <https://doi.org/10.1016/j.chemosphere.2021.130188>.
- Dolatbadi, S., Fattahi, M., Nabati, M., 2021. Solid state dispersion and hydrothermal synthesis, characterization and evaluations of TiO₂/ZnO nanostructures for degradation of rhodamine B. *Desalination Water Treat.* 231, 425–435. <https://doi.org/10.5004/dwt.2021.27496>.
- Dou, M., Wang, J., Gao, B., Xu, C., Yang, F., 2020. Photocatalytic difference of amoxicillin and cefotaxime under visible light by mesoporous g-C₃N₄: mechanism, degradation pathway and DFT calculation. *Chem. Eng. J.* 383, 123134. <https://doi.org/10.1016/j.cej.2019.123134>.
- Dozzi, M.V., Selli, E., 2013. Doping TiO₂ with p-block elements: effects on photocatalytic activity. *J. Photochem. Photobiol. C Photochem. Rev.* <https://doi.org/10.1016/j.jphotochemrev.2012.09.002>.
- Durán, A., Monteagudo, J.M., San Martín, I., 2018. Operation costs of the solar photocatalytic degradation of pharmaceuticals in water: a mini-review. *Chemosphere.* <https://doi.org/10.1016/j.chemosphere.2018.07.170>.
- Ekimov, E.A., Kondrin, M.V., 2020. High-pressure, high-temperature synthesis and doping of nanodiamonds. In: *Semiconductors and Semimetals*, pp. 161–199. <https://doi.org/10.1016/bs.semsem.2020.03.006>.
- El Mouchtari, E.M., Bahsis, L., El Mersly, L., Anane, H., Lebarillier, S., Piram, A., Briche, S., Wong-Wah-Chung, P., Rafiqah, S., 2021. Inhibitors in the aqueous and adsorbed photocatalytic degradation of carbamazepine by a biosourced composite: kinetics, mechanisms and DFT calculations. *Int. J. Environ. Res.* 15, 135–147. <https://doi.org/10.1007/s41742-020-00300-2>.
- Escudero-Curiel, S., Penelas, U., Sanromán, M.A., Pazos, M., 2021. An approach towards Zero-Waste wastewater technology: fluoxetine adsorption on biochar and removal by the sulfate radical. *Chemosphere* 268, 129318. <https://doi.org/10.1016/j.chemosphere.2020.129318>.
- Eskandarloo, H., Badii, A., Behnadjy, M.A., Ziarani, G.M., 2015. UV-LEDs assisted preparation of silver deposited TiO₂ catalyst bed inside microchannels as a high efficiency microphotoreactor for cleaning polluted water. *Chem. Eng. J.* 270, 158–167. <https://doi.org/10.1016/j.cej.2015.01.117>.
- Espíndola, J.C., Cristóvão, R.O., Santos, S.G.S., Boaventura, R.A.R., Dias, M.M., Lopes, J.C.B., Vilar, V.J.P., 2019. Intensification of heterogeneous TiO₂ photocatalysis using the NETmix mini-photoreactor under microscale illumination for oxytetracycline oxidation. *Sci. Total Environ.* 681, 467–474. <https://doi.org/10.1016/j.scitotenv.2019.05.066>.
- Espíndola, J.C., Vilar, V.J.P., 2020. Innovative light-driven chemical/catalytic reactors towards contaminants of emerging concern mitigation: a review. *Chem. Eng. J.* 394, 124865. <https://doi.org/10.1016/j.cej.2020.124865>.
- European Commission, E.C., 2018. COMMISSION IMPLEMENTING DECISION (EU) 2018/840 of 5 June 2018. *Off. J. Eur. Union* 141, 9–12.
- Fan, B., Zhu, Y., Rechenberg, R., Rusinek, C.A., Becker, M.F., Li, W., 2017. Large-scale, all polycrystalline diamond structures transferred onto flexible Polyene-C films for neurotactant sensing. *Lab Chip* 17, 3159–3167. <https://doi.org/10.1039/c7lc00229g>.
- Farabough, E.N., Robins, L., Feldman, A., Johnson, C.E., 1995. Growth and oxidation of boron-doped diamond films. *J. Mater. Res.* 10, 1448–1454. <https://doi.org/10.1557/JMR.1995.1448>.
- Feier, B., Florea, A., Cristea, C., Săndulescu, R., 2018. Electrochemical detection and removal of pharmaceuticals in waste waters. *Curr. Opin. Electrochem.* 11, 1–11. <https://doi.org/10.1016/j.coelec.2018.06.012>.
- Fekadu, S., Alemayehu, E., Dewil, R., Van der Bruggen, B., 2019. Pharmaceuticals in freshwater aquatic environments: a comparison of the African and European challenge. *Sci. Total Environ.* 654, 324–337. <https://doi.org/10.1016/j.scitotenv.2018.11.072>.
- Ferrari, B., Mons, R., Vollat, B., Fraysse, B., Paxéus, N., Lo Giudice, R., Pollio, A., Garric, J., 2004. Environmental risk assessment of six human pharmaceuticals: are the current environmental risk assessment procedures sufficient for the protection of the aquatic environment?. In: *Environmental Toxicology and Chemistry. Environ Toxicol Chem.* pp. 1344–1354. <https://doi.org/10.1897/03-246>.
- Ferreira, V.R.A., Santos, P.R.M., Silva, C.I.Q., Azenha, M.A., 2021. Latest developments on TiO₂-based photocatalysis: a special focus on selectivity and hollowness for enhanced photonic efficiency. *Appl. Catal. Gen.* <https://doi.org/10.1016/j.apcata.2021.118243>.
- Frontistis, Z., Antonopoulou, M., Venieri, D., Konstantinou, I., Mantzavinos, D., 2017. Boron-doped diamond oxidation of amoxicillin pharmaceutical formulation: statistical evaluation of operating parameters, reaction pathways and antibacterial activity. *J. Environ. Manag.* 195, 100–109. <https://doi.org/10.1016/j.jenvman.2016.04.035>.
- Fu, K., Pan, Y., Ding, C., Shi, J., Deng, H., 2021. Photocatalytic degradation of naproxen by Bi₂MoO₆/g-C₃N₄ heterojunction photocatalyst under visible light: mechanisms, degradation pathway, and DFT calculation. *J. Photochem. Photobiol. Chem.* 412, 113235. <https://doi.org/10.1016/j.jphotochem.2021.113235>.
- Fukui, K., 2006. Theory of orientation and stereoselection. In: *Orientation and Stereoselection*. Springer-Verlag, pp. 1–85. <https://doi.org/10.1007/bfb0051113>.
- Gadipelly, C., Pérez-González, A., Yadav, G.D., Ortiz, I., Ibáñez, R., Rathod, V.K., Marathe, K.V., 2014. Pharmaceutical industry wastewater: review of the technologies for water treatment and reuse. *Ind. Eng. Chem. Res.* <https://doi.org/10.1021/ie501210j>.
- García-Espinoza, J.D., Mijaylova-Nacheva, P., Avilés-Flores, M., 2018. Electrochemical carbamazepine degradation: effect of the generated active chlorine, transformation pathways and toxicity. *Chemosphere* 192, 142–151. <https://doi.org/10.1016/j.chemosphere.2017.10.147>.
- García-Segura, S., Brillas, E., 2017. Applied photoelectrocatalysis on the degradation of organic pollutants in wastewaters. *J. Photochem. Photobiol. C Photochem. Rev.* <https://doi.org/10.1016/j.jphotochemrev.2017.01.005>.
- García-Segura, S., Dosta, S., Guilemany, J.M., Brillas, E., 2013. Solar photoelectrocatalytic degradation of Acid Orange 7 azo dye using a highly stable TiO₂ photoanode synthesized by atmospheric plasma spray. *Appl. Catal. B Environ.* 132, 142–150. <https://doi.org/10.1016/j.apcatb.2012.11.037>.
- Garmouhi, A., Kheirollahi, M., Mousavi, S.A., Fattahi, M., Mahvelati, E.H., 2020. Effects of graphene oxide/TiO₂ nanocomposite, graphene oxide nanosheets and Cedr

- extraction solution on IFT reduction and ultimate oil recovery from a carbonate rock. *Petroleum*. <https://doi.org/10.1016/J.PETLM.2020.10.002>.
- Ghasemian, S., Nasuhoglu, D., Omanovic, S., Yargeau, V., 2017. Photoelectrocatalytic degradation of pharmaceutical carbamazepine using Sb-doped Sn80%-W20%-oxide electrodes. *Separ. Purif. Technol.* 188, 52–59. <https://doi.org/10.1016/j.seppur.2017.07.007>.
- Gong, X.Q., Selloni, A., 2005. Reactivity of anatase TiO₂ nanoparticles: the role of the minority (001) surface. *J. Phys. Chem. B* 109, 19560–19562. <https://doi.org/10.1021/jp055311g>.
- Goss, J.P., Eyre, R.J., Briddon, P.R., 2008. Theoretical models for doping diamond for semiconductor applications. In: Koizumi, S., Nebel, C., Nesladek, M. (Eds.), *Physics and Applications of CVD Diamond*. Wiley-VCH Verlag GmbH & Co. KGaA, pp. 199–236. <https://doi.org/10.1002/9783527623174.ch8>.
- Guillery, R.W., 1993. General introduction. *Neuroscience* 57, 181. [https://doi.org/10.1016/0306-4522\(93\)90120-5](https://doi.org/10.1016/0306-4522(93)90120-5).
- Guinea, E., Garrido, J.A., Rodríguez, R.M., Cabot, P.L., Arias, C., Centellas, F., Brillas, E., 2010. Degradation of the fluoroquinolone enrofloxacin by electrochemical advanced oxidation processes based on hydrogen peroxide electrogeneration. *Electrochim. Acta* 55, 2101–2115. <https://doi.org/10.1016/j.electacta.2009.11.040>.
- Guitaya, L., Azaïs, A., Zaviska, F., Drogui, P., Blais, J.F., Gourich, B., 2017. Electrochemical oxidation as treatment for contaminated wastewaters by carbamazepine: process optimization through response surface methodology. *Water. Air. Soil Pollut.* 228, 1–14. <https://doi.org/10.1007/s11270-017-3565-4>.
- Gupta, B., Gupta, A.K., Tiwary, C.S., Ghosal, P.S., 2021. A multivariate modeling and experimental realization of photocatalytic system of engineered S-C₃N₄/ZnO hybrid for ciprofloxacin removal: influencing factors and degradation pathways. *Environ. Res.* 196, 110390. <https://doi.org/10.1016/j.envres.2020.110390>.
- Gurkan, Y.Y., Turkten, N., Hatipoglu, A., Cinar, Z., 2012. Photocatalytic degradation of cefazolin over N-doped TiO₂ under UV and sunlight irradiation: prediction of the reaction paths via conceptual DFT. *Chem. Eng. J.* 184, 113–124. <https://doi.org/10.1016/j.cej.2012.01.011>.
- Han, Y., Qiu, J., Miao, Y., Han, J., Zhang, S., Zhang, H., Zhao, H., 2011. Robust TiO₂/BDD heterojunction photoanodes for determination of chemical oxygen demand in wastewaters. *Anal. Methods* 3. <https://doi.org/10.1039/c1ay05193h>, 2003–2009.
- Han, Y., Ruan, X., Chen, J., Zhang, H., Zhao, H., Zhang, S., 2013. Photoelectrochemical properties and its application of nano-TiO₂/boron-doped diamond heterojunction electrode material. *Asian J. Chem.* 25, 6167–6172. <https://doi.org/10.14233/ajchem.2013.14299>.
- Harada, A., Komori, K., Nakada, N., Kitamura, K., Suzuki, Y., 2008. Biological effects of PPCPs on aquatic lives and evaluation of river waters affected by different wastewater treatment levels. *Water Sci. Technol.* 58, 1541–1546. <https://doi.org/10.2166/wst.2008.742>.
- Hartley, A.C., Moss, J.B., Keesling, K.J., Moore, N.J., Glover, J.D., Boyd, J.E., 2017. PMMA-titanium floating microspheres for the photocatalytic remediation of agro-pharmaceutical wastewater. *Water Sci. Technol.* 75, 1362–1369. <https://doi.org/10.2166/wst.2017.003>.
- He, J., Kumar, A., Khan, M., Lo, I.M.C., 2021. Critical review of photocatalytic disinfection of bacteria: from noble metals- and carbon nanomaterials-TiO₂ composites to challenges of water characteristics and strategic solutions. *Sci. Total Environ.* <https://doi.org/10.1016/j.scitotenv.2020.143953>.
- He, L., Lin, M., Li, H., Kim, N.J., 2010. Surface-enhanced Raman spectroscopy coupled with dendritic silver nanosubstrate for detection of restricted antibiotics. *J. Raman Spectrosc.* 41, 739–744. <https://doi.org/10.1002/jrs.2505>.
- He, M., Wan, Z., Tsang, D.C.W., Sun, Y., Khan, E., Hou, D., Graham, N.J.D., 2021. Performance indicators for a holistic evaluation of catalyst-based degradation—a case study of selected pharmaceuticals and personal care products (PPCPs). *J. Hazard Mater.* 402, 123460. <https://doi.org/10.1016/j.jhazmat.2020.123460>.
- Hébert, C., Scorsoni, E., Mermoux, M., Bergonzo, P., 2015. Porous diamond with high electrochemical performance. *Carbon N. Y.* 90, 102–109. <https://doi.org/10.1016/j.carbon.2015.04.016>.
- Heo, J., Kim, S., Her, N., Park, C.M., Yu, M., Yoon, Y., 2019. Removal of contaminants of emerging concern by FO, RO, and UF membranes in water and wastewater. In: *Contaminants of Emerging Concern in Water and Wastewater: Advanced Treatment Processes*. Elsevier, pp. 139–176. <https://doi.org/10.1016/B978-0-12-813561-7.00005-5>.
- Hitchman, M.L., Tian, F., 2002. Studies of TiO₂ thin films prepared by chemical vapour deposition for photocatalytic and photoelectrocatalytic degradation of 4-chlorophenol. *J. Electroanal. Chem.* 538–539, 165–172. [https://doi.org/10.1016/S0022-0728\(02\)01252-4](https://doi.org/10.1016/S0022-0728(02)01252-4).
- Hoffmann, R., Kriele, A., Obloh, H., Hees, J., Wolfer, M., Smirnov, W., Yang, N., Nebel, C. E., 2010. Electrochemical hydrogen termination of boron-doped diamond. *Appl. Phys. Lett.* 97, 1–4. <https://doi.org/10.1063/1.3476346>.
- Hong, M., Wang, Y., Lu, G., 2020. UV-Fenton degradation of diclofenac, sulphiride, sulfamethoxazole and sulfisomidine: degradation mechanisms, transformation products, toxicity evolution and effect of real water matrix. *Chemosphere* 258, 127351. <https://doi.org/10.1016/j.chemosphere.2020.127351>.
- Hua, Z., Dai, Z., Bai, X., Ye, Z., Wang, P., Gu, H., Huang, X., 2016. Copper nanoparticles sensitized TiO₂ nanotube arrays electrode with enhanced photoelectrocatalytic activity for diclofenac degradation. *Chem. Eng. J.* 283, 514–523. <https://doi.org/10.1016/j.cej.2015.07.072>.
- Huang, D., Sun, X., Liu, Y., Ji, H., Liu, W., Wang, C.C., Ma, W., Cai, Z., 2021. A carbon-rich g-C₃N₄ with promoted charge separation for highly efficient photocatalytic degradation of amoxicillin. *Chin. Chem. Lett.* 32, 2787–2791. <https://doi.org/10.1016/j.ccl.2021.01.012>.
- Huang, H., He, Y., Li, X., Li, M., Zeng, C., Dong, F., Du, X., Zhang, T., Zhang, Y., 2015. Bi₂O₂(OH)(NO₃) as a desirable [Bi₂O₂]²⁺ layered photocatalyst: strong intrinsic polarity, rational band structure and {001} active facets co-beneficial for robust photooxidation capability. *J. Mater. Chem.* 3, 24547–24556. <https://doi.org/10.1039/c5ta07655b>.
- Hurtado, L., Solís-Casados, D.A., Escobar-Alarcón, L., Romero, R., Natividad, R., 2016. Multiphase photo-capillary reactors coated with TiO₂ films: preparation, characterization and photocatalytic performance. *Chem. Eng. J.* 304, 39–47. <https://doi.org/10.1016/j.cej.2016.06.003>.
- Hutton, L.A., Iacobini, J.G., Bitziou, E., Channon, R.B., Newton, M.E., Macpherson, J.V., 2013. Examination of the factors affecting the electrochemical performance of oxygen-terminated polycrystalline boron-doped diamond electrodes. *Anal. Chem.* 85, 7230–7240. <https://doi.org/10.1021/ac401042t>.
- Islam, A., Teo, S.H., Taufiq-Yap, Y.H., Ng, C.H., Vo, D.V.N., Ibrahim, M.L., Hasan, M.M., Khan, M.A.R., Nur, A.S.M., Awual, M.R., 2021. Step towards the sustainable toxic dyes and heavy metals removal and recycling from aqueous solution- A comprehensive review. *Resour. Conserv. Recycl.* <https://doi.org/10.1016/j.resconrec.2021.105849>.
- Ismael, M., 2020. A review on graphitic carbon nitride (g-C₃N₄) based nanocomposites: synthesis, categories, and their application in photocatalysis. *J. Alloys Compd.* 846, 156446. <https://doi.org/10.1016/J.JALLCOM.2020.156446>.
- Ismail, S.A., Ang, W.L., Mohammad, A.W., 2021. Electro-Fenton technology for wastewater treatment: a bibliometric analysis of current research trends, future perspectives and energy consumption analysis. *J. Water Proc. Eng.* <https://doi.org/10.1016/j.jwpe.2021.101952>.
- Jallouli, N., Pastrana-Martínez, L.M., Ribeiro, A.R., Moreira, N.F.F., Faria, J.L., Hentati, O., Silva, A.M.T., Ksibi, M., 2018. Heterogeneous photocatalytic degradation of ibuprofen in ultrapure water, municipal and pharmaceutical industry wastewaters using a TiO₂/UV-LED system. *Chem. Eng. J.* 334, 976–984. <https://doi.org/10.1016/j.cej.2017.10.045>.
- Jaramillo-Gutiérrez, M.L., Rivero, E.P., Cruz-Díaz, M.R., Niño-Gómez, M.E., Pedraza-Avella, J.A., 2016. Photoelectrocatalytic hydrogen production from oilfield-produced wastewater in a filter-press reactor using TiO₂-based photoanodes. *Catal. Today* 266, 17–26. <https://doi.org/10.1016/j.cattod.2015.12.008>.
- Jaria, G., Calisto, V., Gil, M.V., Ferreira, P., Santos, S.M., Otero, M., Esteves, V.I., 2021. Effects of thiol functionalization of a waste-derived activated carbon on the adsorption of sulfamethoxazole from water: kinetic, equilibrium and thermodynamic studies. *J. Mol. Liq.* 323, 115003. <https://doi.org/10.1016/j.molliq.2020.115003>.
- Jayasree, P., Remya, N., 2020. Photocatalytic degradation of paracetamol using aluminosilicate supported TiO₂. *Water Sci. Technol.* 82, 2114–2124. <https://doi.org/10.2166/wst.2020.484>.
- Jelovica Badovinac, I., Peter, R., Omerzu, A., Salamon, K., Šarić, I., Samaržija, A., Perčić, M., Kavre Piltaver, I., Ambrožić, G., Petravčić, M., 2020. Grain size effect on photocatalytic activity of TiO₂ thin films grown by atomic layer deposition. *Thin Solid Films* 709, 138215. <https://doi.org/10.1016/J.TSF.2020.138215>.
- Jeon, T.H., Koo, M.S., Kim, H., Choi, W., 2018. Dual-functional photocatalytic and photoelectrocatalytic systems for energy- and resource-recovering water treatment. *ACS Catal.* 8, 11542–11563. <https://doi.org/10.1021/acscatal.8b03521>.
- Jesić, D., Lašić Jurković, D., Pohar, A., Suhadolnik, L., Likozar, B., 2021. Engineering photocatalytic and photoelectrocatalytic CO₂ reduction reactions: mechanisms, intrinsic kinetics, mass transfer resistances, reactors and multi-scale modelling simulations. *Chem. Eng. J.* <https://doi.org/10.1016/j.cej.2020.126799>.
- Jia, M., Yang, Z., Xu, H., Song, P., Xiong, W., Cao, J., Zhang, Y., Xiang, Y., Hu, J., Zhou, C., Yang, Y., Wang, W., 2020. Integrating N and F co-doped TiO₂ nanotubes with ZIF-8 as photoelectrode for enhanced photo-electrocatalytic degradation of sulfamethazine. *Chem. Eng. J.* 388, 124388. <https://doi.org/10.1016/j.cej.2020.124388>.
- Jia, X., Zhang, B., Chen, C., Fu, X., Huang, Q., 2021. Immobilization of chitosan grafted carboxylic Zr-MOF to porous starch for sulfanilamide adsorption. *Carbohydr. Polym.* 253, 117305. <https://doi.org/10.1016/j.carbpol.2020.117305>.
- Jiang, X., Willich, P., Paul, M., Klages, C.P., 1999. In situ boron doping of chemical-vapor-deposited diamond films. *J. Mater. Res.* 14, 3211–3220. <https://doi.org/10.1557/JMR.1999.0434>.
- Joint Norman, Water Europe Position Paper, 2019. *Contaminants of Emerging Concern in Urban Wastewater Joint NORMAN and Water Europe Position Paper* 1–21.
- Jose, J., Sandra Pinto, J., Kotian, B., Mathew Thomas, A., Narayana Charyulu, R., 2020. Comparison of the regulatory outline of ecopharmacovigilance of pharmaceuticals in Europe, USA, Japan and Australia. *Sci. Total Environ.* 709, 134815. <https://doi.org/10.1016/j.scitotenv.2019.134815>.
- Jum'h, I., Al-Addous, M., Al-Taani, H., Abd El-Sadek, M.S., Ayoub, N., 2017. Effect of boron concentration on nano-crystalline diamond deposited on niobium substrates. *Dig. J. Nanomater. Biostructures* 12, 589–593.
- Kanakaraju, D., Glass, B.D., Oelgemöller, M., 2018. Advanced oxidation process-mediated removal of pharmaceuticals from water: a review. *J. Environ. Manag.* 219, 189–207. <https://doi.org/10.1016/j.jenvman.2018.04.103>.
- Kasha, M., 1950. Characterization of electronic transitions in complex molecules. *Discuss. Faraday Soc.* <https://doi.org/10.1039/DF9500900014>.
- Katal, R., Tanhaei, M., Hu, J., 2021. Photocatalytic degradation of the acetaminophen by nanocrystal-engineered TiO₂ thin film in batch and continuous system. *Front. Environ. Sci. Eng.* 15, 1–4. <https://doi.org/10.1007/s11783-020-1319-9>.
- Katheresan, V., Kansedo, J., Lau, S.Y., 2018. Efficiency of various recent wastewater dye removal methods: a review. *J. Environ. Chem. Eng.* 6, 4676–4697. <https://doi.org/10.1016/J.JECE.2018.06.060>.
- Khandaker, S., Hossain, M.T., Saha, P.K., Rayhan, U., Islam, A., Choudhury, T.R., Awual, M.R., 2021. Functionalized layered double hydroxides composite bio-adsorbent for efficient copper(II) ion encapsulation from wastewater. *J. Environ. Manag.* 300, 113782. <https://doi.org/10.1016/j.jenvman.2021.113782>.

- Khanna, S., Utsav, Patel, R., Marathe, P., Chaudari, R., Vora, J., Banerjee, R., Ray, A., Mukhopadhyay, I., 2020. Growth of titanium dioxide nanorod over shape memory material using chemical vapor deposition for energy conversion application. *Mater. Today Proc.* 28, 475–479. <https://doi.org/10.1016/J.MATPR.2019.10.035>.
- Kharel, S., Stapf, M., Mische, U., Ekblad, M., Cimbritz, M., Falås, P., Nilsson, J., Sehlén, R., Bregendahl, J., Bester, K., 2020. Removal of pharmaceutical metabolites in wastewater ozonation including their fate in different post-treatments. *Sci. Total Environ.* 759, 143989. <https://doi.org/10.1016/j.scitotenv.2020.143989>.
- Khetan, S.K., Collins, T.J., 2007. Human pharmaceuticals in the aquatic environment: a challenge to green chemistry. *Chem. Rev.* <https://doi.org/10.1021/cr020441w>.
- Kim, H., Lee, H., Kim, C.M., Jang, A., 2020. Enhancement of ozonation of seawater-based wastewater containing pharmaceutical compounds by total residual oxidants: salinity, ammonia, and organic matter. *Chemosphere* 259, 127513. <https://doi.org/10.1016/j.chemosphere.2020.127513>.
- Kim, J.R., Kan, E., 2016. Heterogeneous photocatalytic degradation of sulfamethoxazole in water using a biochar-supported TiO₂ photocatalyst. *J. Environ. Manag.* 180, 94–101. <https://doi.org/10.1016/j.jenvman.2016.05.016>.
- Kitanosono, T., Masuda, K., Xu, P., Kobayashi, S., 2018. Catalytic organic reactions in water toward sustainable society. *Chem. Rev.* <https://doi.org/10.1021/acs.chemrev.7b00417>.
- Koiki, B.A., Orimolade, B.O., Zwane, B.N., Nkosi, D., Mabuba, N., Arotiba, O.A., 2020. Cu₂O on anodized TiO₂ nanotube arrays: a heterojunction photoanode for visible light assisted electrochemical degradation of pharmaceuticals in water. *Electrochim. Acta* 340, 135944. <https://doi.org/10.1016/j.electacta.2020.135944>.
- Komaraiah, D., Radha, E., Sivakumar, J., Ramana Reddy, M.V., Sayanna, R., 2020. Photoluminescence and photocatalytic activity of spin coated Ag⁺ doped anatase TiO₂ thin films. *Opt. Mater.* 108, 110401. <https://doi.org/10.1016/j.optmat.2020.110401>.
- Kondo, T., Yajima, K., Kato, T., Okano, M., Terashima, C., Aikawa, T., Hayase, M., Yuasa, M., 2017. Hierarchically nanostructured boron-doped diamond electrode surface. *Diam. Relat. Mater.* 72, 13–19. <https://doi.org/10.1016/j.diamond.2016.12.004>.
- Kovacic, M., Papac, J., Kusic, H., Karamanis, P., Loncaric Bozic, A., 2020. Degradation of polar and non-polar pharmaceutical pollutants in water by solar assisted photocatalysis using hydrothermal TiO₂-SnS₂. *Chem. Eng. J.* 382, 122826. <https://doi.org/10.1016/j.cej.2019.122826>.
- Kubra, K.T., Salman, M.S., Hasan, M.N., Islam, A., Teo, S.H., Hasan, M.M., Sheikh, M.C., Awual, M.R., 2021. Sustainable detection and capturing of cerium(III) using ligand embedded solid-state conjugate adsorbent. *J. Mol. Liq.* 338, 116667. <https://doi.org/10.1016/j.molliq.2021.116667>.
- Lan, Y., Coetsier, C., Causserand, C., Groenen Serrano, K., 2018. An experimental and modelling study of the electrochemical oxidation of pharmaceuticals using a boron-doped diamond anode. *Chem. Eng. J.* 333, 486–494. <https://doi.org/10.1016/j.cej.2017.09.164>.
- Lan, Y., Coetsier, C., Causserand, C., Groenen Serrano, K., 2017. On the role of salts for the treatment of wastewaters containing pharmaceuticals by electrochemical oxidation using a boron doped diamond anode. *Electrochim. Acta* 231, 309–318. <https://doi.org/10.1016/j.electacta.2017.01.160>.
- Lee, H., Jang, H.S., Kim, N.Y., Joo, J.B., 2021. Cu-doped TiO₂ hollow nanostructures for the enhanced photocatalysis under visible light conditions. *J. Ind. Eng. Chem.* 99, 352–363. <https://doi.org/10.1016/j.jiec.2021.04.045>.
- Li, D., Ohashi, N., Hishita, S., Kolodiazny, T., Haneda, H., 2005. Origin of visible-light-driven photocatalysis: a comparative study on N/F-doped and N-F-codoped TiO₂ powders by means of experimental characterizations and theoretical calculations. *J. Solid State Chem.* 178, 3293–3302. <https://doi.org/10.1016/j.jssc.2005.08.008>.
- Li, G., Zhou, S., Shi, Z., Meng, X., Li, L., Liu, B., 2019. Electrochemical degradation of ciprofloxacin on BDD anode using a differential column batch reactor: mechanisms, kinetics and pathways. *Environ. Sci. Pollut. Res.* 26, 17740–17750. <https://doi.org/10.1007/s11356-019-04900-0>.
- Li, Y., Fu, Y., Zhu, M., 2020. Green synthesis of 3D tripyramid TiO₂ architectures with assistance of aloe extracts for highly efficient photocatalytic degradation of antibiotic ciprofloxacin. *Appl. Catal. B Environ.* 260, 118149. <https://doi.org/10.1016/j.apcatb.2019.118149>.
- Li, Y., Yang, Y., Lei, J., Liu, W., Tong, M., Liang, J., 2021. The degradation pathways of carbamazepine in advanced oxidation process: a mini review coupled with DFT calculation. *Sci. Total Environ.* 779, 146498. <https://doi.org/10.1016/j.scitotenv.2021.146498>.
- Linley, S., Liu, Y., Ptacek, C.J., Blowes, D.W., Gu, F.X., 2014. Recyclable graphene oxide-supported titanium dioxide photocatalysts with tunable properties. *ACS Appl. Mater. Interfaces* 6, 4658–4668. <https://doi.org/10.1021/am4039272>.
- Liu, C.M., Diao, Z.H., Huo, W.Y., Kong, L.J., Du, J.J., 2018. Simultaneous removal of Cu²⁺ and bisphenol A by a novel biochar-supported zero valent iron from aqueous solution: synthesis, reactivity and mechanism. *Environ. Pollut.* 239, 698–705. <https://doi.org/10.1016/j.envpol.2018.04.084>.
- Liu, D., Li, H., Gao, R., Zhao, Q., Yang, Z., Gao, X., Wang, Z., Zhang, F., Wu, W., 2021. Enhanced visible light photoelectrocatalytic degradation of tetracycline hydrochloride by I and P co-doped TiO₂ photoelectrode. *J. Hazard Mater.* 406, 124309. <https://doi.org/10.1016/j.jhazmat.2020.124309>.
- Liu, D., Tian, R., Wang, J., Nie, E., Piao, X., Li, X., Sun, Z., 2017. Photoelectrocatalytic degradation of methylene blue using F doped TiO₂ photoelectrode under visible light irradiation. *Chemosphere* 185, 574–581. <https://doi.org/10.1016/j.chemosphere.2017.07.071>.
- Liu, F., Liang, J., Chen, L., Tong, M., Liu, W., 2019. Photocatalytic removal of diclofenac by Ti doped BiOI microspheres under visible light irradiation: kinetics, mechanism, and pathways. *J. Mol. Liq.* 275, 807–814. <https://doi.org/10.1016/j.molliq.2018.11.119>.
- Liu, G., Wang, L., Yang, H.G., Cheng, H.M., Lu, G.Q., 2010. Titania-based photocatalysts - crystal growth, doping and heterostructuring. *J. Mater. Chem.* 20, 831–843. <https://doi.org/10.1039/b909930a>.
- Liu, H., Xu, G., Li, G., 2021. Preparation of porous biochar based on pharmaceutical sludge activated by NaOH and its application in the adsorption of tetracycline. *J. Colloid Interface Sci.* 587, 271–278. <https://doi.org/10.1016/j.jcis.2020.12.014>.
- Liu, J., Li, J., Li, Y., Guo, J., Xu, S.M., Zhang, R., Shao, M., 2020. Photoelectrochemical water splitting coupled with degradation of organic pollutants enhanced by surface and interface engineering of BiVO₄ photoanode. *Appl. Catal. B Environ.* 278, 119268. <https://doi.org/10.1016/j.apcatb.2020.119268>.
- Liu, J.J., Diao, Z.H., Liu, C.M., Jiang, D., Kong, L.J., Xu, X.R., 2018. Synergistic reduction of copper (II) and oxidation of norfloxacin over a novel sewage sludge-derived char-based catalyst: performance, fate and mechanism. *J. Clean. Prod.* 182, 794–804. <https://doi.org/10.1016/J.JCLEPRO.2018.02.045>.
- Liu, S., Zhao, X., Zeng, H., Wang, Y., Qiao, M., Guan, W., 2017. Enhancement of photoelectrocatalytic degradation of diclofenac with persulfate activated by Cu cathode. *Chem. Eng. J.* 320, 168–177. <https://doi.org/10.1016/j.cej.2017.03.047>.
- Liu, W., Li, Y., Liu, F., Jiang, W., Zhang, D., Liang, J., 2019. Visible-light-driven photocatalytic degradation of diclofenac by carbon quantum dots modified porous g-C₃N₄: mechanisms, degradation pathway and DFT calculation. *Water Res.* 151, 8–19. <https://doi.org/10.1016/j.watres.2018.11.084>.
- Liu, X., Ji, H., Li, S., Liu, W., 2019. Graphene modified anatase/titanate nanosheets with enhanced photocatalytic activity for efficient degradation of sulfamethazine under simulated solar light. *Chemosphere* 233, 198–206. <https://doi.org/10.1016/j.chemosphere.2019.05.229>.
- Liu, Y., Gan, X., Zhou, B., Xiong, B., Li, J., Dong, C., Bai, J., Cai, W., 2009. Photoelectrocatalytic degradation of tetracycline by highly effective TiO₂ nanopore arrays electrode. *J. Hazard Mater.* 171, 678–683. <https://doi.org/10.1016/j.jhazmat.2009.06.054>.
- Liu, Y., Wang, X., Sun, Q., Yuan, M., Sun, Z., Xia, S., Zhao, J., 2022. Enhanced visible light photo-Fenton-like degradation of tetracyclines by expanded perlite supported FeMo₃O₄/g-C₃N₄ floating Z-scheme catalyst. *J. Hazard Mater.* 424, 127387. <https://doi.org/10.1016/J.JHAZMAT.2021.127387>.
- Liu, Y.J., Hu, C.Y., Lo, S.L., 2019. Direct and indirect electrochemical oxidation of amine-containing pharmaceuticals using graphite electrodes. *J. Hazard Mater.* 366, 592–605. <https://doi.org/10.1016/j.jhazmat.2018.12.037>.
- Loos, G., Scheers, T., Van Eyck, K., Van Schepdael, A., Adams, E., Van der Bruggen, B., Cabooter, D., Dewil, R., 2018. Electrochemical oxidation of key pharmaceuticals using a boron doped diamond electrode. *Separ. Purif. Technol.* 195, 184–191. <https://doi.org/10.1016/j.seppur.2017.12.009>.
- Low, J., Yu, J., Jaronec, M., Wageh, S., Al-Ghamdi, A.A., 2017. Heterojunction photocatalysts. *Adv. Mater.* <https://doi.org/10.1002/adma.201601694>.
- Luo, C., Ren, X., Dai, Z., Zhang, Y., Qi, X., Pan, C., 2017. Present perspectives of advanced characterization techniques in TiO₂-based photocatalysts. *ACS Appl. Mater. Interfaces.* <https://doi.org/10.1021/acsami.7b00496>.
- Luong, J.H.T., Male, K.B., Glennon, J.D., 2009. Boron-doped diamond electrode: synthesis, characterization, functionalization and analytical applications. *Analyst.* <https://doi.org/10.1039/b910206j>.
- Ma, B., Xin, S., Xin, Y., Ma, X., Zhang, C., Gao, M., Ma, F., Ma, Y., 2021. Visible-light-driven photoelectrocatalytic degradation of p-chloronitrobenzene by BiOBr/TiO₂ nanotube arrays photoelectrodes: mechanisms, degradation pathway and DFT calculation. *Separ. Purif. Technol.* 268, 118699. <https://doi.org/10.1016/j.seppur.2021.118699>.
- Ma, Q., Zhang, H., Guo, R., Li, B., Zhang, X., Cheng, X., Xie, M., Cheng, Q., 2018. Construction of CuS/TiO₂ nano-tube arrays photoelectrode and its enhanced visible light photoelectrocatalytic decomposition and mechanism of penicillin G. *Electrochim. Acta* 283, 1154–1162. <https://doi.org/10.1016/j.electacta.2018.07.026>.
- Macpherson, J.V., 2015. A practical guide to using boron doped diamond in electrochemical research. *Phys. Chem. Chem. Phys.* 17, 2935–2949. <https://doi.org/10.1039/c4cp04022h>.
- Malato, S., Maldonado, M.I., Fernández-Ibáñez, P., Oller, I., Polo, I., Sánchez-Moreno, R., 2016. Decontamination and disinfection of water by solar photocatalysis: the pilot plants of the Plataforma Solar de Almería. *Mater. Sci. Semicond. Process.* <https://doi.org/10.1016/j.mssp.2015.07.017>.
- Manassero, A., Satuf, M.L., Alfano, O.M., 2017. Photocatalytic degradation of an emerging pollutant by TiO₂-coated glass rings: a kinetic study. *Environ. Sci. Pollut. Res.* 24, 6031–6039. <https://doi.org/10.1007/s11356-016-6855-2>.
- Manassero, A., Satuf, M.L., Alfano, O.M., 2015. Kinetic modeling of the photocatalytic degradation of clofibrac acid in a slurry reactor. *Environ. Sci. Pollut. Res.* 22, 926–937. <https://doi.org/10.1007/s11356-014-2682-5>.
- Mancuso, A., Sacco, O., Vaiano, V., Sannino, D., Pragliola, S., Venditto, V., Morante, N., 2021. Visible light active Fe-Pr co-doped TiO₂ for water pollutants degradation. *Catal. Today* 380, 93–104. <https://doi.org/10.1016/j.cattod.2021.04.018>.
- Marinho, B.A., Cristóvão, R.O., Boaventura, R.A.R., Vilar, V.J.P., 2019. As(III) and Cr(VI) oxyanion removal from water by advanced oxidation/reduction processes—a review. *Environ. Sci. Pollut. Res.* <https://doi.org/10.1007/s11356-018-3595-5>.
- Marinho, B.A., Cristóvão, R.O., Djellabi, R., Caseiro, A., Miranda, S.M., Loureiro, J.M., Boaventura, R.A.R., Dias, M.M., Lopes, J.C.B., Vilar, V.J.P., 2018. Strategies to reduce mass and photons transfer limitations in heterogeneous photocatalytic processes: hexavalent chromium reduction studies. *J. Environ. Manag.* 217, 555–564. <https://doi.org/10.1016/j.jenvman.2018.04.003>.
- Marinho, B.A., Cristóvão, R.O., Djellabi, R., Loureiro, J.M., Boaventura, R.A.R., Vilar, V.J.P., 2017. Photocatalytic reduction of Cr(VI) over TiO₂-coated cellulose acetate monolithic structures using solar light. *Appl. Catal. B Environ.* 203, 18–30. <https://doi.org/10.1016/j.apcatb.2016.09.061>.

- Marinho, B.A., de Souza, S.M.A.G.U., de Souza, A.A.U., Hotza, D., 2021. Electrospun TiO₂ nanofibers for water and wastewater treatment: a review. *J. Mater. Sci.* <https://doi.org/10.1007/s10853-020-05610-6>.
- Marinko, Z., Suhadolnik, L., Setina Batić, B., Selih, V.S., Majaron, B., Kovač, J., Čeh, M., 2021. Toward a flexible and efficient TiO₂ photocatalyst immobilized on a titanium foil. *ACS Omega* 6, 23233–23242. <https://doi.org/10.1021/acsomega.1c02862>.
- Martínez-Huitle, C.A., Rodrigo, M.A., Sirés, I., Scialdone, O., 2015. Single and coupled electrochemical processes and reactors for the abatement of organic water pollutants: a critical review. *Chem. Rev.* 115, 13362–13407. <https://doi.org/10.1021/acs.chemrev.5b00361>.
- Martínez, C., Canle, L.M., Fernández, M.I., Santaballa, J.A., Faria, J., 2011. Aqueous degradation of diclofenac by heterogeneous photocatalysis using nanostructured materials. *Appl. Catal. B Environ.* 107, 110–118. <https://doi.org/10.1016/j.apcatb.2011.07.003>.
- Mathon, B., Coquery, M., Liu, Z., Penru, Y., Guillon, A., Esperanza, M., Miège, C., Choubert, J.M., 2021. Ozonation of 47 organic micropollutants in secondary treated municipal effluents: direct and indirect kinetic reaction rates and modelling. *Chemosphere* 262, 127969. <https://doi.org/10.1016/j.chemosphere.2020.127969>.
- May, P.W., 2000. Diamond thin films: a 21st-century material. *Philos. Trans. R. Soc. A Math. Phys. Eng. Sci.* 358, 473–495. <https://doi.org/10.1098/rsta.2000.0542>.
- Mazierski, P., Borzyszkowska, A.F., Wilczewska, P., Białk-Bielińska, A., Zaleska-Medynska, A., Siedlecka, E.M., Pieczyńska, A., 2019. Removal of 5-fluorouracil by solar-driven photoelectrocatalytic oxidation using Ti/TiO₂(NT) photoelectrodes. *Water Res.* 157, 610–620. <https://doi.org/10.1016/j.watres.2019.04.010>.
- Mehrabadi, Z., Faghhihian, H., 2018. Comparative photocatalytic performance of TiO₂ supported on clinoptilolite and TiO₂/Salicylaldehyde-NH₂-MIL-101(Cr) for degradation of pharmaceutical pollutant atenolol under UV and visible irradiations. *J. Photochem. Photobiol. Chem.* 356, 102–111. <https://doi.org/10.1016/j.jphotochem.2017.12.042>.
- Meng, F., Wang, Y., Chen, Z., Hu, J., Lu, G., Ma, W., 2021. Synthesis of CQDs@FeOOH nanoneedles with active edges for efficient electro-catalytic degradation of levofloxacin: degradation mechanism and toxicity assessment. *Appl. Catal. B Environ.* 282, 119597. <https://doi.org/10.1016/j.apcatb.2020.119597>.
- Mitsika, E.E., Christophoridis, C., Kouinoglou, N., Lazaridis, N., Zacharis, C.K., Fytianos, K., 2021. Optimized Photo-Fenton degradation of psychoactive pharmaceuticals alprazolam and diazepam using a chemometric approach—structure and toxicity of transformation products. *J. Hazard Mater.* 403, 123819. <https://doi.org/10.1016/j.jhazmat.2020.123819>.
- Miyashita, K., Kondo, T., Sugai, S., Tei, T., Nishikawa, M., Tojo, T., Yuasa, M., 2019. Boron-doped nanodiamond as an electrode material for aqueous electric double-layer capacitors. *Sci. Rep.* 9, 1–10. <https://doi.org/10.1038/s41598-019-54197-9>.
- Mohammed, M.K.A., 2020. Sol-gel synthesis of Au-doped TiO₂ supported SWCNT nanohybrid with visible-light-driven photocatalytic for high degradation performance toward methylene blue dye. *Optik* 223, 165607. <https://doi.org/10.1016/j.jlleo.2020.165607>.
- Mohapatra, D.P., Brar, S.K., Dagher, R., Tyagi, R.D., Picard, P., Surampalli, R.Y., Drogui, P., 2014a. Photocatalytic degradation of carbamazepine in wastewater by using a new class of whey-stabilized nanocrystalline TiO₂ and ZnO. *Sci. Total Environ.* 485–486, 263–269. <https://doi.org/10.1016/j.scitotenv.2014.03.089>.
- Mohapatra, D.P., Brar, S.K., Tyagi, R.D., Picard, P., Surampalli, R.Y., 2014b. Analysis and advanced oxidation treatment of a persistent pharmaceutical compound in wastewater and wastewater sludge-carbamazepine. *Sci. Total Environ.* 470, 58–75. <https://doi.org/10.1016/j.scitotenv.2013.09.034>–471.
- Moradmand Jalali, H., Dezhmanpanah, H., 2021. Kinetic investigation of photo-degradation of amoxicillin, ampicillin, and cloxacillin by semiconductors using Monte Carlo simulation. *Chem. Eng. Commun.* 208, 159–165. <https://doi.org/10.1080/00986445.2019.1694918>.
- Moreira, F.C., Boaventura, R.A.R., Brillas, E., Vilar, V.J.P., 2017. Electrochemical advanced oxidation processes: a review on their application to synthetic and real wastewaters. *Appl. Catal. B Environ.* <https://doi.org/10.1016/j.apcatb.2016.08.037>.
- Nabi, G., Majid, A., Riaz, A., Alharbi, T., Arshad Kamran, M., Al-Habardi, M., 2021. Green synthesis of spherical TiO₂ nanoparticles using Citrus Limetta extract: excellent photocatalytic water decontamination agent for Rh dye. *Inorg. Chem. Commun.* 129, 108618. <https://doi.org/10.1016/j.inoche.2021.108618>.
- Nakata, K., Fujishima, A., 2012. TiO₂ photocatalysis: design and applications. *J. Photochem. Photobiol. C Photochem. Rev.* <https://doi.org/10.1016/j.jphotochemrev.2012.06.001>.
- Nakata, K., Liu, B., Ishikawa, Y., Sakai, M., Saito, H., Ochiai, T., Sakai, H., Murakami, T., Abe, M., Takagi, K., Fujishima, A., 2011. Fabrication and photocatalytic properties of TiO₂ nanotube arrays modified with phosphate. *Chem. Lett.* 40, 1107–1109. <https://doi.org/10.1246/cl.2011.1107>.
- Naraginti, S., Yu, Y.Y., Fang, Z., Yong, Y.C., 2019. Visible light degradation of macrolide antibiotic azithromycin by novel ZrO₂/Ag@TiO₂ nanorod composite: transformation pathways and toxicity evaluation. *Process Saf. Environ. Protect.* 125, 39–49. <https://doi.org/10.1016/j.psep.2019.02.031>.
- Neghi, N., Kumar, M., Burkhalov, D., 2019. Synthesis and application of stable, reusable TiO₂ polymeric composites for photocatalytic removal of metronidazole: removal kinetics and density functional analysis. *Chem. Eng. J.* 359, 963–975. <https://doi.org/10.1016/j.cej.2018.11.090>.
- NHMRC, 2018. Australian Drinking Water Guidelines Paper 6 National Water Quality Management Strategy. Version 3.5. 2018.
- Nie, X., Chen, J., Li, G., Shi, H., Zhao, H., Wong, P.K., An, T., 2013. Synthesis and characterization of TiO₂ nanotube photoanode and its application in photoelectrocatalytic degradation of model environmental pharmaceuticals. *J. Chem. Technol. Biotechnol.* 88, 1488–1497. <https://doi.org/10.1002/jctb.3992>.
- Orimolade, B.O., Arotiba, O.A., 2020. Towards visible light driven photoelectrocatalysis for water treatment: application of a FTO/BiVO₄/Ag₂S heterojunction anode for the removal of emerging pharmaceutical pollutants. *Sci. Rep.* 10, 1–13. <https://doi.org/10.1038/s41598-020-62425-w>.
- Oseghe, E.O., Ofomaja, A.E., 2018. Facile microwave synthesis of pine cone derived Cd-doped TiO₂ for the photodegradation of tetracycline hydrochloride under visible-LED light. *J. Environ. Manag.* 223, 860–867. <https://doi.org/10.1016/j.jenvman.2018.07.003>.
- Oturan, N., Brillas, E., Oturan, M.A., 2012. Unprecedented total mineralization of atrazine and cyanuric acid by anodic oxidation and electro-Fenton with a boron-doped diamond anode. *Environ. Chem. Lett.* 10, 165–170. <https://doi.org/10.1007/s10311-011-0337-z>.
- Palanivel, B., Lallimathi, M., Arjankumar, B., Shkir, M., Alshahrani, T., Al-Namshah, K. S., Hamdy, M.S., Shanavas, S., Venkatachalam, M., Ramalingam, G., 2021. rGO supported g-C₃N₄/CoFe₂O₄ heterojunction: visible-light-active photocatalyst for effective utilization of H₂O₂ to organic pollutant degradation and OH radicals production. *J. Environ. Chem. Eng.* 9, 104698. <https://doi.org/10.1016/j.jece.2020.104698>.
- Palmisano, G., Loddò, V., Augugliaro, V., Bellardita, M., Camera Roda, G., Parrino, F., 2015. Validation of a two-dimensional modeling of an externally irradiated slurry photoreactor. *Chem. Eng. J.* 262, 490–498. <https://doi.org/10.1016/j.cej.2014.10.013>.
- Panizza, M., Cerisola, G., 2009. Direct and mediated anodic oxidation of organic pollutants. *Chem. Rev.* 109, 6541–6569. <https://doi.org/10.1021/cr9001319>.
- Paredes, L., Murgolo, S., Dzinun, H., Dzarfan Othman, M.H., Ismail, A.F., Carballa, M., Mascolo, G., 2019. Application of immobilized TiO₂ on PVDF dual layer hollow fibre membrane to improve the photocatalytic removal of pharmaceuticals in different water matrices. *Appl. Catal. B Environ.* 240, 9–18. <https://doi.org/10.1016/j.apcatb.2018.08.067>.
- Patel, M., Kumar, R., Kishor, K., Mlsna, T., Pittman, C.U., Mohan, D., 2019. Pharmaceuticals of emerging concern in aquatic systems: chemistry, occurrence, effects, and removal methods. *Chem. Rev.* <https://doi.org/10.1021/acs.chemrev.8b00299>.
- Pelaez, M., Nolan, N.T., Pillai, S.C., Seery, M.K., Falaras, P., Kontos, A.G., Dunlop, P.S.M., Hamilton, J.W.J., Byrne, J.A., O’Shea, K., Entezari, M.H., Dionysiou, D.D., 2012. A review on the visible light active titanium dioxide photocatalysts for environmental applications. *Appl. Catal. B Environ.* <https://doi.org/10.1016/j.apcatb.2012.05.036>.
- Pelalak, R., Heidari, Z., Alizadeh, R., Gharehabani, E., Nasseh, N., Marjani, A., Albadarin, A.B., Shirazian, S., 2021. Efficient oxidation/mineralization of pharmaceutical pollutants using a novel Iron (III) oxyhydroxide nanostructure prepared via plasma technology: experimental, modeling and DFT studies. *J. Hazard Mater.* 411, 125074. <https://doi.org/10.1016/j.jhazmat.2021.125074>.
- Pereira, J.H.O.S., Reis, A.C., Queirós, D., Nunes, O.C., Borges, M.T., Vilar, V.P., Boaventura, R.A.R., 2013. Insights into solar TiO₂-assisted photocatalytic oxidation of two antibiotics employed in aquatic animal production, oxolinic acid and oxytetracycline. *Sci. Total Environ.* 463, 274–283. <https://doi.org/10.1016/j.scitotenv.2013.05.098>, 464.
- Perisic, D.J., Kovacic, M., Kusic, H., Stangar, U.L., Marin, V., Bozic, A.L., 2016. Comparative analysis of UV-C/H₂O₂ and UV-A/TiO₂ processes for the degradation of diclofenac in water. *React. Kinet. Mech. Catal.* 118, 451–462. <https://doi.org/10.1007/s11144-016-1027-4>.
- Porcar-Santos, O., Cruz-Alcalde, A., López-Vinent, N., Zanganas, D., Sans, C., 2020. Photocatalytic degradation of sulfamethoxazole using TiO₂ in simulated seawater: evidence for direct formation of reactive halogen species and halogenated by-products. *Sci. Total Environ.* 736, 139605. <https://doi.org/10.1016/j.scitotenv.2020.139605>.
- Prakash, J., Samrithi, Kumar, A., Dai, H., Janegitz, B.C., Krishnan, V., Swart, H.C., Sun, S., 2021. Novel rare earth metal-doped one-dimensional TiO₂ nanostructures: fundamentals and multifunctional applications. *Mater. Today Sustain.* <https://doi.org/10.1016/j.mtsust.2021.100066>.
- Prasannamedha, K., Kumar, P.S., 2020. A review on contamination and removal of sulfamethoxazole from aqueous solution using cleaner techniques: present and future perspective. *J. Clean. Prod.* 250, 119553. <https://doi.org/10.1016/j.jclepro.2019.119553>.
- Prawer, S., Kalish, R., 1995. Ion-beam-induced transformation of diamond. *Phys. Rev. B* 51, 15711–15722. <https://doi.org/10.1103/PhysRevB.51.15711>.
- Qu, X., Lin, J., Chaudhary, J.P., Sun, B., Wei, F., Fan, M., Sun, D., 2021. Defect enrich ultrathin TiO₂ nanosheets for rapid adsorption and visible light mediated PPCPs degradation. *Chemosphere* 268, 128782. <https://doi.org/10.1016/j.chemosphere.2020.128782>.
- Raymundo-Pereira, P.A., Campos, A.M., Mendonça, C.D., Calegari, M.L., Machado, S.A.S., Oliveira, O.N., 2017. Printex 6L carbon nanoballs used in electrochemical sensors for simultaneous detection of emerging pollutants hydroquinone and paracetamol. *Sensor. Actuator. B Chem.* 252, 165–174. <https://doi.org/10.1016/j.snb.2017.05.121>.
- Reddy, S.R., Saritha, V., Karnena, K., Dwarapureddi, B.K., 2017. Combined SBR and RO pilot scale treatment for pharmaceutical wastewater. <https://doi.org/10.5004/dwt.2017.21579>.
- Regmi, C., Kshetri, Y.K., Dhakal, D., Sohng, J.K., Rosei, F., Lee, S.W., 2019a. Insight into phosphate doped BiVO₄ heterostructure for multifunctional photocatalytic performances: a combined experimental and DFT study. *Appl. Surf. Sci.* 466, 787–800. <https://doi.org/10.1016/j.apsusc.2018.10.069>.
- Regmi, C., Kshetri, Y.K., Kim, T.H., Dhakal, D., Lee, S.W., 2019b. Mechanistic understanding of enhanced photocatalytic activity of N-doped BiVO₄ towards

- degradation of ibuprofen: an experimental and theoretical approach. *Mol. Catal.* 470, 8–18. <https://doi.org/10.1016/j.mcat.2019.03.014>.
- Reinholds, I., Pugajeva, I., Perkons, I., Lundanes, E., Rusko, J., Kizane, G., Nikolajeva, V., Mutere, O., Petrina, Z., Baumane, L., Bartkevics, V., 2017. Decomposition of multi-class pharmaceutical residues in wastewater by exposure to ionising radiation. *Int. J. Environ. Sci. Technol.* 14, 1969. <https://doi.org/10.1007/s13762-017-1290-6>, 1980.
- Rezaei, R., Mohseni, M., 2017. Impact of natural organic matter on the degradation of 2,4-dichlorophenoxy acetic acid in a fluidized bed photocatalytic reactor. *Chem. Eng. J.* 310, 457–463. <https://doi.org/10.1016/j.cej.2016.05.086>.
- Rodríguez-Mozaz, S., Vaz-Moreira, I., Varela Della Giustina, S., Llorca, M., Barceló, D., Schubert, S., Berendonk, T.U., Michael-Kordatou, I., Fatta-Kassinos, D., Martinez, J. L., Elpers, C., Henriques, I., Jaeger, T., Schwartz, T., Paulshus, E., O'Sullivan, K., Pärnänen, K.M.M., Virta, M., Do, T.T., Walsh, F., Manaia, C.M., 2020. Antibiotic residues in final effluents of European wastewater treatment plants and their impact on the aquatic environment. *Environ. Int.* 140, 1–11. <https://doi.org/10.1016/j.envint.2020.105733>.
- Sági, G., Szabacs, K., Szabó, L., Homlok, R., Kovács, K., Mohácsi-Farkas, C., Pillai, S.D., Takács, E., Wojnárovits, L., 2018. Influence of ionizing radiation on the antimicrobial activity of the antibiotics sulfamethoxazole and trimethoprim. *J. Environ. Sci. Heal. - Part A Toxic/Hazardous Subst. Environ. Eng.* 53, 687–693. <https://doi.org/10.1080/10934529.2018.1439821>.
- Salazar, C., Contreras, N., Mansilla, H.D., Yáñez, J., Salazar, R., 2016. Electrochemical degradation of the antihypertensive losartan in aqueous medium by electro-oxidation with boron-doped diamond electrode. *J. Hazard Mater.* 319, 84–92. <https://doi.org/10.1016/j.jhazmat.2016.04.009>.
- Samarghandi, M.R., Dargahi, A., Rahmani, A., Shabanloo, A., Ansari, A., Nematollahi, D., 2021. Application of a fluidized three-dimensional electrochemical reactor with Ti/SnO₂-Sb/β-PbO₂ anode and granular activated carbon particles for degradation and mineralization of 2,4-dichlorophenol: process optimization and degradation pathway. *Chemosphere* 279, 130640. <https://doi.org/10.1016/j.chemosphere.2021.130640>.
- Sanabria, P., Scunderlick, D., Wilde, M.L., Lüdtk, D.S., Sirtori, C., 2021. Solar photo-Fenton treatment of the anti-cancer drug anastrozole in different aqueous matrices at near-neutral pH: transformation products identification, pathways proposal, and in silico (Q)SAR risk assessment. *Sci. Total Environ.* 754, 142300. <https://doi.org/10.1016/j.scitotenv.2020.142300>.
- Santana, M.H.P., Faria, L.A.D., Boodts, J.F.C., 2005. Electrochemical characterisation and oxygen evolution at a heavily boron doped diamond electrode. *Electrochim. Acta* 50, 2017–2027. <https://doi.org/10.1016/j.electacta.2004.08.050>.
- Sarkar, S., Chakraborty, S., Bhattacharjee, C., 2015. Photocatalytic degradation of pharmaceutical wastes by alginate supported TiO₂ nanoparticles in packed bed photo reactor (PBPR). *Ecotoxicol. Environ. Saf.* 121, 263–270. <https://doi.org/10.1016/j.ecoenv.2015.02.035>.
- Savun-Hekimoğlu, B., Eren, Z., Ince, N.H., 2020. Photocatalytic destruction of caffeine on sepiolite-supported TiO₂ nanocomposite. *Sustain. Times* 12, 1–16. <https://doi.org/10.3390/su122410314>.
- Scaria, J., Gopinath, A., Nidheesh, P.V., 2021. A versatile strategy to eliminate emerging contaminants from the aqueous environment: heterogeneous Fenton process. *J. Clean. Prod.* <https://doi.org/10.1016/j.jclepro.2020.124014>.
- Seitz, W., Schulz, W., Weber, W.H., 2006. Novel applications of highly sensitive liquid chromatography/mass spectrometry/mass spectrometry for the direct detection of ultra-trace levels of contaminants in water. *Rapid Commun. Mass Spectrom.* 20, 2281–2285. <https://doi.org/10.1002/rcm.2554>.
- Šešlovská, R., Štěpánková, M., Janíková, L., Nováková, K., Vojs, M., Marton, M., Behl, M., 2016. Surface and electrochemical characterization of boron-doped diamond electrodes prepared under different conditions. *Monatshfte fur Chemie* 147, 1353–1364. <https://doi.org/10.1007/s00706-015-1640-3>.
- Seo, J.-H., Mikael, S., Mi, H., Venkataraman, G., Blanchard, J.P., Zhou, W., Gong, S., Ma, Z., 2014. Thermal diffusion doping of single crystal diamond. *J. Appl. Phys.* 119, 1–35.
- Seshan, V., Ullien, D., Castellanos-Gomez, A., Sachdeva, S., Murthy, D.H.K., Savenije, T. J., Ahmad, H.A., Nunnery, T.S., Janssens, S.D., Haenen, K., Nešládek, M., Van Der Zant, H.S.J., Sudhölter, E.J.R., De Smet, L.C.P.M., 2013. Hydrogen termination of CVD diamond films by high-temperature annealing at atmospheric pressure. *J. Chem. Phys.* 138, 1–6. <https://doi.org/10.1063/1.4810866>.
- Shen, Y., Chu, L., Zhuan, R., Xiang, X., Sun, H., Wang, J., 2019a. Degradation of antibiotics and antibiotic resistance genes in fermentation residues by ionizing radiation: a new insight into a sustainable management of antibiotic fermentative residuals. *J. Environ. Manag.* 232, 171–178. <https://doi.org/10.1016/j.jenvman.2018.11.050>.
- Shen, Y., Zhuan, R., Chu, L., Xiang, X., Sun, H., Wang, J., 2019b. Inactivation of antibiotic resistance genes in antibiotic fermentation residues by ionizing radiation: exploring the development of recycling economy in antibiotic pharmaceutical factory. *Waste Manag.* 84, 141–146. <https://doi.org/10.1016/j.wasman.2018.11.039>.
- Shi, L., Yan, C., Guo, Z., Chi, W., Wei, J., Liu, W., Liu, X., Tian, H., Zhu, W.H., 2020. De novo strategy with engineering anti-Kasha/Kasha fluorophores enables reliable ratiometric quantification of biomolecules. *Nat. Commun.* 11 <https://doi.org/10.1038/s41467-020-14615-3>.
- Sichel, C., Garcia, C., Andre, K., 2011. Feasibility studies: UV/chlorine advanced oxidation treatment for the removal of emerging contaminants. *Water Res.* 45, 6371–6380. <https://doi.org/10.1016/j.watres.2011.09.025>.
- Singh, N.B., Nagpal, G., Agrawal, S., Rachna, 2018. Water purification by using adsorbents: a review. *Environ. Technol. Innovat.* <https://doi.org/10.1016/j.eti.2018.05.006>.
- Sirés, I., Brillas, E., Oturan, M.A., Rodrigo, M.A., Panizza, M., 2014. Electrochemical advanced oxidation processes: today and tomorrow. A review. *Environ. Sci. Pollut. Res.* 21, 8336–8367. <https://doi.org/10.1007/s11356-014-2783-1>.
- Smaali, A., Berkani, M., Merouane, F., Le, V.T., Vasseghian, Y., Rahim, N., Kouachi, M., 2021. Photocatalytic-persulfate-oxidation for diclofenac removal from aqueous solutions: modeling, optimization and biotoxicity test assessment. *Chemosphere* 266, 129158. <https://doi.org/10.1016/j.chemosphere.2020.129158>.
- Sodhi, K.K., Kumar, M., Singh, D.K., 2021. Insight into the amoxicillin resistance, ecotoxicity, and remediation strategies. *J. Water Proc. Eng.* 39, 101858. <https://doi.org/10.1016/j.jwpe.2020.101858>.
- Song, C.W., Cho, D.S., Lee, J.M., Song, P.K., 2020. Effect of boron doping on diamond film and electrochemical properties of BDD according to thickness and morphology. *Coatings* 10, 1–11. <https://doi.org/10.3390/coatings10040331>.
- Sopaj, F., Rodrigo, M.A., Oturan, N., Podvorica, F.I., Pinson, J., Oturan, M.A., 2015. Influence of the anode materials on the electrochemical oxidation efficiency. Application to oxidative degradation of the pharmaceutical amoxicillin. *Chem. Eng. J.* 262, 286–294. <https://doi.org/10.1016/j.cej.2014.09.100>.
- Srikanth, V.V.S.S., Sampath Kumar, P., Kumar, V.B., 2012. A brief review on the in situ synthesis of boron-doped diamond thin films. *Int. J. Electrochem.* 1–7. <https://doi.org/10.1155/2012/218393>, 2012.
- Strobel, P., Riedel, M., Ristein, J., Ley, L., 2004. Surface transfer doping of diamond. *Nature* 430, 439–441. <https://doi.org/10.1038/nature02751>.
- Su, Y., fan, Wang, G.B., Kuo, D.T.F., Chang, M., ling, Shih, hsin, Y., 2016. Photoelectrocatalytic degradation of the antibiotic sulfamethoxazole using TiO₂/Ti photoanode. *Appl. Catal. B Environ.* 186, 184–192. <https://doi.org/10.1016/j.apcatb.2016.01.003>.
- Suhadolnik, L., Lasić Jurković, D., Likozar, B., Bele, M., Drev, S., Čeh, M., 2019a. Structured titanium oxynitride (TiO_xN_y) nanotube arrays for a continuous electrocatalytic phenol-degradation process: synthesis, characterization, mechanisms and the chemical reaction micro-kinetics. *Appl. Catal. B Environ.* 257 <https://doi.org/10.1016/j.apcatb.2019.117894>.
- Suhadolnik, L., Pohar, A., Novak, U., Likozar, B., Mihelić, A., Čeh, M., 2019b. Continuous photocatalytic, electrocatalytic and photo-electrocatalytic degradation of a reactive textile dye for wastewater-treatment processes: batch, microreactor and scaled-up operation. *J. Ind. Eng. Chem.* 72, 178–188. <https://doi.org/10.1016/j.jiec.2018.12.017>.
- Surenjan, A., Pradeep, T., Philip, L., 2019. Application and performance evaluation of a cost-effective vis-LED based fluidized bed reactor for the treatment of emerging contaminants. *Chemosphere* 228, 629–639. <https://doi.org/10.1016/j.chemosphere.2019.04.179>.
- Talwar, S., Verma, A.K., Sangal, V.K., 2021. Synergistic degradation employing photocatalysis and photo-Fenton process of real industrial pharmaceutical effluent utilizing the Iron-Titanium dioxide composite. *Process Saf. Environ. Protect.* 146, 564–576. <https://doi.org/10.1016/j.psep.2020.11.029>.
- Tang, H., Shang, Q., Tang, Y., Yi, X., Wei, Y., Yin, K., Liu, M., Liu, C., 2020. Static and continuous flow photoelectrocatalytic treatment of antibiotic wastewater over mesh of TiO₂ nanotubes implanted with g-C₃N₄ nanosheets. *J. Hazard Mater.* 384, 121248. <https://doi.org/10.1016/j.jhazmat.2019.121248>.
- Tang, L., Wang, J., Jun, Jia, C., tao, Lv, G., xin, Xu, G., Li, W., tao, Wang, L., Zhang, J., ye, Wu, M., hong, 2017. Simulated solar driven catalytic degradation of psychiatric drug carbamazepine with binary BiVO₄ heterostructures sensitized by graphene quantum dots. *Appl. Catal. B Environ.* 205, 587–596. <https://doi.org/10.1016/j.apcatb.2016.10.067>.
- Telegan Chekem, C., Chiron, S., Mancaux, J.M., Plantard, G., Goetz, V., 2020. Thermal activation of persulfates for wastewater depollution on pilot scale solar equipment. *Sol. Energy* 205, 372–379. <https://doi.org/10.1016/j.solener.2020.04.075>.
- Tirado, P., Alcantar-Peña, J.J., De Obaldia, E., Kudriavtsev, Y., García, R., Auciello, O., 2018. Boron doping of ultrananocrystalline diamond films by thermal diffusion process. *MRS Commun* 8, 1111–1118. <https://doi.org/10.1557/mrc.2018.157>.
- Tran, H.T.T., Kosslick, H., Ibad, M.F., Fischer, C., Benstrup, U., Vuong, T.H., Nguyen, L.Q., Schulz, A., 2017. Photocatalytic performance of highly active brookite in the degradation of hazardous organic compounds compared to anatase and rutile. *Appl. Catal. B Environ.* 200, 647–658. <https://doi.org/10.1016/j.apcatb.2016.07.017>.
- Turkay, O., Barışçi, S., Ulusoy, E., Şeker, M.G., Dimoglo, A., 2018. Anodic oxidation of anti-cancer drug Imatinib on different electrodes: kinetics, transformation by-products and toxicity assessment. *Electrochim. Acta* 263, 400–408. <https://doi.org/10.1016/j.electacta.2018.01.079>.
- Turro, N.J., Ramamurthy, V., Cherry, W., Farneth, W., 1978. The effect of wavelength on organic photoreactions in solution. Reactions from upper excited states. *Chem. Rev.* 78, 125–145. <https://doi.org/10.1021/cr60312a003>.
- U.S. Environmental Protection Agency, 2016. Revisions to the unregulated contaminant monitoring regulation (UCMR 4) for public water systems. *Fed. Regist.* 81, 92666–92692.
- Umukoro, E.H., Kumar, N., Ngila, J.C., Arotiba, O.A., 2018. Expanded graphite supported p-n MoS₂-SnO₂ heterojunction nanocomposite electrode for enhanced photo-electrocatalytic degradation of a pharmaceutical pollutant. *J. Electroanal. Chem.* 827, 193–203. <https://doi.org/10.1016/j.jelechem.2018.09.027>.
- Vafajoo, L., Khorasheh, F., Nakhjavani, M.H., Fattahi, M., 2014. Kinetic parameters optimization and modeling of catalytic dehydrogenation of heavy paraffins to Olefins. *Petrol. Sci. Technol.* 32, 813–820. <https://doi.org/10.1080/10916466.2011.604061>.
- Valério, A., Sárria, M.P., Rodríguez-Lorenzo, L., Hotza, D., Espiña, B., Gómez González, S.Y., 2020. Are TiO₂ nanoparticles safe for photocatalysis in aqueous media? *Nanoscale Adv* 2, 4951–4960. <https://doi.org/10.1039/d0na00584c>.

- Vokhmyanin, D.S., Oglezneva, S.A., 2019. Growth features of diamond films on the tungsten carbide surface with a copper sublayer. *Russ. J. Non-Ferrous Metals* 60, 754–761. <https://doi.org/10.3103/S1067821219060208>.
- Wang, C., Lin, C.Y., Liao, G.Y., 2020. Degradation of antibiotic tetracycline by ultrafine-bubble ozonation process. *J. Water Proc. Eng.* 37, 101463. <https://doi.org/10.1016/j.jwpe.2020.101463>.
- Wang, D., He, Y., Zhong, N., He, Z., Shen, Y., Zeng, T., Lu, X., Ma, J., Song, S., 2021. In situ chloride-mediated synthesis of TiO₂ thin film photoanode with enhanced photoelectrochemical activity for carbamazepine oxidation coupled with simultaneous cathodic H₂ production and CO₂ conversion to fuels. *J. Hazard Mater.* 410, 124563. <https://doi.org/10.1016/j.jhazmat.2020.124563>.
- Wang, J., Gao, B., Dou, M., Huang, X., Ma, Z., 2020. A porous g-C₃N₄ nanosheets containing nitrogen defects for enhanced photocatalytic removal meropenem: mechanism, degradation pathway and DFT calculation. *Environ. Res.* 184, 109339. <https://doi.org/10.1016/j.envres.2020.109339>.
- Wang, J., Wang, S., 2020. Reactive species in advanced oxidation processes: formation, identification and reaction mechanism. *Chem. Eng. J.* 401 <https://doi.org/10.1016/j.cej.2020.126158>.
- Wang, J., Zhuan, R., 2020. Degradation of antibiotics by advanced oxidation processes: an overview. *Sci. Total Environ.* 701, 135023. <https://doi.org/10.1016/j.scitotenv.2019.135023>.
- Wang, L., Lan, X., Peng, W., Wang, Z., 2020. Uncertainty and misinterpretation over identification, quantification and transformation of reactive species generated in catalytic oxidation processes: a review. *J. Hazard Mater.* <https://doi.org/10.1016/j.jhazmat.2020.124436>.
- Wang, P., Bu, L., Wu, Y., Ma, W., Zhu, S., Zhou, S., 2021. Mechanistic insight into the degradation of ibuprofen in UV/H₂O₂ process via a combined experimental and DFT study. *Chemosphere* 267, 128883. <https://doi.org/10.1016/j.chemosphere.2020.128883>.
- Wang, Q., Zhu, H., Li, B., 2019. Synergy of Ti-O-based heterojunction and hierarchical 1D nanobelt/3D microflower heteroarchitectures for enhanced photocatalytic tetracycline degradation and photoelectrochemical water splitting. *Chem. Eng. J.* 378, 122072. <https://doi.org/10.1016/j.cej.2019.122072>.
- Wang, X., Brigante, M., Dong, W., Wu, Z., Mailhot, G., 2020. Degradation of Acetaminophen via UVA-induced advanced oxidation processes (AOPs). Involvement of different radical species: HO[•], SO₄^{•-} and HO₂[•]/O₂^{•-}. *Chemosphere* 258, 127268. <https://doi.org/10.1016/j.chemosphere.2020.127268>.
- Wang, X., Cui, Y., Zhang, J., Shen, B., Sun, F., 2014. Erosive wear performance of boron-doped diamond films on different substrates. *Proc. Inst. Mech. Eng. Part J J. Eng. Tribol.* 228, 352–361. <https://doi.org/10.1177/1350650113508380>.
- Wang, X.H., Ma, G.H.M., Zhu, W., Glass, J.T., Bergman, L., Turner, K.F., Nemanich, R.J., 1992. Effects of boron doping on the surface morphology and structural imperfections of diamond films. *Diam. Relat. Mater.* 1, 828–835. [https://doi.org/10.1016/0925-9635\(92\)90109-2](https://doi.org/10.1016/0925-9635(92)90109-2).
- Wang, Y., Jing, B., Wang, F., Wang, S., Liu, X., Ao, Z., Li, C., 2020. Mechanism Insight into enhanced photodegradation of pharmaceuticals and personal care products in natural water matrix over crystalline graphitic carbon nitrides. *Water Res.* 180, 115925. <https://doi.org/10.1016/j.watres.2020.115925>.
- Wang, Zhuangzhuang, Jiang, L., Wang, K., Li, Y., Zhang, G., 2021. Novel AgI/BiSbO₄ heterojunction for efficient photocatalytic degradation of organic pollutants under visible light: interfacial electron transfer pathway, DFT calculation and degradation mechanism study. *J. Hazard Mater.* 410, 124948. <https://doi.org/10.1016/j.jhazmat.2020.124948>.
- Wang, Zichen, Li, H., Ma, W., Wang, Y., Cui, P., Qi, J., Chen, Z., Zhu, Z., Meng, F., 2021. Highly efficient electro-catalysis activation of peroxydisulfate by “used” As/Cr/Mo/FeOOH material for the degradation of metronidazole: degradation mechanism and toxicity assessment. *J. Taiwan Inst. Chem. Eng.* 121, 302–312. <https://doi.org/10.1016/j.jtice.2021.03.050>.
- Watanabe, I., Yata, M., Kanatani, M., Kawaguchi, Y., 2002. Effect of high-temperature annealing in vacuum and hydrogen on paramagnetic defects in diamond films grown by chemical vapor deposition. *Japanese J. Appl. Physics, Part 1 Regul. Pap. Short Notes Rev. Pap.* 41, 770–774. <https://doi.org/10.1143/jjap.41.770>.
- Welter, J.B., da Silva, S.W., Schneider, D.E., Rodrigues, M.A.S., Ferreira, J.Z., 2020. Performance of Nb/BDD material for the electrochemical advanced oxidation of prednisone in different water matrix. *Chemosphere* 248, 126062. <https://doi.org/10.1016/j.chemosphere.2020.126062>.
- Wu, C., Zuo, H., Du, H., Zhang, S., Wang, L., Yan, Q., 2022. Construction of layered embedding dual Z-Scheme Bi₂O₃/g-C₃N₄/Bi₂O₃: tetracycline degradation pathway, toxicity analysis and mechanism insight. *Separ. Purif. Technol.* 282, 120096. <https://doi.org/10.1016/J.SEPUR.2021.120096>.
- Xie, R., Meng, X., Sun, P., Niu, J., Jiang, W., Bottomley, L., Li, D., Chen, Y., Crittenden, J., 2017. Electrochemical oxidation of ofloxacin using a TiO₂-based SnO₂-Sb/polytetrafluoroethylene resin-PbO₂ electrode: reaction kinetics and mass transfer impact. *Appl. Catal. B Environ.* 203, 515–525. <https://doi.org/10.1016/j.apcatb.2016.10.057>.
- Xie, X., Li, S., Zhang, H., Wang, Z., Huang, H., 2019. Promoting charge separation of biochar-based Zn-TiO₂/pBC in the presence of ZnO for efficient sulfamethoxazole photodegradation under visible light irradiation. *Sci. Total Environ.* 659, 529–539. <https://doi.org/10.1016/J.SCITOTENV.2018.12.401>.
- Xing, Y., Ni, G., Liu, J., Tian, Y., Que, W., 2018. New insights into photocatalytic mechanism and photoelectrochemical property of bismuth oxybromide heterostructure with DFT investigation. *Appl. Surf. Sci.* 458, 464–477. <https://doi.org/10.1016/j.apsusc.2018.07.030>.
- Xu, L., Zhang, H., Xiong, P., Zhu, Q., Liao, C., Jiang, G., 2021. Occurrence, fate, and risk assessment of typical tetracycline antibiotics in the aquatic environment: a review. *Sci. Total Environ.* 753, 141975. <https://doi.org/10.1016/j.scitotenv.2020.141975>.
- Xue, J., Bao, J., 2021. Interfacial charge transfer of heterojunction photocatalysts: characterization and calculation. *Surface. Interfac.* 25, 101265. <https://doi.org/10.1016/j.surfin.2021.101265>.
- Yamashita, N., Yasojima, M., Nakada, N., Miyajima, K., Komori, K., Suzuki, Y., Tanaka, H., 2006. Effects of antibacterial agents, levofloxacin and clarithromycin, on aquatic organisms. In: *Water Science and Technology. Water Sci Technol*, pp. 65–72. <https://doi.org/10.2166/wst.2006.338>.
- Yang, C., Fan, Y., Li, P., Gu, Q., Li, X., yan, 2021. Freestanding 3-dimensional macroporous SnO₂ electrodes for efficient electrochemical degradation of antibiotics in wastewater. *Chem. Eng. J.* 422, 130032. <https://doi.org/10.1016/j.cej.2021.130032>.
- Yang, H., 2021. A short review on heterojunction photocatalysts: carrier transfer behavior and photocatalytic mechanisms. *Mater. Res. Bull.* <https://doi.org/10.1016/j.materresbull.2021.111406>.
- Yang, L., Li, Z., Jiang, H., Jiang, W., Su, R., Luo, S., Luo, Y., 2016. Photoelectrocatalytic oxidation of bisphenol A over mesh of TiO₂/graphene/Cu₂O. *Appl. Catal. B Environ.* 183, 75–85. <https://doi.org/10.1016/j.apcatb.2015.10.023>.
- Yang, Q., Chen, W., Xiao, C., Sannayanaik, R., Hirose, A., 2005. Synthesis of diamond films and nanotips through graphite etching. *Carbon N. Y.* 43, 748–754. <https://doi.org/10.1016/j.carbon.2004.10.047>.
- Yang, Y., Hoffmann, M.R., 2016. Synthesis and stabilization of blue-black TiO₂ nanotube arrays for electrochemical oxidant generation and wastewater treatment. *Environ. Sci. Technol.* 50, 11888–11894. <https://doi.org/10.1021/acs.est.6b03540>.
- Yang, Y., Ok, Y.S., Kim, K.H., Kwon, E.E., Tsang, Y.F., 2017. Occurrences and removal of pharmaceuticals and personal care products (PPCPs) in drinking water and water/sewage treatment plants: a review. *Sci. Total Environ.* 596, 303–320. <https://doi.org/10.1016/j.scitotenv.2017.04.102> –597.
- Yang, Z., Ding, X., Guo, Q., Wang, Y., Lu, Z., Ou, H., Luo, Z., Lou, X., 2017. Second generation of signaling-probe displacement electrochemical aptasensor for detection of picomolar ampicillin and sulfadimethoxine. *Sensor. Actuator. B Chem.* 253, 1129–1136. <https://doi.org/10.1016/j.snb.2017.07.119>.
- Yang, Z., Xia, X., Shao, L., Wang, L., Liu, Y., 2021. Efficient photocatalytic degradation of tetracycline under visible light by Z-scheme Ag₃PO₄/mixed-valence MIL-88A(Fe) heterojunctions: mechanism insight, degradation pathways and DFT calculation. *Chem. Eng. J.* 410, 128454. <https://doi.org/10.1016/j.cej.2021.128454>.
- Yin, Z., Han, M., Hu, Z., Feng, L., Liu, Y., Du, Z., Zhang, L., 2020. Peroxymonosulfate enhancing visible light photocatalytic degradation of bezafibrate by Pd/g-C₃N₄ catalysts: the role of sulfate radicals and hydroxyl radicals. *Chem. Eng. J.* 390, 124532. <https://doi.org/10.1016/j.cej.2020.124532>.
- Yu, H., Zhang, M., Wang, Y., Lv, J., Liu, Y., He, G., Sun, Z., 2021. Low-temperature strategy for vapor phase hydrothermal synthesis of C₃N₄-doped TiO₂ nanorod arrays with enhanced photoelectrochemical and photocatalytic activity. *J. Ind. Eng. Chem.* <https://doi.org/10.1016/j.jiec.2021.03.021>.
- Yu, Y., bo, Zhang, Q., Wu, L., ying, Zhou, Y., lian, Wang, B. xin, Chen, B.Y., Hong, J. ming, 2021. Reaction mechanism of N-(4-hydroxyphenyl)ethanamide electrodegradation via phosphorus-graphene prepared from triphenylphosphine: generation and destruction of the reactive species. *Chem. Eng. J.* 403, 126322. <https://doi.org/10.1016/j.cej.2020.126322>.
- Yuan, J., Li, Hongdong, Gao, S., Lin, Y., Li, Haiyan, 2010. A facile route to n-type TiO₂-nanotube/p-type boron-doped-diamond heterojunction for highly efficient photocatalysts. *Chem. Commun.* 46, 3119–3121. <https://doi.org/10.1039/c003172k>.
- Zanoni, M.V.B., Sene, J.J., Anderson, M.A., 2003. Photoelectrocatalytic degradation of Remazol Brilliant Orange 3R on titanium dioxide thin-film electrodes. *J. Photochem. Photobiol. Chem.* 157, 55–63. [https://doi.org/10.1016/S1010-6030\(02\)00320-9](https://doi.org/10.1016/S1010-6030(02)00320-9).
- Zhang, D., Qi, J., Ji, H., Li, S., Chen, L., Huang, T., Xu, C., Chen, X., Liu, W., 2020. Photocatalytic degradation of ofloxacin by perovskite-type NaNbO₃ nanorods modified g-C₃N₄ heterojunction under simulated solar light: theoretical calculation, ofloxacin degradation pathways and toxicity evolution. *Chem. Eng. J.* 400, 125918. <https://doi.org/10.1016/j.cej.2020.125918>.
- Zhang, J., Tao, H., Wu, S., Yang, J., Zhu, M., 2021. Enhanced durability of nitric oxide removal on TiO₂ (P25) under visible light: enabled by the direct Z-scheme mechanism and enhanced structure defects through coupling with C₃N₄. *Appl. Catal. B Environ.* 296, 120372. <https://doi.org/10.1016/j.apcatb.2021.120372>.
- Zhang, J., Zhou, P., Liu, J., Yu, J., 2014. New understanding of the difference of photocatalytic activity among anatase, rutile and brookite TiO₂. *Phys. Chem. Chem. Phys.* 16, 20382–20386. <https://doi.org/10.1039/c4cp02201g>.
- Zhang, Q., Du, R., Tan, C., Chen, P., Yu, G., Deng, S., 2021. Efficient degradation of typical pharmaceuticals in water using a novel TiO₂/ONLH nano-photocatalyst under natural sunlight. *J. Hazard Mater.* 403, 123582. <https://doi.org/10.1016/j.jhazmat.2020.123582>.
- Zhang, Q., Tan, C., Zheng, X., Chen, P., Zhuo, M., Chen, T., Xie, Z., Wang, F., Liu, H., Liu, Y., Zhang, X., Lv, W., Liu, G., 2019. Dual metal-free polymer reactive sites for the efficient degradation of diclofenac by visible light-driven oxygen reduction to superoxide radical and hydrogen peroxide. *Environ. Sci. Nano* 6, 2577–2590. <https://doi.org/10.1039/c9en00482c>.
- Zhang, Q., Wang, B.X., Yu, Y.B., Chen, B.Y., Hong, J. ming, 2020a. Sulfur doped-graphene for enhanced acetaminophen degradation via electro-catalytic activation: efficiency and mechanism. *Sci. Total Environ.* 715, 136730. <https://doi.org/10.1016/j.scitotenv.2020.136730>.
- Zhang, Q., Zhou, Y., lian, Yu, bo, Y., Chen, B.Y., Hong, J. ming, 2020b. Exploring catalytic performance of boron-doped graphene electrode for electrochemical degradation of acetaminophen. *Appl. Surf. Sci.* 508, 145111. <https://doi.org/10.1016/j.apsusc.2019.145111>.
- Zhang, X.X., Li, R., Jia, M., Wang, S., Huang, Y., Chen, C., 2015. Degradation of ciprofloxacin in aqueous bismuth oxybromide (BiOBr) suspensions under visible

- light irradiation: a direct hole oxidation pathway. *Chem. Eng. J.* 274, 290–297. <https://doi.org/10.1016/j.cej.2015.03.077>.
- Zhang, Y., Zhang, B.T., Teng, Y., Zhao, J., Sun, X., 2021. Heterogeneous activation of persulfate by carbon nanofiber supported Fe₃O₄@carbon composites for efficient ibuprofen degradation. *J. Hazard Mater.* 401, 123428. <https://doi.org/10.1016/j.jhazmat.2020.123428>.
- Zhao, C., Liao, Z., Liu, W., Liu, F., Ye, J., Liang, J., Li, Y., 2020. Carbon quantum dots modified tubular g-C₃N₄ with enhanced photocatalytic activity for carbamazepine elimination: mechanisms, degradation pathway and DFT calculation. *J. Hazard Mater.* 381, 120957. <https://doi.org/10.1016/j.jhazmat.2019.120957>.
- Zhao, J., Wang, J., Zhi, J., Zhang, Z., 2010. Preparation of grain size controlled boron-doped diamond thin films and their applications in selective detection of glucose in basic solutions. *Sci. China Chem.* 53, 1378–1384. <https://doi.org/10.1007/s11426-010-3099-8>.
- Zheng, K., Sun, Y., Gong, S., Jiang, G., Zheng, X., Yu, Z., 2019. Degradation of sulfamethoxazole in aqueous solution by dielectric barrier discharge plasma combined with Bi₂WO₆-rMoS₂ nanocomposite: mechanism and degradation pathway. *Chemosphere* 222, 872–883. <https://doi.org/10.1016/j.chemosphere.2019.02.004>.
- Zhong, X., Zhang, K.X., Wu, D., Ye, X.Y., Huang, W., Zhou, B.X., 2020. Enhanced photocatalytic degradation of levofloxacin by Fe-doped BiOCl nanosheets under LED light irradiation. *Chem. Eng. J.* 383, 123148. <https://doi.org/10.1016/j.cej.2019.123148>.
- Zhou, M., Tan, Q., Wang, Q., Jiao, Y., Oturan, N., Oturan, M.A., 2012. Degradation of organics in reverse osmosis concentrate by electro-Fenton process. *J. Hazard Mater.* 215–216, 287–293. <https://doi.org/10.1016/j.jhazmat.2012.02.070>.
- Zhou, R., Lu, G., Yan, Z., Jiang, R., Bao, X., Lu, P., 2020. A review of the influences of microplastics on toxicity and transgenerational effects of pharmaceutical and personal care products in aquatic environment. *Sci. Total Environ.* 732, 139222. <https://doi.org/10.1016/j.scitotenv.2020.139222>.
- Zhu, Y., Deng, F., Qiu, S., Ma, F., Zheng, Y., Lian, R., 2021. Enhanced electro-Fenton degradation of sulfonamides using the N, S co-doped cathode: mechanism for H₂O₂ formation and pollutants decay. *J. Hazard Mater.* 403, 123950. <https://doi.org/10.1016/j.jhazmat.2020.123950>.